To the Graduate Council:

I am submitting herewith a thesis written by William D. Newmyer entitled "The Analysis of a Hypothetical Criticality Accident Involving Dry Highly-Enriched Uranium Powder." I have examined the final copy of this thesis for form and content and recommend that it be accepted in partial fulfillment of the requirements for the degree of Master of Science, with a major in Nuclear Engineering.

H. L. Dodds

Dr. H.L.Dodds, Major Professor

We have read this thesis
and recommend its acceptance:

L F Miller

Paul M Stevens

Accepted for the Council:

Lee Minkel

Associate Vice Chancellor and
Dean of The Graduate School

The Analysis of a Hypothetical Criticality Accident Involving Dry Highly-Enriched Uranium Powder

A Thesis

Presented for the

Master of Science

Degree

The University of Tennessee, Knoxville

William D. Newmyer

May 1992

ACKNOWLEDGEMENTS

I would like to thank some of the people who have helped make the completion of this thesis possible. First, I must thank my major professor, Dr. H. L. Dodds, Jr. The many hours he spent with me on this project are sincerely appreciated. I thank him for all of his support.

Also, a great deal of thanks goes to Davis Reed, Richard Taylor and Dick Vornehm of the Y-12 Plant in Oak Ridge. Their willingness to help answer questions and address problems encountered in this project was exceptional.

The Criticality Safety Research Group at the University of Tennessee, Dan Hollenbach, Benan Basoglu, Roger Brewer and Chris Haught, have all been there to help solve the tough problems when they arose. I would also like to thank Tom Radcliffe who contributed to this work via interesting technical discussions.

Appreciation is also expressed to the numerous folks at the Oak Ridge National Laboratory who gave their time to help me when I needed it; specifically, Mike Westfall, Maurice Green, Pat Fox, Nancy Landers, Bill Herman, and the other staff members in Bulding 6011.

In addition, I wish to express my appreciation to Martin Marietta Energy

Systems who provided financial support for this work via a research contract with the University of Tennessee, Department of Nuclear Engineering.

Finally, I must thank my parents and my wife for all of their support. It is to them that this thesis is dedicated.

ABSTRACT

Nuclear Criticality Safety is a major field of interest in nuclear engineering today. The analyses of hypothetical criticality accident scenarios are an important part of this field. To safely mitigate the consequences of such an accident, the results of the accident must be known. This thesis presents a theoretical model for predicting the consequences of a hypothetical criticality accident involving dry highly-enriched uranium(HEU) powder. The results obtained with the model include power histories, integrated fission yields, temperature histories, and reactivity histories of the systems analyzed.

The materials of concern in this study are 93.2% U^{235} enriched dry uranium powders, UO_3 and UF_4. To simulate a powder pile on a concrete floor, a finite slab geometry (1x1xh and 2x2xh meters) is used where the pile height, h, determines the system reactivity. The model employs point neutronics with simple, lumped parameter thermal feedback. Feedback reactivity effects are caused by changes in temperature, density and volume. Temperature is calculated using an energy balance equation. Density and volume changes are calculated from an empirical relationship which is a function of temperature.

Results of excursion calculations involving different feedback models, geometries, powders, etc. are presented. Peak temperatures for the excursions range from 1000K to 2000K and total fission yields are calculated to be around 10^{19} fissions.

Some validation work is performed for the neutronics portion of the computational model. Finally, conclusions of the study and suggestions for future work are presented.

TABLE OF CONTENTS

List of Figures

List of Tables

Chapter 1

INTRODUCTION

1.1. Background

Nuclear criticality safety analysis is very important in support of any facility that deals with fissile materials. Care must be taken in all operations and procedures to insure the safety of all concerned. Current technology used to prevent criticality excursions is working well. Along with safe procedures and operations to prevent criticality accidents, emergency procedures must be determined to insure that the least possible harm comes to personnel and equipment in the unlikely event of an accident. A prerequisite for defining these emergency procedures is to understand the consequences of possible accidents that may occur in the facility. The analysis of hypothetical criticality excursions is one way to determine the possible effects of criticality accidents.

Since the beginning of the nuclear industry, only 8 accidents have occurred in processing facilities that deal with fissile materials.[1] The results of these accidents have been used to upgrade the emergency procedures in place at these and other sites. Along with actual accident data, experimental results are also available from criticality excursion experiments performed at critical mass laboratories throughout the world. These data can be applied to situations in a

facility that is similar to those of the experimental setup.

Facilities dealing with fissile materials must also rely on mathematical and computer models to calculate the results of hypothetical criticality excursions that may occur within their facility. Since most critical mass laboratories have closed and no accidents have occurred since 1978, computational results from these models are now relied upon to determine appropriate emergency responses.

The work presented in this thesis analyzes the results of a hypothetical nuclear criticality excursion involving dry highly-enriched uranium (HEU) powder. To the best of this author's knowledge, no accidents involving dry HEU powder have occurred nor have any mathematical or computer models been developed for calculating excursions involving dry HEU powder. Hence, this research should be considered as a "first attempt" at modelling a criticality excursion involving dry HEU powder.

1.2. Previous Work

In the area of nuclear criticality safety, a considerable amount of work has been performed to analyze hypothetical criticality excursions. A good example is the analysis of postulated, moderated criticality accidents at the Y-12 plant in

Oak Ridge involving fissile liquid systems.[2] This analysis calculated the initial fission pulse due to a hypothetical excursion and the resulting radiation doses on and off site. The approach used was the "weak neutron source method" developed by G.Hansen.[3] Hansen demonstrates in his paper that there is a non-zero probability that a system may achieve a supercritical configuration before an actual sustained chain reaction occurs. Hansen's method uses the Fuch's Energy Model[1] to predict the energy released in the first fission pulse. An empirical quenching constant "b" with units of $\Delta k/k$/fission is multiplied by the energy release to estimate the amount of feedback reactivity. Using data collected about fissile liquid systems at the Y-12 plant and data from the CRAC experiments,[4] the initial fission pulse yields for hypothetical criticality accidents involving fissile solutions at the Y-12 plant were calculated.[2]

The CRAC experiments[4] were performed from 1968 through 1971 by the French Atomic Energy Commission with highly-enriched uranium fissile solutions. The results of these experiments are also used frequently by nuclear criticality safety analysts to validate studies of fissile solution systems.

A document written by E.R.Woodcock presents estimations of the total fission yield associated with different types of criticality excursions.[5] Predictions are included for fissile solutions, heterogenous liquid/powder systems, solid fissile materials, and arrays of fissile units.

Examples of research on the modelling of criticality excursions for fissile solutions using the point kinetics model with simple thermal-hydraulic feedback solutions are the computer codes CRITEX[6] and CREST[7]. The CRITEX code was developed in the United Kingdom and the CREST code was developed in Japan. Both codes consider Hansen's weak neutron source method. A method for solving this stochastic problem when using the deterministic point kinetics model is discussed by H.Lutz.[8] Lutz states that given the ramp reactivity addition and the inherent neutron source, a delay time for early, most likely, and late initiation of the criticality excursion can be calculated. These times are then used to determine the reactivity of the system as a step at the onset of the excursion(i.e., early, most likely, and late) at time zero followed by continuation of the ramp insertion.

Other computer modeling codes exist to perform a wide range of criticality transient calculations. They include SKINATH[9], SLOPUS[10] and PAD[11]. Further information on these codes are presented in the body of this thesis. More recent excursion studies have been performed for damp low-enriched UO_2 powder. This work included experimental studies[12] as well as computer modelling[13]. Again the computer model uses point kinetics with simple reactivity feedback models. The computer model was compared to experimental work which was also performed by the same research group.[12,13] No comparison between experimental work and the computer model is currently available in the literature.

1.3. Scope and Organization

This research provides a theoretical model for computing transient histories of power, total fission yield, reactivity, and temperature for hypothetical criticality accident scenarios involving dry HEU powders of UO_3 and UF_4.

Chapter 2 provides a description of the entire accident scenario, the model, and the transient computer code used to calculate the hypothetical excursions. The effects of temperature on system properties and system reactivity is also discussed in Chapter 2.

Chapter 3 contains results for all transient calculations performed for dry HEU powder systems. Several parameter variations which are important when calculating criticality excursions are described. The small amount of validation work that could be done on the solution code is presented in Chapter 4. These validation efforts are primarily for the neutronics portion of the methodology only.

Conclusions and some suggestions for future work are presented in Chapter 5. Also included are two appendixes which discuss future work topics and a third that presents a listing of the computer code developed in this work.

Chapter 2

ACCIDENT MODELING

2.1. Hypothetical Accident Scenario

The material of interest in this work is dry highly-enriched uranium (HEU) powder; either UO_3 or UF_4, enriched to 93.2% U^{235}. The material density of the powder is 3.5 gm/cm^3 at 20°C.[14] The powder considered is dry(i.e., no moisture present); however, UO_3 may contain as much as 1.5w/o H_2O which is considered in Appendix B.[15] It is postulated that the powder is pouring continuously onto a concrete floor forming a powder pile which is approximated as a rectangular prism(i.e. a finite slab). For an easy analysis, the width and depth are chosen to be the same. One meter square and two meter square powder slabs with a variable height are used for the hypothetical accidents considered in this work. The height of the slab determines the system reactivity. The external reactivity insertion is caused by the mass addition to the system. Postulated reactivity insertion rates of \$.10/sec, \$1/sec and \$10./sec are considered. The height of the powder slab at delayed critical is taken as the starting point for the excursion calculations. A concrete reflector, 0.2 meters thick, is assumed on the bottom of the slab.

2.2 Transient Solution Methodology

The major objective of this study is to calculate the coupled neutronic and thermal response of an excursion involving dry highly-enriched uranium powder. A simple model for the time response of neutronics is the point kinetics model. The thermal response of the system can be treated simply by considering a one lump energy balance for the system. These equations are coupled since the neutronic power constitutes a heat generation source in the system that effects temperature, density, and volume which, in turn, affects the power via reactivity feedback.

A computer code named SKINATH[9] was developed several years ago at the Oak Ridge National Laboratory to solve the point kinetics equations with simple thermal-hydraulic feedback. This code was developed to calculate criticality excursions for fissile systems having the form of a long horizontal cylinder externally cooled by natural convection. It uses the Livermore Solver of Ordinary Differential Equations[16], LSODE, to solve the coupled set of point kinetics and thermal equations. Since SKINATH was designed to calculate results similar to those needed in this work, it can be modified to solve the more complex thermal equations for the HEU dry powder system. The original

SKINATH code will be referred to as SKINATH and the SKINATH code modified for the dry HEU powder system will be refered to as SKINATH-DP.

More complex methods of solution could involve consideration of the spatial dependence of the neutronic and thermal equations. A one-, two-, or three-dimensional spatial neutron kinetics model could be employed along with thermal considerations in multi-dimensional space. The PAD[11] code developed at Los Alamos National Laboratory models dynamic systems with transport theory neutronics, thermodynamics, and hydrodynamics in one-dimensional spherical, cylindrical, and planar geometries. However, such spatial detail is probably not needed unless the geometrical shape of the powder pile changes appreciably during the transient(e.g., during powder dispersal or disassembly). Moreover, the simple point models employed in this work are considered adequate for this "first attempt" at modelling excursions in powder systems. Therefore, a more complex code with spatial dependence such as PAD, is not required in this work. Also, since SKINATH is available on the Oak Ridge Computer System, it is easier to use and to modify than a code imported from another laboratory.

2.3. Point Kinetics

The point kinetics equations[8] are used in this work to calculate the power and neutron density responses of a nuclear system as a function of time. The point kinetics equations with six precursor groups are shown below:

$$\frac{dn}{dt} = \frac{(\rho-\beta)\ n}{\Lambda} + \sum_{i=1}^{6} C\lambda_i \ , \ and \tag{2.1}$$

$$For\ i=1,6$$
$$\frac{dC_i}{dt} = \frac{\beta_i\ n}{\Lambda} - \lambda_i C_i \ , \tag{2.2}$$

where n(t) = time-dependent system power (fissions/sec),
$\rho(t)$ = total system reactivity, ($\Delta k/k$)
β = total delayed neutron fraction,
β_i = delayed neutron fraction for precursor group i,
Λ = generation time, (sec)
$C_i(t)$ = precursor concentration for group i, (same units as n)
λ = decay constant for precursor group i, (sec^{-1})

If an extraneous neutron source, S(t), is present in equation 2.1 and has the units of neutrons/sec, then n(t) must have units of neutrons. For most of the applications in this work, S(t)=0, which permits n(t) to have units of fissions/sec. The units on n(t) are usually determined by the interpretation placed on the value of n(t) at t=0; namely, the initial power level.

A more detailed discussion of the initial power level is presented in section 3.2. The initial precursor concentrations are assumed to be in equilibrium with the initial power level.

2.3.1. Reactivity Changes

The total system reactivity is modeled as the sum of external and feedback reactivities as shown in equation 2.3:

$$\rho_{total} = \rho_{external} + \rho_{feedback} \qquad \textbf{(2.3)}$$

The external reactivity is calculated from a postulated powder pouring rate that results in a certain reactivity addition rate. The external reactivity insertion rates considered in this work are \$.10/sec, \$1./sec and \$10./sec.

The reactivity feedback effects are caused by changes in system properties due to system temperature changes. Reactivity feedback effects are calculated using reactivity feedback coefficients which are calculated *a priori*. The feedback effects considered are the changes in density and volume caused by temperature changes and the Doppler effect. A complete discussion on the calculation of external and feedback reactivities is presented in section 2.6.

2.3.2. Delayed Neutron Precursors

Delayed neutrons play an important role in nuclear systems. They dictate how fast or slow nuclear systems will respond to reactivity changes because they appear and disappear at times dictated by their production and decay.

The use of incorrect delayed neutron data in the point kinetics equations can produce inaccurate results. Therefore, care must be taken when selecting the values of the delayed neutron decay constants and delayed neutron fractions. These values usually come from Keepin's book, Physics of Nuclear Kinetics.[17] However, an updated report of delayed neutron data is given by J.E.Cahalan and K.O.Ott.[18] The data employed in the present analyses are presented in Table 2.1. These data are for a fast U^{235} system.

Table 2.1 : Delayed Neutron Data for U^{235}

i	$\lambda_i(sec^{-1})$	β_i
1	.0129	.00023
2	.0311	.00142
3	.1340	.00136
4	.3310	.00240
5	1.260	.00070
6	3.210	.00027

$$\beta = \Sigma \beta_i = .00642$$

2.3.3. Generation Time

The generation time[8] used by the point kinetics equations is defined as the average time it takes one neutron to produce either a prompt neutron or a delayed-neutron precursor. The generation time is defined as shown below:[19]

$$\Lambda \equiv \frac{\int dV \int dE\ W(r,E)[1/v(E)]\Phi(r,E,t)}{\int dV \int dE\ W(r,E)\sum_j \chi^j(E) F^j\Phi(r,E,t)}, \quad \textbf{(2.4)}$$

where r, E, V, t = position, energy, volume, and time, respectively,
W(r,E) = weighting function (see ref. 19),
v = neutron speed,
$\Phi(r,E,t)$ = time dependent flux density,
χ^j = neutron spectrum of neutrons emitted by isotope, j,
$F^j\Phi(r,E,t)$ = operator on $\Phi(r,E,t)$, =

$$\int_0^\infty \nu_j \Sigma_f^j(r,E',t)\phi(r,E',t)dE'$$

Accurate evaluations of the generation time using this expression are usually accomplished using a neutron diffusion code and can be quite cumbersome.

The Monte Carlo code KENO Va[20] also calculates a number which is interpreted as the generation time. It is effectively the average time between successive generations of neutrons averaged over all generations but the first

three in the Monte Carlo calculation. KENO Va[a] was executed to determine the generation time for each dry HEU powder system analyzed. These results are shown in table 2.2. The value of the generation time in each case is for a slab that is critical.

Table 2.2 : Generation Time Results using KENO Va

System Definition	UO_3 1-m x 1-m slab (10^{-5} sec)	UO_3 2-m x 2-m slab (10^{-5} sec)	UF_4 1-m x 1-m slab (10^{-5} sec)
Generation Time Λ	2.40 ± .067	2.80 ± .062	2.84 ± .063

2.4. Energy Balance

To calculate the system temperature, $T_{sys}(t)$, during the excursion, an overall energy balance for the system is used. Considering the slab as the control volume, the overall energy balance may be written as

$$Q(t)_{storage} = Q(t)_{generation} - Q(t)_{loss} , \qquad (2.5)$$

where Q(t) is a time rate of change of energy.

---

[a] KENO Va was executed as part of the CSAS25[21] sequence found in the SCALE 4 release. CSAS25 executes BONAMI-S, NITAWL-S, and KENO Va. BONAMI-S performs resonance shielding through the application of the Bonderenko shielding factor method. NITAWL-S applies the Nordheim Integral Treatment to perform neutron cross section processing in the resonance energy range. KENO Va is a multigroup Monte Carlo computer code. The 27-group ENDF/B-IV master cross section library was used in these calculations.

2.4.1. Internal Energy Storage Rate

The derivation of the stored internal energy will be treated first. The powder system is comprised of powder particles and air which occupies the interstitial volume. The powder particles have far more mass than the air and are also the source of heat generation in the system; therefore, it is assumed that the powder is the only material that stores internal energy. The internal energy storage rate is given by

$$Q_{storage}(t) = m_p(t) C_p(T_{sys}) \frac{dT_{sys}(t)}{dt} , \qquad (2.6)$$

where $Q_{storage}(t)$ = internal system energy storage rate at time t, (J/s)
$m_p(t)$ = mass of powder in the system at time t, (kg)
$C_p(T_{sys})$ = specific heat of the powder at T_{sys}, (J/s/kg)
$T_{sys}(t)$ = system temperature at time t, (K).

The mass of powder in the system changes with time because the addition of mass to the system is the external reactivity insertion. The calculation of the mass of powder in the system at time t is given by

$$m_p(t) = m_0 + \rho(t)_{ext} \frac{\partial m}{\partial \rho} , \qquad (2.7)$$

where $m_p(t)$ = mass of powder in system at time t, (kg)
m_0 = initial mass of powder, (kg)
$\rho_{ext}(t)$ = total external reactivity inserted at time t, ($)
$\partial m/\partial \rho$ = external reactivity coefficient, (kg/$)

The external reactivity coefficient is used to determine the amount of mass required to insert a specific amount of reactivity in the system. The actual calculation of this coefficient is presented in section 2.6.1.

Equations for the specific heats for UO_3 and UF_4 as functions of temperature are given by[22]

$$C_p^{UO_3}(T_{sys}) = 14.78\ (22.1 + 2.6x10^{-3}T_{sys} - 2.65x10^{5}T_{sys}^{-2})$$
$$C_p^{UF_4}(T_{sys}) = 13.45\ (25.7 + 7.0x10^{-3}T_{sys} - 0.06x10^{5}T_{sys}^{-2}). \qquad (2.8)$$

2.4.2. Energy Generation Rate

The energy generation takes place inside the powder particles. Since the power is calculated in fissions/sec from the point kinetics equations described earlier, the energy generation rate in joules/sec is the product of power and a conversion constant. The energy generation rate is given by

$$Q(t)_{generated} = \varepsilon \times FP(t)\ , \qquad (2.9)$$

where $Q_{generated}(t)$ = energy generation rate in the system, (J/s)
ε = energy released per fission, $3.2x10^{-11}$ J/fission,
FP(t) = power (fissions/s).

2.4.3. Energy Loss Rate

The energy loss rate from the system is the summation of three energy loss effects: conduction through the concrete floor, natural convection from the slab to the surrounding air, and radiative cooling to the surrounding environment. These three effects require knowledge of the three fundamental heat transfer mechanisms: conduction, natural convenction, and radiative.

Conduction occurs through the concrete floor located below the powder slab. The rate of energy loss due to conduction in one dimension is described by Fourier's Law[23] as

$$Q(t)_{conduction} = kA\frac{dT}{dx} \qquad (2.10)$$

where $Q_{conduction}(t)$ = energy loss rate due to conduction,
k = thermal conductivity,
A = area, and
dT/dx = temperature gradient.

Two different ways to estimate the temperature gradient are considered in this research. The first approach is a simple thermal resistance model. In the thermal resistance model, the temperature gradient is approximated as

$$\frac{dT}{dx} = \frac{[T_{sys}(t) - T_c]}{L} \qquad (2.11)$$

where $T_{sys}(t)$ = system temperature at time t, (K)
T_c = temperature of the bottom of the concrete, 293K, and
L = thickness of concrete, 0.2 meters.

This is the conventional steady state temperature gradient except that the temperature difference in the numerator is assumed to be time dependent.

The resulting expression for $Q(t)_{conduction}$ is

$$Q(t)_{conduction} = \frac{k\ A_b(t)\ [T_{sys}(t) - T_c]}{L} \qquad (2.12)$$

The second model considered is an analytic solution of the heat conduction equation. The heat conduction equation is solved for the following conditions: (1) A semi-infinite solid, (2) a prescribed surface temperature, F(t), and (3) the temperature of the powder, $T_{sys}(t)$, is equal to F(t). The resulting expression for $Q(t)_{conduction}$ is[23]

$$Q(t)_{conduction} = \frac{A(t)_b k}{\sqrt{\pi / a}} \int_0^t \frac{F'(t-\tau)}{\sqrt{\tau}} d\tau \qquad (2.13)$$

where a = thermal diffusivity of concrete, 5.16×10^{-7} m^2/sec, and
F'(t) = the time derivative of the prescribed surface temperature, dF/dt.

The time derivative of the prescribed surface temperature is simply the calculated derivative, dT_{sys}/dt, from the overall energy balance shown at the end of this

section in equation 2.22. By storing the value of this derivative during the calculation, the integral in equation 2.13 can be evaluated numerically at any time, t. This gives the energy loss rate at time t due to conduction using the second model.

Results of the thermal resistance and analytic models are compared along with a no conduction model in section 3.3. The thermal resistance model is used in this work for the reasons stated in section 3.3.

Natural Convection occurs from the sides and top of the powder slab. The heat loss rate caused by natural convection is given by

$$Q_{convection}(t) = (\hat{h}_{top}A_{top}(t) + \hat{h}_{sides}A_{sides}(t))(T_{sys}(t)-T_{air}) , \qquad (2.14)$$

where $Q_{convection}(t)$ = energy loss rate due to convection, (J/s)
$\hat{h}_{top}$ = heat transfer coefficient for top of slab, (J/s/m^2/K)
$\hat{h}_{sides}$ = heat transfer coefficient for sides of slab, (J/s/m^2/K)
$A_{top}(t)$ = area of the top of the slab at time t, (m^2)
$A_{sides}(t)$ = area of the sides of the slab at time t, (m^2)
$T_{sys}(t)$ = system temperature at time t, (K)
T_{air} = surrounding air temperature, 293K.

Natural convection heat transfer coefficients are found from experimental correlations in terms of the dimensionless Nusselt number, Nu, and the dimensionless Raleigh number, Ra.[24] The Nusselt number, Nu, is defined as

$$Nu_L = \frac{hL}{k}, \qquad (2.15)$$

where h = heat transfer coefficient, (J/s/m^2/K)
k = thermal conductivity of gas, (J/s/m/K)
L = characteristic length, (m).

and the Raleigh, Ra, is defined as

$$Ra_L = \frac{g\beta(T_{sys}-T_{air})L^3}{\alpha\nu}, \qquad (2.16)$$

where g = acceleration due to gravity, (m/s^2),
β = 1 / T_f, T_f is the film temperature = (T_{sys} + T_{air}) / 2,
T_{sys} = system temperature, (K)
T_{air} = ambient air temperature, (K)
α = thermal diffusivity, (m^2/s)
ν = kinematic viscosity, (m^2/s)
L = characteristic length, (m).

The correlations of Nu_L and Ra_L for the top of a heated horizontal surface are given by[24]

$$\begin{aligned} Nu_L^{top} &= 0.54Ra_L^{1/4} \quad (10^4 \le Ra_L \le 10^7) \\ Nu_L^{top} &= 0.15Ra_L^{1/3} \quad (10^7 < Ra_L \le 10^{11}), \end{aligned} \qquad (2.17)$$

where L = $A_s(t)$ / P(t),
A_s = top surface area of slab at time t, (m^2)
P = perimeter of top surface area of slab at time t, (m)

The heat transfer coefficient for the top of the slab is found by multiplying Nu_L^{top} by the thermal conductivity, k, and dividing by the characteristic length, L.

The correlations for the sides of the slab are given by[24]

$$Nu_L^{sides} = 0.59 Ra_L^{1/4} \quad (10^4 \le Ra_L \le 10^9)$$
$$Nu_L^{sides} = 0.10 Ra_L^{1/3} \quad (10^9 \le Ra_L \le 10^{13}) , \qquad (2.18)$$

where L = height of slab, (m)

The heat transfer coefficient for the sides is also found by multiplying Nu_L^{sides} by k, and dividing by L.

The determination of $\hat{h}_{top}$ and $\hat{h}_{sides}$ as described above uses the properties of the air found from tabulated data available in reference 20. These tabulated data were fit to polynomials as follows

$$k_{air} = 1.0x10^{-3}(13.68 + .004456\ T_f + 1.28x10^{-4}\ T_f^2 - 9.939x10^{-8}\ T_f^3 + 2.452x10^{-11} T_f^4) \qquad (2.19)$$
$$\alpha_{air} = 1.0x10^{-6}(-32.39 + .2055\ T_f - 5.98x10^{-5}\ T_f^2 + 5.57x10^{-8}\ T_f^3)$$
$$\nu_{air} = 1.0x10^{-6}(-2.451 + .044\ T_f + 7.787x10^{-5}\ T_f^2).$$

Radiative Cooling is described as follows

$$Q(t)_{radiative} = \varepsilon\sigma(A_{top}(t)+A_{sides}(t))(T_{sys}^4 - T_{air}^4) , \qquad (2.20)$$

where $Q_{radiative}$ = heat loss rate due to radiative cooling, (J/s)
ε = emissivity of powder slab,
σ = Boltzmann's constant, ($J/s/K^4/m^2$)
T_{sys} = temperature of the slab, (K)
T_{air} = temperature of the surrounding air, 293K.

The emissivity is a measure of how close the system is to a black body radiator for which $\varepsilon = 1$.[25] Data for the emissivity of UO_3 or UF_4 were not found. However, data for UO_2 are available[26]. The emissivity of UO_2 powder is given by

$$\begin{array}{ll} \varepsilon = 0.850 & 293\ K - 1020\ K \\ \varepsilon = .020357 + .001265\ T - 6.1715 \times 10^{-7}\ T^2 & 1020\ K - 1800\ K \\ \varepsilon = 0.40 & 1800\ K - 3000\ K \end{array} \qquad (2.21)$$

2.4.4. Energy Balance Equation

With all the necessary terms in the energy balance equation defined, the overall differential energy balance for the system may be written as

$$m_p(t)C_p(t)\frac{dT_{sys}}{dt} = \varepsilon FP - \frac{kA_b(t)[T_{sys}-T_c]}{L} - [\hat{h}_{top}A_{top}(t)+\hat{h}_{sides}A_{sides}(t)][T_{sys}-T_{air}] - \varepsilon\sigma[A_T(t)+A_{sides}(t)][T_{sys}^4-T_{air}^4]. \qquad (2.22)$$

2.5. System Properties Changing With Temperature

2.5.1. Powder Density Change

In the powder slab system, an increase in the system temperature causes the powder to increase its volume. This expansion is due to heating of the air voids trapped by the powder particles and the expansion of the powder particles. To calculate this effect, a relationship between system temperature and powder density must be known. A relationship for UO_3 or UF_4 was not found. However, a relationship between temperature and powder density for UO_2 was found[27]. This relationship is given by

$$D(T) = D_0 \left(1 + 2.04x10^{-5}(T_{sys} - 273) + 8.7x10^{-9}(T_{sys} - 273)^2\right)^{-1}, \quad (2.23)$$

where D_0 = initial density of the powder, in kg/m^3

The density change of the powder will have a feedback effect on reactivity due to number density changes which is discussed later. It also will have an effect on the dimensions of the powder slab which affects reactivity via a change in neutron leakage and is discussed next.

2.5.2. System Dimensions Change

An increase in system temperature causes an increase in the volume of the system which affects neutron leakage and, thus, the reactivity of the system. This increased volume can be calculated by using the new density according to equation 2.24. A simple mass ratio is used to calculate the new system volume

$$V_T = V_0 \frac{D_0}{D_T}. \qquad (2.24)$$

The volume change of the powder can be related to the change in dimensions of the powder system by using a simple expansion model. The fractional change in the system volume is approximately equal to three times the linear expansion coefficient, α[25]

$$\frac{V_T - V_0}{V_0} = 3\alpha , \qquad (2.25)$$

where V_T = the system volume at temperature T, (m^3)
V_0 = the initial system volume, (m^3)
α = the coefficient of linear expansion.

This coefficient of linear expansion is used to determine the change in side length, ΔS. The new side length, S_T, is equal to the original side length, S_0, plus the change in side length, ΔS and is given by

$$S_T = S_0 (1 + \alpha) \tag{2.26}$$

The new height is given by

$$H_T = H_0(1 + \alpha). \tag{2.27}$$

The new system height and side length of the slab are used to calculate the reactivity feedback coefficient associated with a volume change. They are also used in the energy balance equation to define the surface area for heat transfer.

2.6. External and Feedback Reactivity

2.6.1. External Reactivity Addition

The external reactivity addition to the HEU dry powder system is caused by mass addition to the powder slab. This increase is assumed to change the height only. If the reactivity change associated with this mass addition is known, the reactivity insertion is known. The reactivity change associated with a mass change can be determined by calculating the reactivity of the system at various

heights, plotting the results, and fitting a line to the plot. This method of determining the external reactivity addition requires the mass addition rate of the powder to be known. In this research, no specification is made on the mass addition rate of powder. The mass addition rate corresponding to a reactivity insertion rate may be calculated as

$$\frac{dm}{dt} = \frac{d\rho}{dt}\frac{dm}{d\rho}, \qquad (2.28)$$

where dm/dt = mass addition rate in kg/sec
dρ/dt = external reactivity addition rate, ($/s)
dm/dρ = external reactivity coefficient, (kg/$)

The reactivity insertion rates considered in this research are $.10/sec, $1./sec, and $10./sec. External reactivity coefficients used in the excursion analysis are calculated using the discrete-ordinates code, XSDRNPM-S[b]. A concrete reflector of 0.2 meters is included on one side for each of the powder slabs to model the concrete floor. The results are shown in figure 2.1.

[b] XSDRNPM-S[26] was executed as part of the CSAS1X[27] sequence found in the SCALE 4 release. CSAS1X executes BONAMI-S, NITAWL-S, and XSDRNPM-S. BONAMI-S performs resonance shielding through the application of the Bonderenko shielding factor method. NITAWL-S applies the Nordheim Integral Treatment to perform neutron cross section processing in the resonance energy range. XSDRNPM-S is a one-dimensional, discrete ordinates, transport theory computer code. The 27-group ENDF/B-IV master cross section library was used in these calculations.

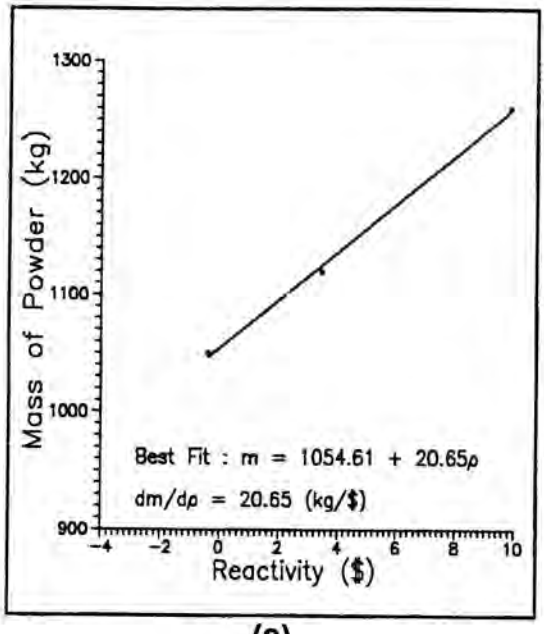

(a)

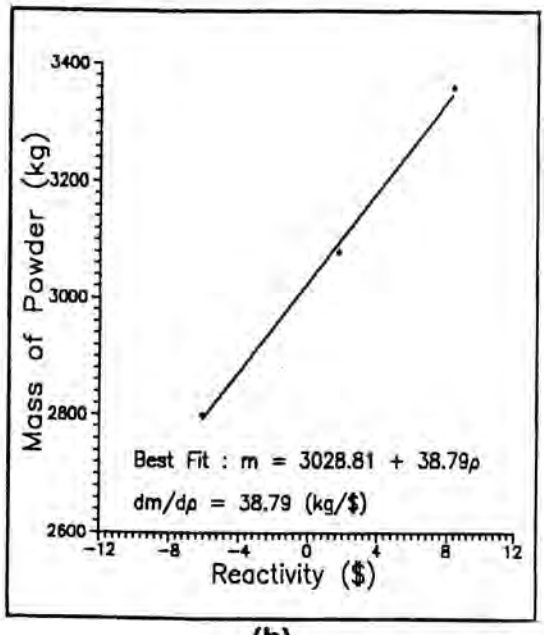

(b)

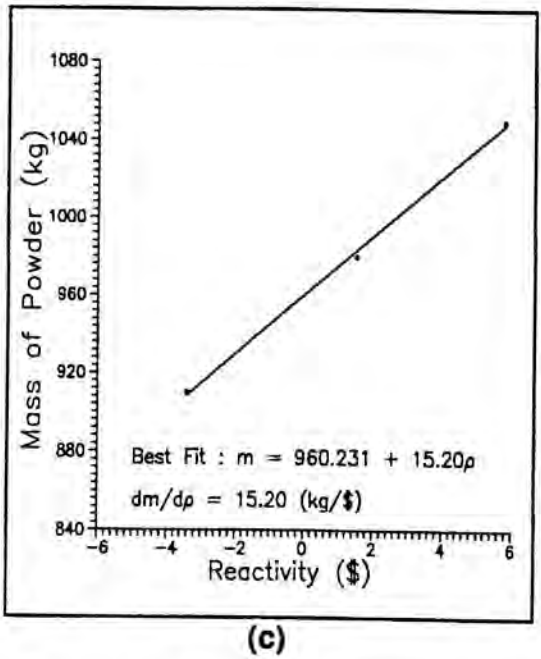

(c)

Figure 2.1 : External Reactivity Coefficient for a (a) UO_3, 1-m x 1-m slab, (b) a UO_3, 2-m x 2-m slab, and (c) a UF_4, 1-m x 1-m slab.

2.6.2. Feedback Reactivity

Reactivity feedback is directly or indirectly caused by the temperature change calculated from the energy balance equation. The temperature change in the powder slab will cause the reactivity to change due to the Doppler effect on the microscopic cross sections and the change in density and volume of the system. The decrease in the density of the powder decreases the reactivity of the system and the increase in the dimensions of the system increases the reactivity. These three effects, Doppler, density and volume can be treated as separate feedback coefficients for reactivity or as one lumped feedback coefficient dependent on temperature only. The next two sections discuss both of these approaches.

Separated Feedback Coefficients are found by treating each of the reactivity feedback effects separately using the discrete ordinates code, XSDRNPM-S. The critical height of each of the powder slabs analyzed is found from the external reactivity addition rate calculations described in section 2.6.1. The initial powder density is 3.5 gm/cc and the initial temperature is 293 K. Changes in the initial conditions of density, volume, and temperature(i.e. Doppler) are made separately to determine the reactivity feedback effect of each parameter. The Doppler effect is calculated by changing the powder temperature and holding the dimensions and density of the system constant. The density

effect is calculated by changing the density of the powder and holding the powder temperature and dimensions constant. Finally, the volume change effect is calculated by changing the dimensions of the system according to the expansion model discussed in section 2.5.2 and leaving the powder density and temperature constant. The separate feedback coefficients are then used to calculate the total(or combined) feedback reactivity as

$$\rho_{fdbk} = \frac{\partial \rho}{\partial D}\left(D(t) - D_0\right) + \frac{\partial \rho}{\partial V}\left(V(t) - V_0\right) + \frac{\partial \rho}{\partial T}\left(T(t) - T_0\right), \quad \textbf{(2.29)}$$

where D = density
V = volume
T = temperature (Doppler).

Results of the individual feedback coefficient calculations for a one meter by one meter slab of UO_3 powder are shown in figure 2.2. A simpler and more accurate way to calculate the feedback reactivity is discussed next.

A Combined Feedback Coefficient can be calculated by assuming that a change in temperature causes a simultaneous change in density, volume, and the microscopic cross sections(i.e., the Doppler effect). The new density and system dimensions are calculated using the equations discussed in section 2.5. The new reactivity of the system is calculated at the new increased temperature by CSAS1X where the density assumes its new value, the dimensions are changed accordingly, and the powder temperature is the new temperature that

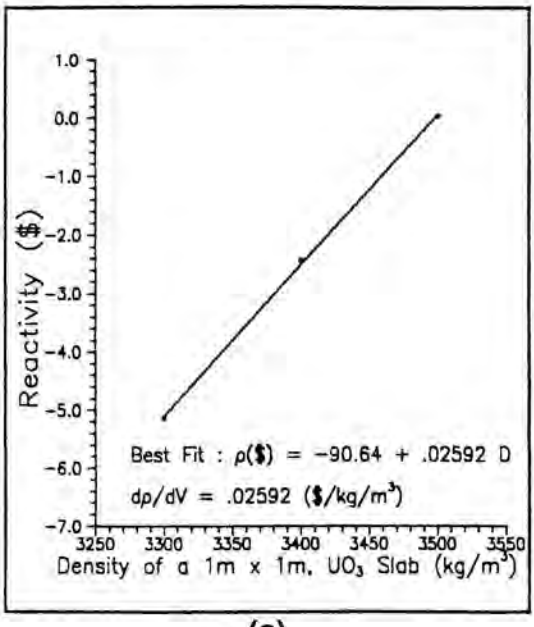

(a)

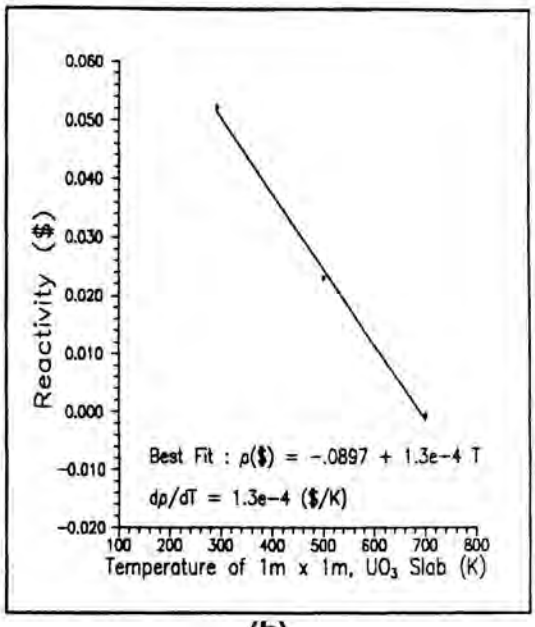

(b)

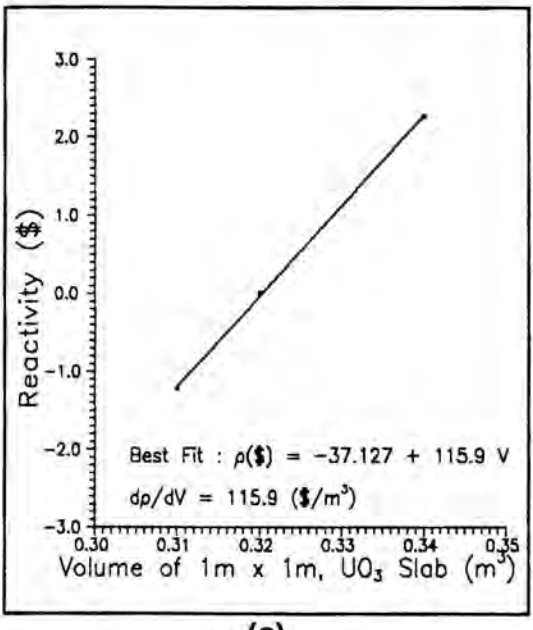

(c)

Figure 2.2 : Reactivity Feedback Coefficients for the Seperated Effects of Temperature in the 1-m x 1-m UO_3 Slab where (a) is the Density Coefficient, (b) is the Doppler Coefficient, and (c) is the Volume Coefficient.

caused these new conditions. These reactivity values will yield a single reactivity feedback coefficient that takes all three effects into consideration. The feedback reactivity is then calculated on-line during a transient by multiplying the combined feedback coefficient times the calculated temperature change. The results using the combined feedback coefficients are shown in figure 2.3 for each of the three powder systems considered in this work.

The combined method of determining feedback reactivity is also simpler because it requires knowledge of the temperature change only to calculate reactivity feedback. The separated feedback model requires calculation of the new density, volume and temperature at each time step to determine the feedback reactivity. The combined reactivity feedback coefficient is more accurate because it takes all three effects into consideration simultaneously. The separated feedback model ignores changes in the other parameters caused by the change in the one parameter alone(i.e., sometimes referred to as cross terms). The cross term feedback effects may be important and are accounted for implicitly in the combined feedback model. Because the combined method should be more accurate, it is used in all calculations presented in this work except section 3.3 which shows a comparison of the two methods.

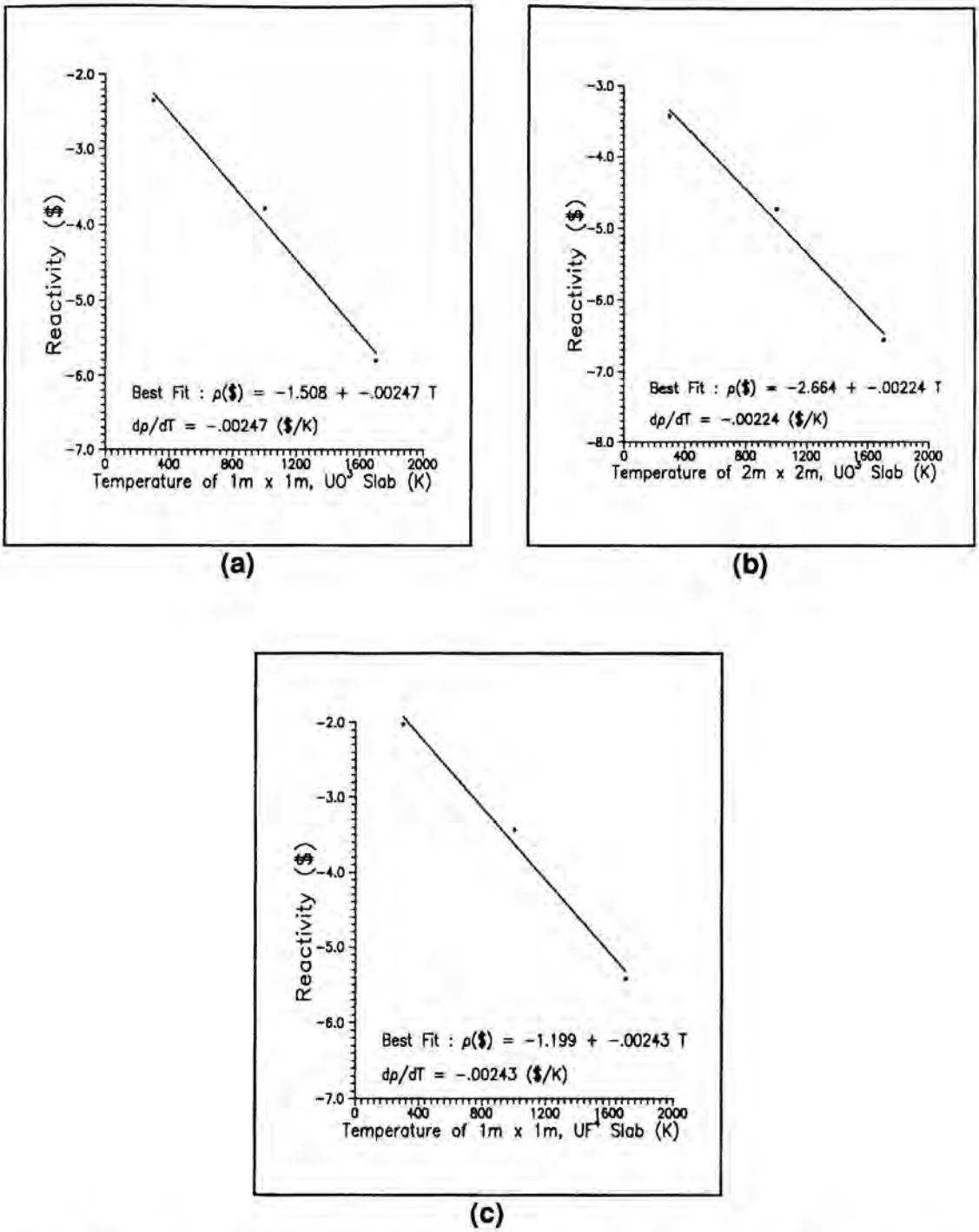

Figure 2.3 : Reactivity Feedback Coefficient with the Combined Effects of Temperature for (a) a UO_3, 1-m x 1-m slab, (b) a UO_3, 2-m x 2-m slab, and (c) a UF_4, 1-m x 1-m slab.

Chapter 3

EXCURSION ANALYSIS RESULTS

3.1. Weak Neutron Source Considerations

The assembly of fissionable material in the presence of a weak neutron source was first considered in 1960 by Hansen.[3] His theory is based on the fact that assembly of fissionable material in the presence of a weak neutron source, where the statistical nature of fission chains are important, can significantly affect the amount of energy released in the first pulse of a criticality excursion. In other words, it is possible to assemble a highly super critical configuration before the power begins to rise if only a weak neutron source is present in the system. Hansen shows that the actual amount of energy release can be 200 to 250 times higher than that predicted by conventional point kinetics.

A delay in the initiation of the sustained chain reaction which allows the system to become super-critical causes the increased energy release. Hansen identifies the "weak source" condition as

$$\frac{2S\tau}{\bar{\nu}\Gamma_2} < 1 \ , \qquad (3.1)$$

where S = neutron source strength, (neutrons/s)
τ = the mean neutron lifetime, (s)
ν = the average number of neutrons emitted per fission, 2.57 for fast fission of U^{235},
$\Gamma_2 = \nu(\nu-1)/\nu^2 \cong 0.8$

Hansen derives two equations that are important in determining the amount of energy release during the first pulse of a criticality excursion. Equation 3.2, describes the probability for the first persistent fission chain being sponsored at time, t_1, in a fissile system undergoing a ramp external reactivity insertion, where delayed critical occurs at t=0. This equation can be used to calculate the probability that a sustained chain reaction will take place at time, t_1, past delayed critical

$$P(t_1) = \sqrt{\frac{2\alpha\tau S^2}{\pi\bar{\nu}^2\Gamma_2^2}}\left[\frac{1-erf\left[\left(\frac{\alpha}{2\tau}\right)^{1/2}t_1\right]}{2}\right]^{\left(\frac{2S\tau}{\bar{\nu}\Gamma_2}-1\right)}\exp\left(-\frac{\alpha t_1^2}{2\tau}\right) \qquad (3.2)$$

where $P(t_1)$ = the probability that a sustained chain reaction will take place at time, t_1, past delayed critical,
t_1 = the time past delayed critical, (s)
α = ramp reactivity insertion rate, ($\Delta k/k/sec$),

The second important equation in Hansen's work, equation 3.3, is the fission yield of a fissile assembly undergoing a ramp reactivity insertion

$$E(t_1) = \frac{1}{b}\left[\alpha^2 t_1^2 + 2\alpha\tau\ln\left(\frac{2\alpha\tau W(t_1)}{b}\right)\right]^{1/2}, \qquad (3.3)$$

where $W(t_1)$ is given by

$$W(t_1) = \frac{\left(\frac{8\alpha\tau}{\pi\bar{\nu}^2\bar{I}_2^2}\right)^{1/2} \exp\left(-\frac{\alpha t_1^2}{2\tau}\right)}{1-erf\left[\left(\frac{\alpha}{2\tau}\right)^{1/2} t_1\right]}.$$

Equation 3.3 is based on the energy model of reactivity quenching (Fuch's Energy Model[1]) which postulates that negative reactivity introduced by the first fission pulse is proportional to the total energy released in the pulse as shown in equation 3.4

$$\rho_{fdbk}(t) = -b\int_{-\infty}^{t} P(t')dt' = -b\int_{0}^{t} P(t')dt' , \qquad (3.4)$$

where $\rho_{fdbk}(t)$ = the feedback reactivity at time, t, ($\Delta k/k$)
b = quenching constant, ($\Delta k/k$/fission)
P(t′) = power at dummy variable, t′, (fissions/sec).

The quenching constant, b, characterizes a fissile system and must be known to employ the above fission yield estimate. However, values of b are not known for fissile powder systems.

Since the value of b in equation 3.3 is unknown for the dry HEU powder system due to the unavailability of experimental data, another way to handle the weak neutron source problem has been suggested by Lutz.[8] In 1985, Lutz described a method to employ the weak neutron consideration using the point kinetics equations. By using equation 3.2, three delay times corresponding to

early, most likely, and late initiation times for the sustained chain reaction can be calculated. Multiplying each delay time by the ramp rate gives three different initial values of reactivity, each of which is considered to be a step at time t=0 followed by continuation of the ramp insertion. Thus, three different transient calculations can be performed corresponding to early, most likely, and late initiation times of the chain reaction producing three different transient responses.

To illustrate, both Hansen and Lutz demonstrate that the expected, or most likely, delay time, $<t_1>$, for a ramp insertion of reactivity is given by

$$<t_1> = \sqrt{\frac{\pi \bar{\nu} \Gamma_2}{4 \alpha S}} ,$$

The standard deviation of the expected value is given by

$$\sigma_1 = \sqrt{\left(1 - \frac{\pi}{4}\right) \frac{\bar{\nu} \Gamma_2}{\alpha S}}$$

Assuming a normal distribution of delay times, the 10% and 90% probability delay times are

$$t_{1,10\%} = <t_1> - 1.28\sigma_1 \text{ ; early}$$
$$t_{1,50\%} = <t_1> \text{ ; most likely}$$
$$t_{1,90\%} = <t_1> + 1.28\sigma_1 \text{ ; late.}$$

An example of this methodology is demonstrated in the next section for the GODIVA critical assembly.

3.1.1. GODIVA Facility Calculation

The GODIVA critical assembly at the Los Alamos National Laboratory is a bare sphere of highly enriched uranium metal. The neutron lifetime, neutron source strength, and quenching coefficient, b, are all known for this system[3] and are 0.6×10^{-8} sec, 90 neutrons/sec and 0.5×10^{-19} $\Delta k/k$/fission, respectively. For a ramp insertion of 10^{-2} $\Delta k/k$/fission, the method based on early, most likely, and late initiation times can be used to show the effect of the delay time on the energy release during the first pulse.

For GODIVA, the most probable delay time is 1.32 seconds and the standard deviation is 0.69 seconds. The 10% and 90% probability delay times are 0.44 seconds and 2.20 seconds, respectively. The GODIVA system was modeled with the SKINATH-DP code using the reactivity quenching model with the b parameter in lieu of the thermal feedback model for a powder pile. The results are shown in Table 3.1 for a steady state initial power of 10 fissions/sec.

These results show that using the delay time concept with the point kinetics equations yield a result almost 200 times higher than the point kinetics

result without a delay time present. These results also show the need to understand and to take into consideration the presence of a weak neutron source when an excursion analysis is being performed.

Table 3.1 : SKINATH-DP Results for GODIVA with and without Delay Times.

Delay Time (sec)	Peak Power (fissions/sec)	Energy Release (fissions)
0.0	2.5×10^{17}	1.72×10^{15}
0.44 (early)	6.6×10^{18}	1.53×10^{16}
1.32 (most likely)	7.5×10^{22}	9.20×10^{16}
2.20 (late)	4.0×10^{23}	3.10×10^{17}

3.1.2. Neutron Source Strength in Dry HEU Powder System

To accurately calculate power histories of the HEU dry powder system, the inherent neutron source strengths of both UO_3 and UF_4 were determined. Because experimental methods are difficult, costly, and time-consuming, a calculational method was used. Specifically, the computer code, ORIGEN-S[c], in the SCALE IV system at Oak Ridge National Laboratory was used to calculate inherent neutron source strengths for both UO_3 and UF_4 on a per kilogram of uranium basis. Table 3.2 shows the results of the ORIGEN-S calculations.

---

[c]ORIGEN-S[28] is a SCALE system module used to calculate fuel depletion, actinide transmutation, fission product buildup and decay, and associated radiation source terms.

Table 3.2 : Neutron Source Strength Spectrum for UO_3 and UF_4 as calculated by ORIGEN-S

Energy Boundaries, Mev	Neutron Source Strength, neutrons/sec/kg	
	UO_3	UF_4
Spontaneous Fission	.862	.862
	(α,n)	(α,n)
6.43 - 20.0	0.0	2.905
3.00 - 6.43	12.10	2268.0
1.85 - 3.00	25.06	1162.0
1.40 - 1.85	6.266	229.4
0.90 - 1.40	3.420	249.6
0.40 - 0.90	0.949	185.8
0.10 - 0.40	0.171	76.16
.017 - 0.10	0.0	11.53
TOTAL	48.836	4186.3

The inherent neutron source in UO_3 and UF_4 powders come mostly from the (α,n) reactions in oxygen and fluorine. The alphas come from the decay of U^{234} which is about 1w/o in dry HEU powders. Very few neutrons are produced from spontaneous fission. The source strength at delayed critical is the neutron source strength of concern. This configuration will either sustain a chain reaction or wait until some supercritical state is achieved. The neutron source strengths of each of the three critical finite slab geometries considered in this work are shown in Table 3.3.

Table 3.3 : Neutron Source Strength for Critical Slab Geometries

Material and Geometry	Critical Volume (m^3)	Critical Uranium Mass (kg)	Neutron Source (neut/sec)
UO_3, 1 x 1 meter	0.3013	875.7	4.277×10^4
UO_3, 2 x 2 meter	0.8653	2514.9	1.228×10^5
UF_4, 1 x 1 meter	0.2743	725.4	3.037×10^6

Because these source strengths are large, the condition for a weak neutron source, equation 3.1, is not met. Therefore, Lutz's method was not applied to compute any significant delay times because the neutron source strength is strong. However, Hansen's probability equation, equation 3.2, was evaluated to determine if delay times were significant. The results of these calculations showed that delay times are negligibly small due to the large inherent neutron source strength associated with the large critical masses. In other words, a sustained chain reaction should occur at delayed critical.

3.2. Initial Power

The approach used to address the effect of the initial power on the excursion results is described in the following section.

3.2.1. Initial Power Sensitivity

The initial power of the dry HEU powder system is caused by initial fission events taking place in the system at delayed critical. To know the initial power exactly, experimental data are needed. Since none are available, calculational methods are used.

The smallest initial power of the system can be calculated from the number of spontaneous fission events (see Table 3.2). If the production rate of spontaneous fission neutrons is divided by the average number of neutrons emitted per fission, assuming 2.57, then the actual rate of spontaneous fission events is 755 fissions/sec. This could be considered a lower limit on the initial fission power of the dry HEU powder system.

The spontaneous fission events are not the only fission events occurring at delayed critical. A finite amount of subcritical multiplication of the source

neutrons will also occur in the system. This multiplication, given by equation 3.5, is simple to calculate. However, mathematically it becomes infinite as k_{eff} becomes one.

$$M = \frac{1}{1-k_{eff}} \tag{3.5}$$

Since the subcritical multiplication is impossible to calculate exactly at the moment of delayed criticality, a value for k_{eff} close to one is assumed to calculate an upper limit on the initial fission power for this study. Assuming a k_{eff} of 0.999 which yields a multiplication of 1000, the upper limit on the initial power for this study will be assumed to be 1000 times the total initial neutron source strength divided by 2.57 which is 1.66×10^7 fissions/sec.

A sensitivity study was performed on the 1 meter by 1 meter UO_3 slab, to determine the effects that the lower and upper limits on the initial power have on the calculated results. The results of power and total fissions for both the lower and upper initial power limits are shown in Figure 3.1. Comparing data from both calculations shows only a factor of 2 difference between the power peaks. The total fission yields are even closer in value. These differences are not significant, therefore the transient response is viewed as insensitive to the initial power. For the excursions analyzed in this report, the lower limit of the initial power is used because it yielded the higher power peak and is therefore considered more

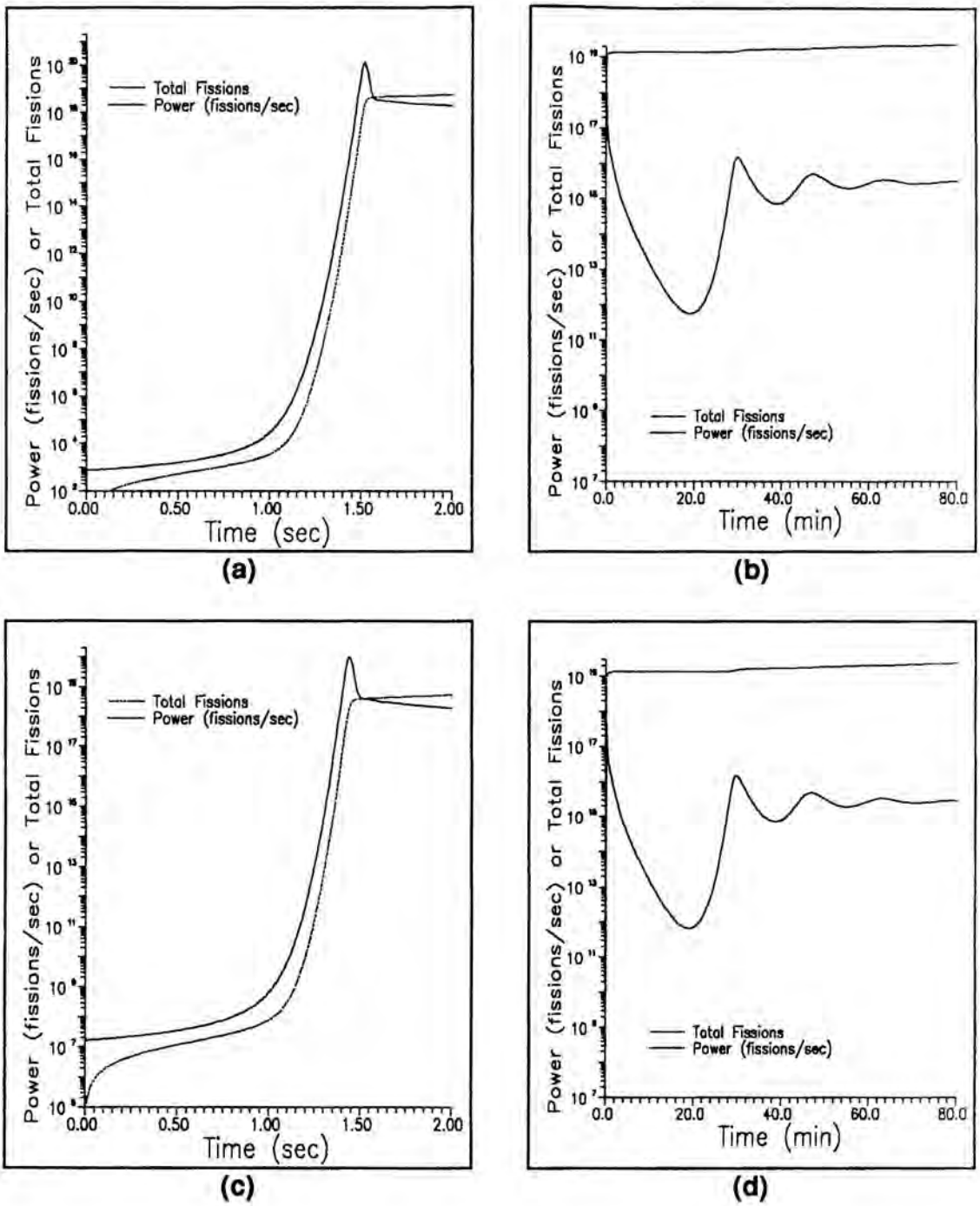

Figure 3.1 : Effect of Initial Power on Power and Total Fissions for a UO_3, 1-m x 1-m Slab, with a \$1.0/sec Reactivity Addition Rate with (a) & (b) a low initial power of 755 fiss/sec, and (c) & (d) a high initial power of 1.66×10^7 fiss/sec.

conservative. The initial power used in the analysis of the finite slabs of dry HEU powder are presented in Table 3.4.

Table 3.4 : Initial Power Values for the Dry HEU Power Systems

Material and Geometry	Initial Power (fissions/sec)
UO_3, 1 x 1 meter	754.9
UO_3, 2 x 2 meter	2167.8
UF_4, 1 x 1 meter	625.3

3.2.2. Starting Transient at Subcritical Level

The transient analyses considered so far have only been concerned with the results of excursions which begin at delayed critical without a source present. However, since the inherent neutron source strength(i.e., a fixed extraneous source) may be calculated at any level of subcriticality, the transient could be started from this subcritical level with the fixed source present. This idea was investigated to see what would result from such a transient calculation.

Because of the presence of a fixed neutron source, a source term must be added to the point kinetics equation

$$\frac{dn(t)}{dt} = \frac{(\rho(t)-\beta)\ n(t)}{\Lambda} + \sum_{i=1}^{6} C_i(t)\lambda_i + S(t) \qquad (3.6)$$

where S(t) is a constant, S_0, and the steady state initial value of n is $n_0=S_0\Lambda/(-\rho)$.

When a source term is present in the point kinetics equation, care must be taken to ensure that the units of the source term and of the dependent variable, n, are consistent. In this problem, the units of the source term are neutrons/sec. Therefore, the time derivative of n is also neutrons/sec and the variable, n, must therefore have units of neutrons. Thus, instead of calculating fission power in fissions/sec as previously described, the point kinetics equations will calculate the neutron population, n, in units of neutrons.

To use the neutron population, n, in the energy balance equation, equation 2.19, the neutron population must be converted to power in fissions/sec. A crude derivation of this conversion using a simple monoenergetic model[8] is presented. The power in fissions/sec is calculated as

$$F.P. = \Sigma_f \phi V, \qquad (3.7)$$

where Σ_f is the macroscopic fission cross section,
ϕ is the volume averaged flux, and
V is the system volume.

The volume average flux is defined as

$$\phi = vn/V, \qquad (3.8)$$

where v is the speed of the neutrons, and
n is the neutron population.

The generation time in a one speed model is defined as

$$\Lambda=1/(v\nu\Sigma_f). \quad (3.9)$$

Rearrange this expression to solve for Σ_f,

$$\Sigma_f=1/(v\nu\Lambda). \quad (3.10)$$

When the above expressions for ϕ and Λ are substituted into equation 3.7, the power becomes

$$F.P. = n/(\nu\Lambda). \quad (3.11)$$

The average number of neutrons per fission, the generation time, and the neutron population are known, hence the fission power is also known. This expression was used to provide the correct power to the energy balance equation.

Results using the method described above were calculated for the one-meter by one-meter UO_3 slab at a subcritical k_{eff} of .96654 or a reactivity of \$ -5.33. The source term present in the point kinetics equation is 3.82×10^4 neutrons/sec as determined by ORIGEN-S. The corresponding fission rate at this subcritical level is 4.23×10^5 fissions/sec. The generation time for this configuration is 2.40×10^{-5} seconds and the average number of neutrons per fission is 2.57. Therefore, the starting neutron population, n_0, used in the subcritical calculation is 26.1 neutrons.

The results of the fission power and total fissions for this calcualtion that starts at subcritical with a fixed source present in the point kinetics model are

shown in Figure 3.2. Figure 3.2 also shows, for comparison, the fission power and total fission results of the delayed critical start calculation with no source term present in the point kinetics model. The initial power for the delayed critical case is found by using the fission power level at delayed critical from the subcritical start results. The time response of reactivity for both cases are shown in Figure 3.3. These two figures show that the subcritical and delayed critical starts do not differ significantly. The plots of fission power and integrated fissions are very similar. The method selected to calculate excursions in this work is the delayed critical start for the following reasons:

(1) Hansen's delay time concept, as currently formulated, assumes that the system is at delayed critical at t=0. In other words, the delay time incorporation is not currently possible in the subcritical start method. In the subcritical start, the transient begins at a negative value of reactivity. The delay time causes a positive reactivity effect at the start of the transient and cannot be implemented, as currently formulated, in the subcritical start method.

(2) The point kinetics equations are not necessarily valid at subcritical start levels because the neutron population may not be sufficiently large to preclude statistical fluctuations.

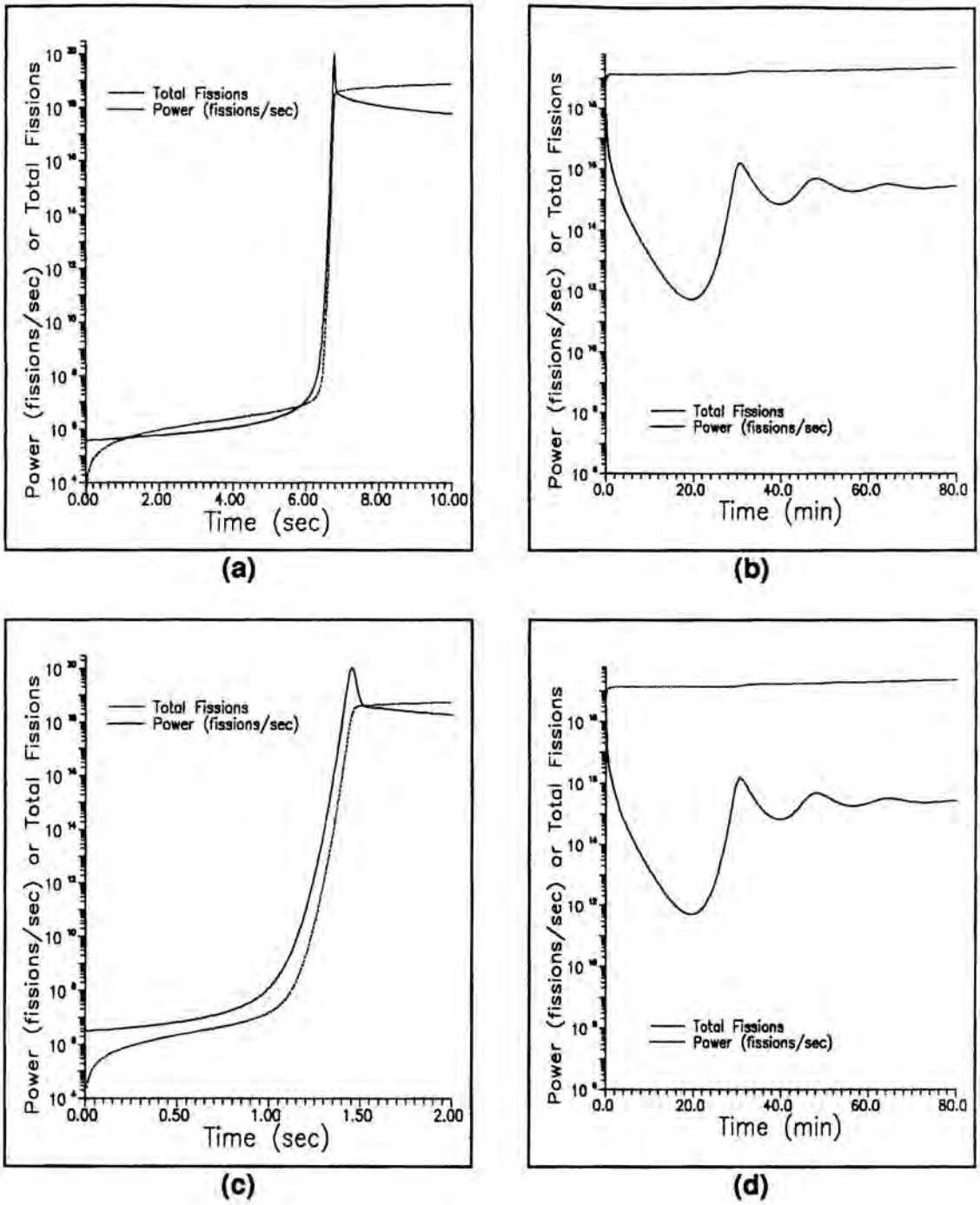

Figure 3.2 : Comparison of Power and Total Fissions for a UO_3, 1-m x 1-m Slab, with a \$1.0/sec Reactivity Addition Rate that Starts (a) & (b) at subcritical with a source present, and (c) & (d) at delayed critical without a source.

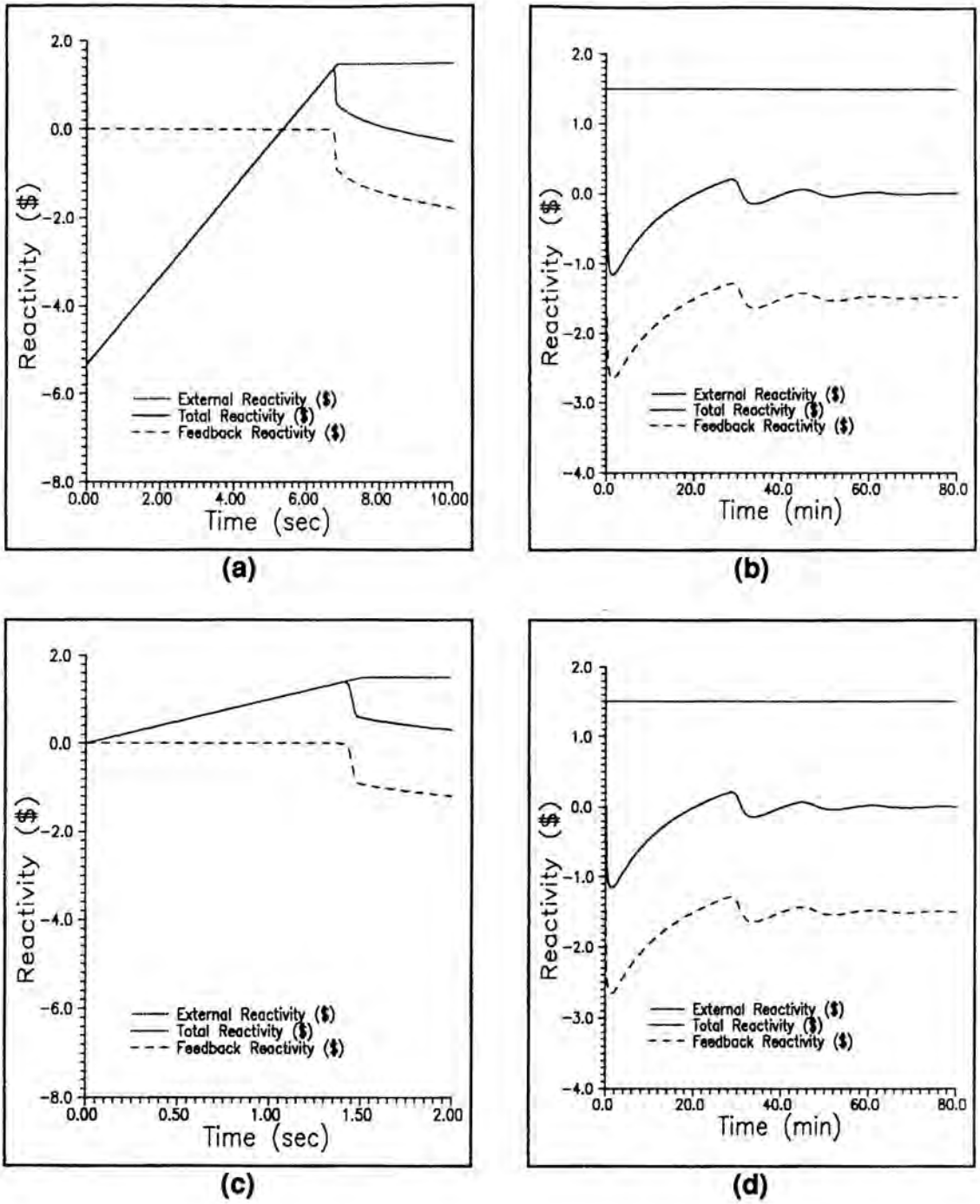

Figure 3.3 : Comparison of Reactivity for a UO_3, 1-m x 1-m Slab, with a \$1.0/sec Reactivity Addition Rate that Starts (a) & (b) at subcritical with a source present, and (c) & (d) at delayed critical without a source.

(3) The conversion between the fission power and the neutron population shown above is very crude. Also, the accuracy of the generation time is not well known since the KENO Va code was used to obtain an approximate value of the generation time.

(4) There is less computer cost when starting the transient from delayed critical. Nothing significant happens to the power until the reactivity becomes positive; however, the computer is spending time calculating the power for negative reactivities.

3.3. Effect of Different Conduction Models

Results of temperature for both the thermal resistance and the analytic conduction models are shown in figure 3.4. Also shown in this figure are the results with no energy loss by conduction.

The thermal resistance and analytic models do not differ significantly as shown in figure 3.4. The results on a short time scale show no difference in the three models. On a long time scale, the analytic model cannot be distinguished from the no conduction model. The analytic model shows the concrete acting as

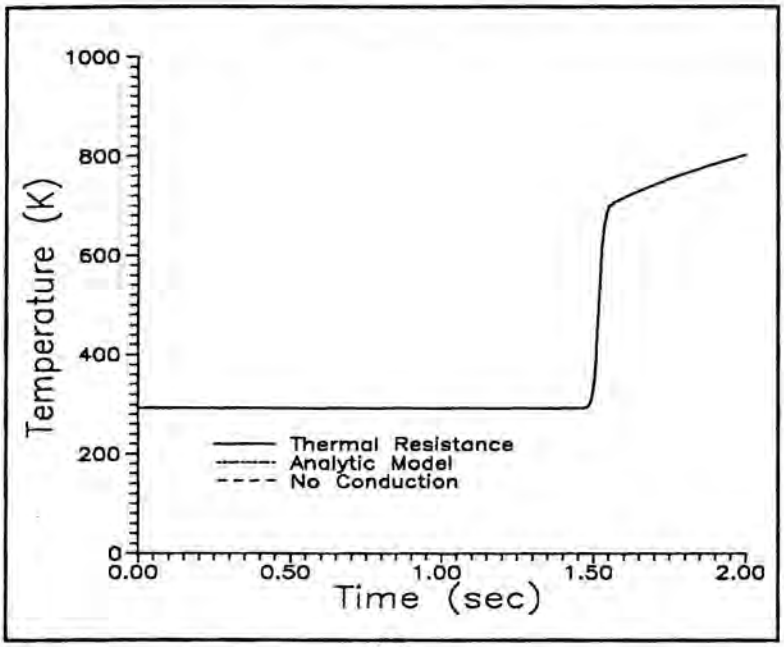

(a)

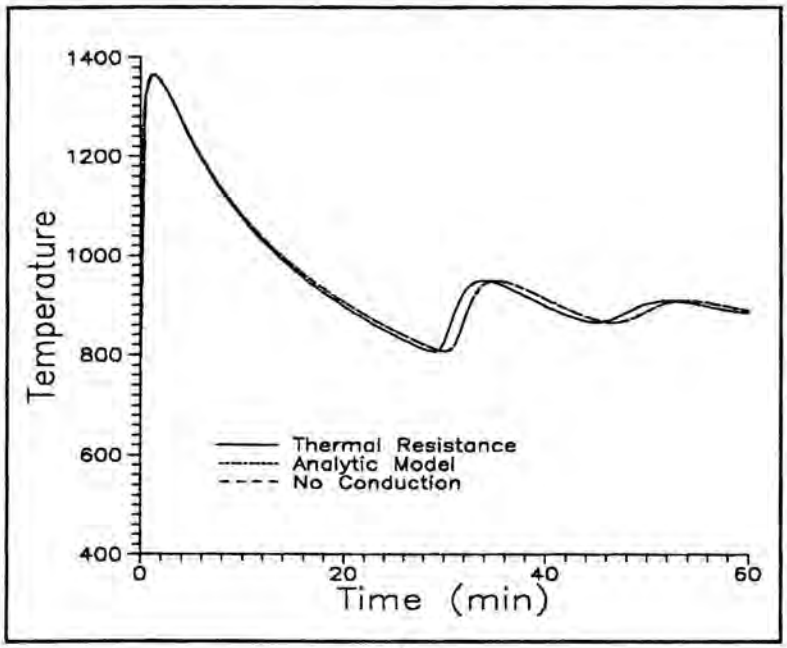

(b)

Figure 3.4 : Effect of Different Conduction Models on Temperature of a UO_3, 1-m x 1-m Slab, with a $.10/sec Reactivity Addition Rate on a (a) short time scale, and (b) long time scale.

an insulator. This is expected because thermal conductivity of concrete is very small.

The analytic model is an exact treatment of the heat conduction from the powder into the concrete. The thermal resistance model although approximate does predict a small amount of energy loss due to conduction. If no conduction is assumed, the results may not be conservative. Conservative results are calculated with the thermal resistance model because it removes more energy from the powder system thereby reducing the thermal reactivity feedback. Using either method will have very little effect on the final results as shown in figure 3.4.

3.4. Effect of Different Reactivity Feedback Models

Results of temperature, reactivity, fission power and total fissions for the different feedback models discussed in section 2.6.2 are shown in Figures 3.5 - 3.8. These figures show that the separated feedback model predicts higher temperatures than the combined feedback model. This effect is caused by the underprediction of the feedback reactivity in the separated case. The feedback reactivity in the separated case is less negative because the coefficient for volume expansion is calculated with the same density at each new volume. Therefore, the real situation, where the density is decreasing while the volume

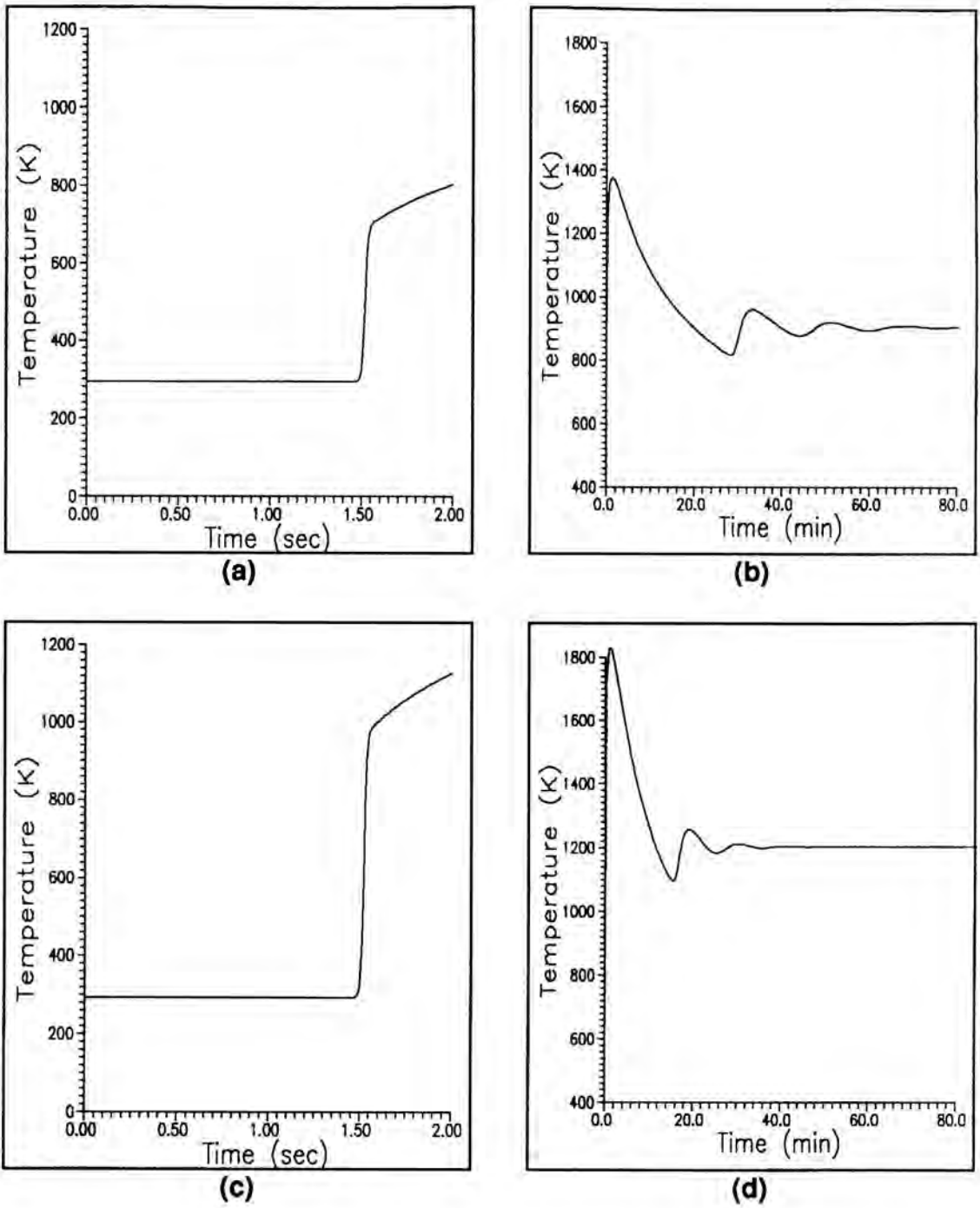

Figure 3.5 : Comparison of Temperature for a UO_3, 1-m x 1-m Slab, with a $1.0/sec Reactivity Addition Rate with (a) & (b) a combined feedback coefficient, and (c) & (d) seperated feedback coefficients.

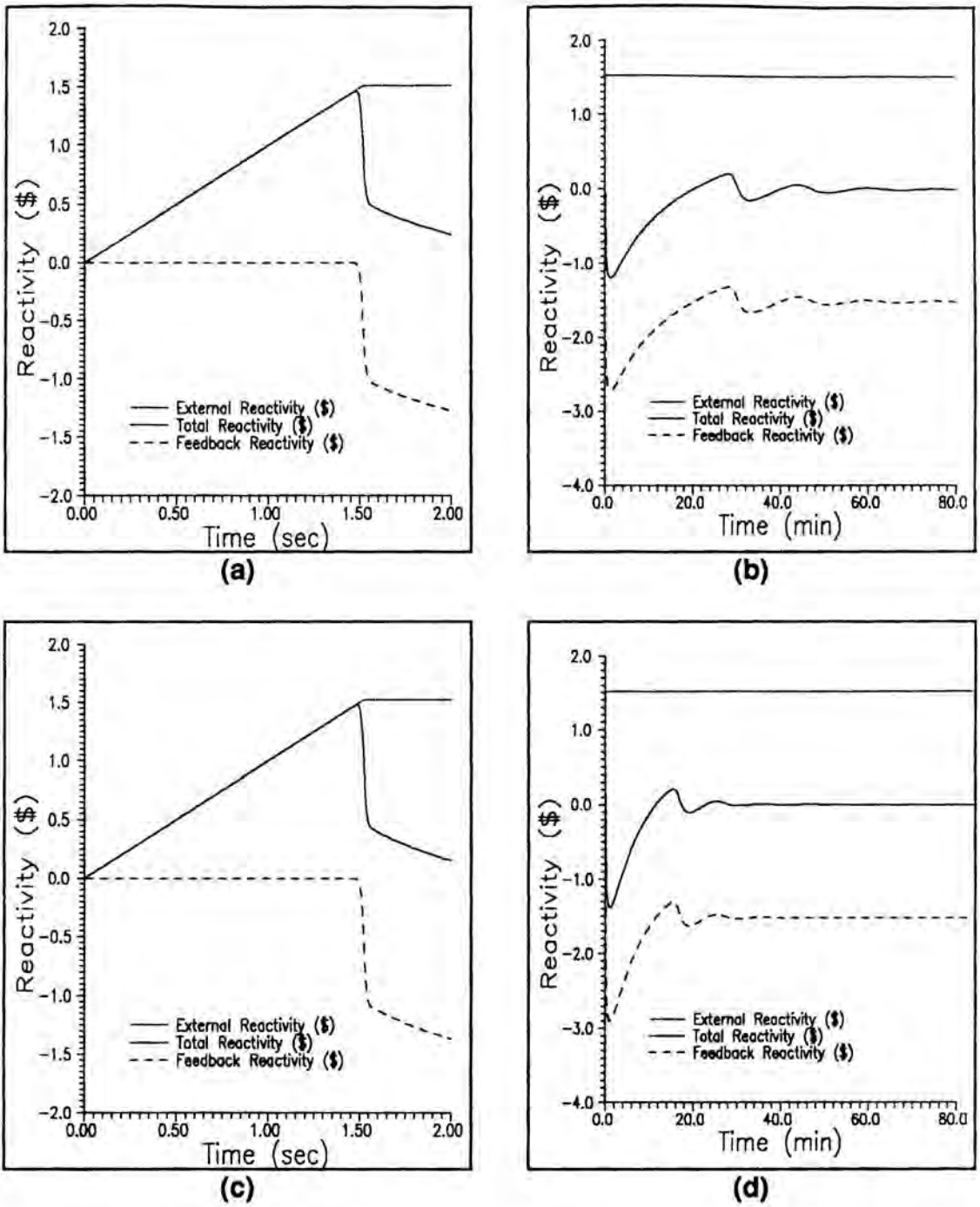

Figure 3.6 : Comparison of Reactivity for a UO_3, 1-m x 1-m Slab, with a \$1.0/sec Reactivity Addition Rate with (a) & (b) a combined feedback coefficient, and (c) & (d) seperated feedback coefficients.

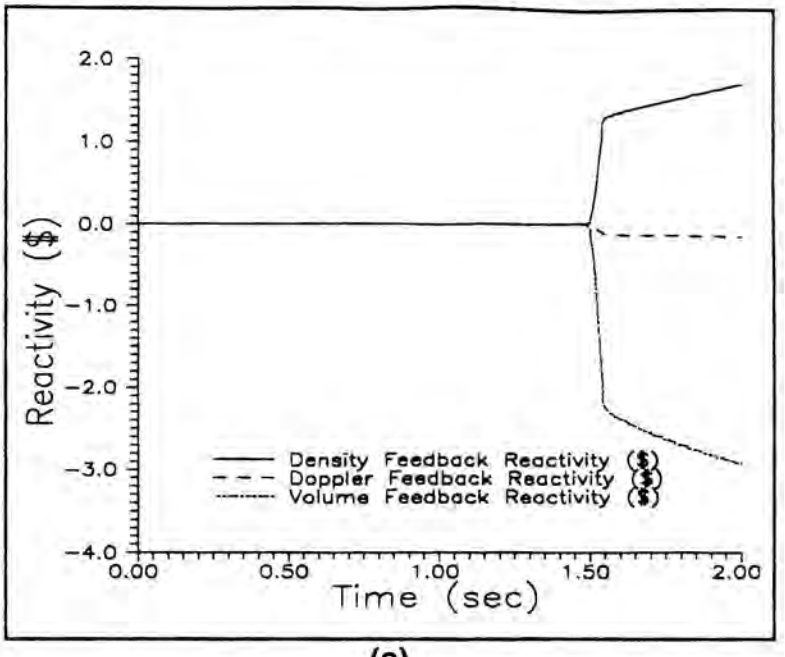

(a)

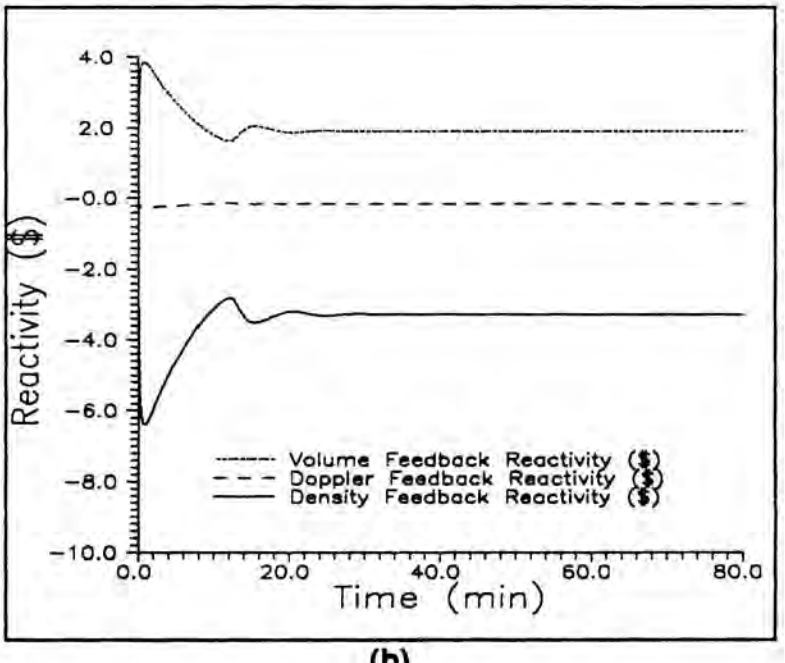

(b)

Figure 3.7 : Seperated Reactivity Feedback Effects of a UO_3, 1-m by 1-m slab, with a \$1.0/sec Reactivity Addition Rate on a (a) short time scale, and (b) long time scale.

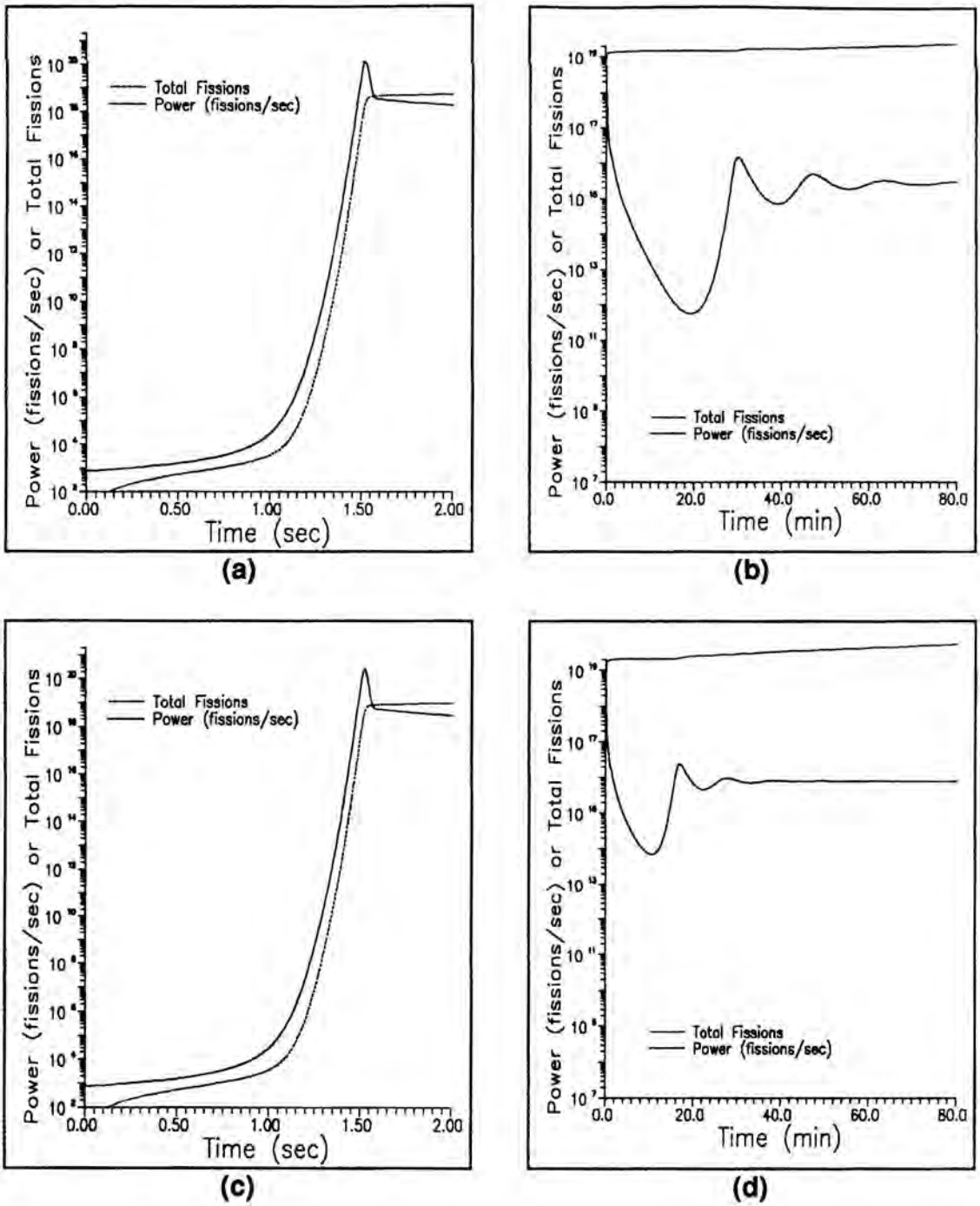

Figure 3.8 : Comparison of Power and Total Fissions for a UO_3, 1-m x 1-m Slab, with a \$1.0/sec Reactivity Addition Rate with (a) & (b) a combined feedback coefficient, and (c) & (d) separated feedback coefficients.

is increasing, is not being considered by the separated model. This effect is considered in the combined effects model. The combined effects model is used in all calculations presented in the other sections of this thesis.

3.5. Effect of a Change in the Reactivity Addition Ramp Rate

Figures 3.9 - 3.11, show temperature, reactivity, power, and total fissions for the UO_3 powder, 1-meter by 1-meter slab for a reactivity addition rate of \$1/sec. These results were generated with the combined feedback coefficient and a low initial starting power. The external reactivity addition was arbitrarily terminated at the power peak. The next three figures, Figures 3.12 - 3.14, show results for a reactivity addition rate of \$.10/sec and Figures 3.15 - 3.17, show the same results for a reactivity addition rate of \$10/sec. All of the results presented show increases in the system temperature with the shapes of the temperature transient varying greatly. In the \$.10/sec case, the temperature rises slowly, but in the \$1.0 and \$10/sec transients the temperature rises sharply - increasing 1000K in .01 sec in the \$10/sec case. Also, the peak temperature is much greater for the larger reactivity addition rates. The peak temperature is about 1.7 times greater in the \$10/sec case than in the \$.10/sec case. The final equilibrium temperature is also higher in each case; however, this is mostly due to the different values of total external reactivity insertion (see section 3.7).

The reactivities of the three cases with changing ramp rates show the same trends as the temperature transients. This is expected since temperature changes cause reactivity feedback. The more the temperature rises, the greater the feedback reactivity. The external reactivity addition rate is terminated at a lower value for a lower reactivity addition rate. This is due to the power peak occurring sooner and the external reactivity addition being terminated at the power peak.

The power response shows the power peaking and oscillations occurring until an equilibrium is reached. The power peaks because of the increase in temperature which results in negative reactivity feedback to the system. The power oscillations occur in the system because of cooling that takes place because of the heat loss mechanisms. The different total external reactivity additions and the different feedback coefficients cause a difference in the number of oscillations and in the amplitude of the oscillations before equilibrium is reached (see section 3.7). Again, the power traces follow the temperature and reactivity trends.

Total fission values for the various cases differ only slightly. Since power is being integrated over time, a large power released during a small time interval will deposit essentially the same amount of energy as a small power in a large time interval.

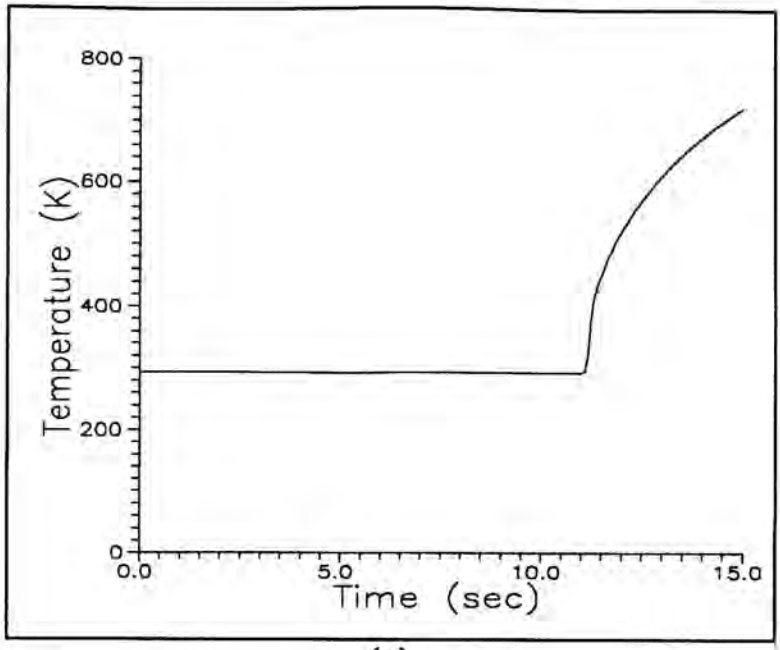

(a)

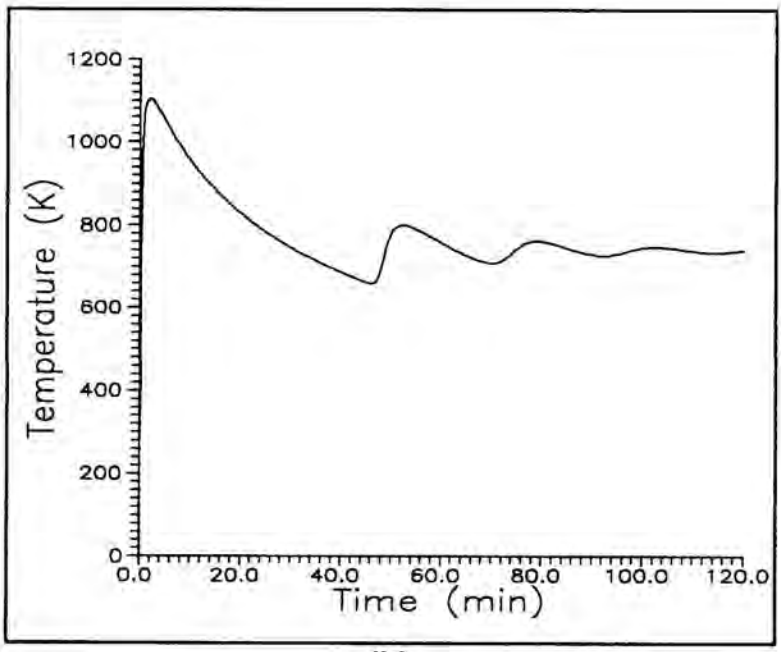

(b)

Figure 3.9 : Temperature of a UO_3, 1-m x 1-m Slab, with a $.10/sec Reactivity Addition Rate on a (a) short time scale, and (b) long time scale.

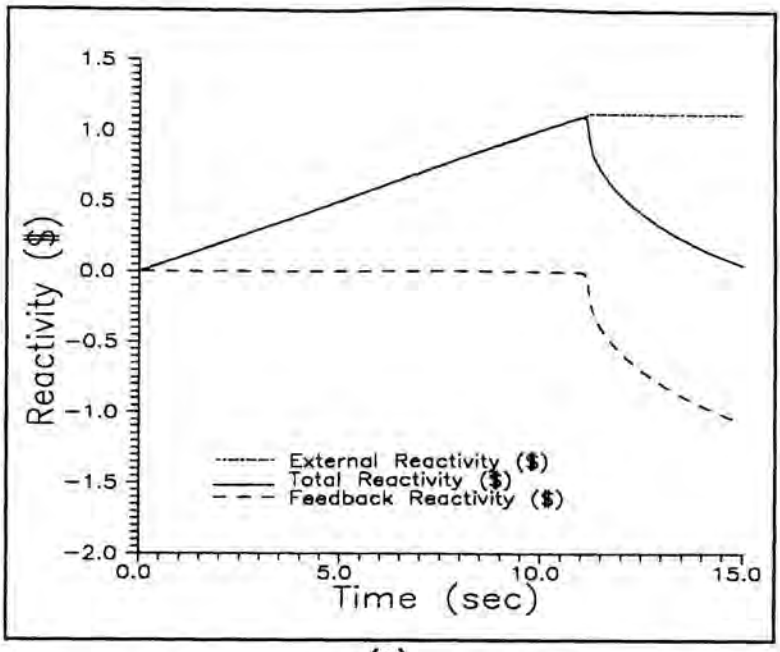

(a)

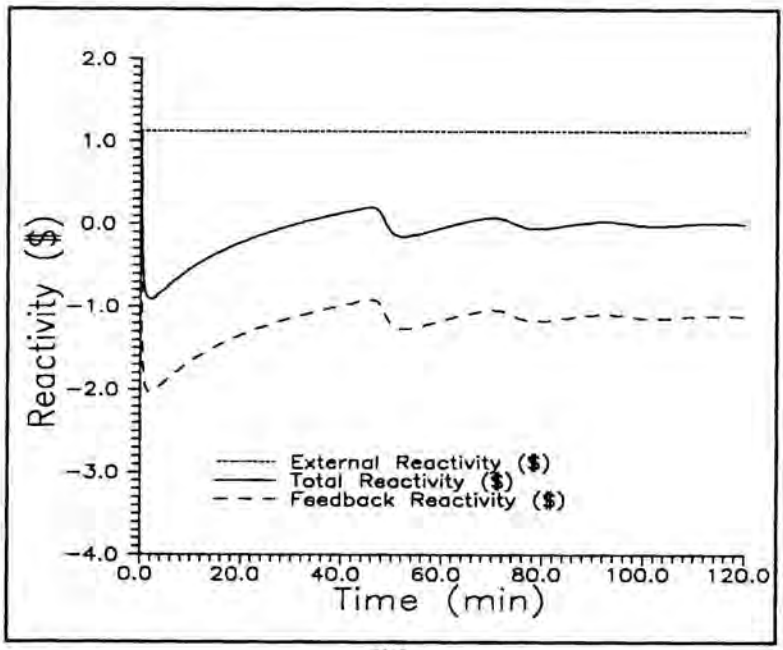

(b)

Figure 3.10 : Reactivity of a UO_3, 1-m x 1-m Slab, with a $.10/sec Reactivity Addition Rate on a (a) short time scale, and (b) long time scale.

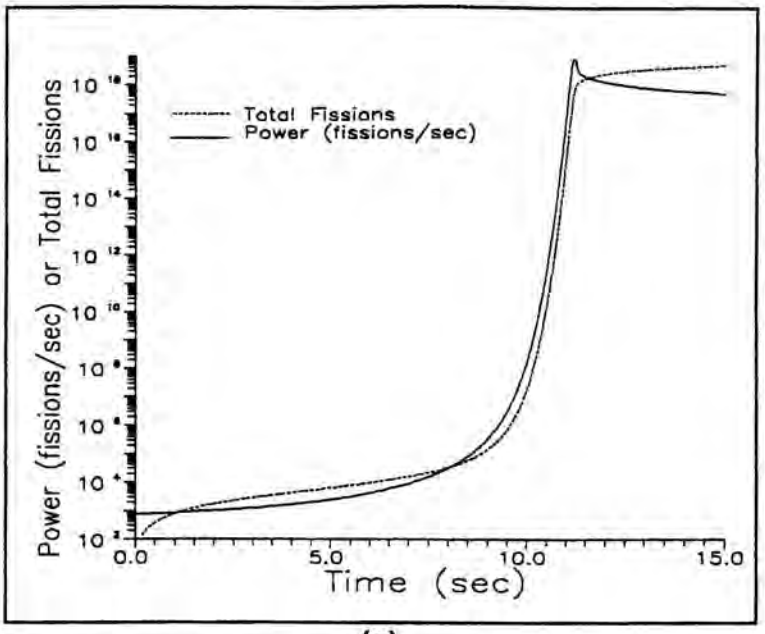

(a)

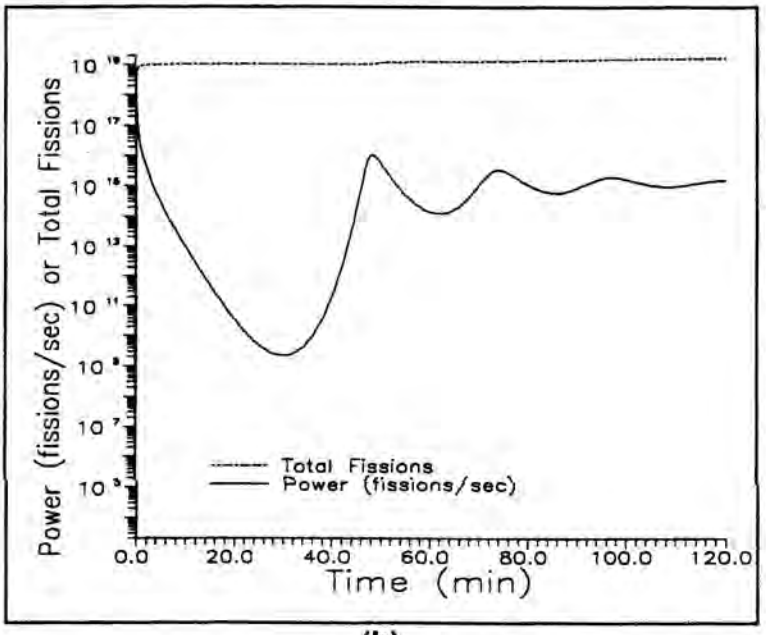

(b)

Figure 3.11 : Power and Total Fissions of a UO_3, 1-m x 1-m Slab, with a $.10/sec Reactivity Addition Rate on a (a) short time scale, and (b) long time scale.

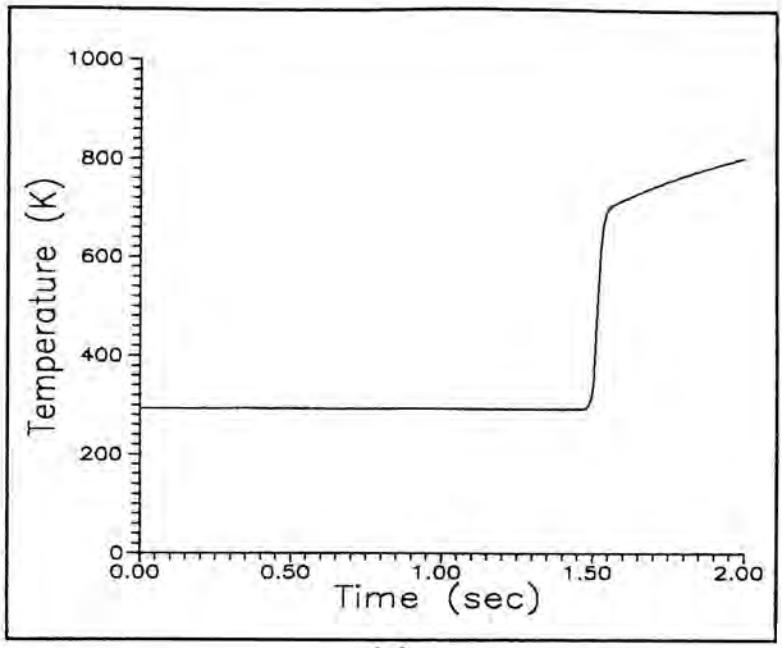

(a)

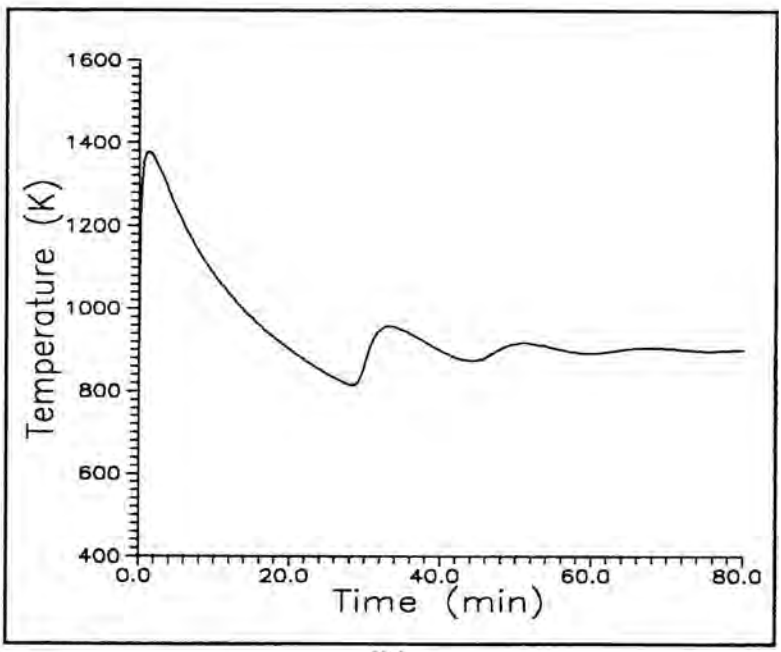

(b)

Figure 3.12 : Temperature of a UO_3, 1-m x 1-m Slab, with a \$1.0/sec Reactivity Addition Rate on a (a) short time scale, and (b) long time scale.

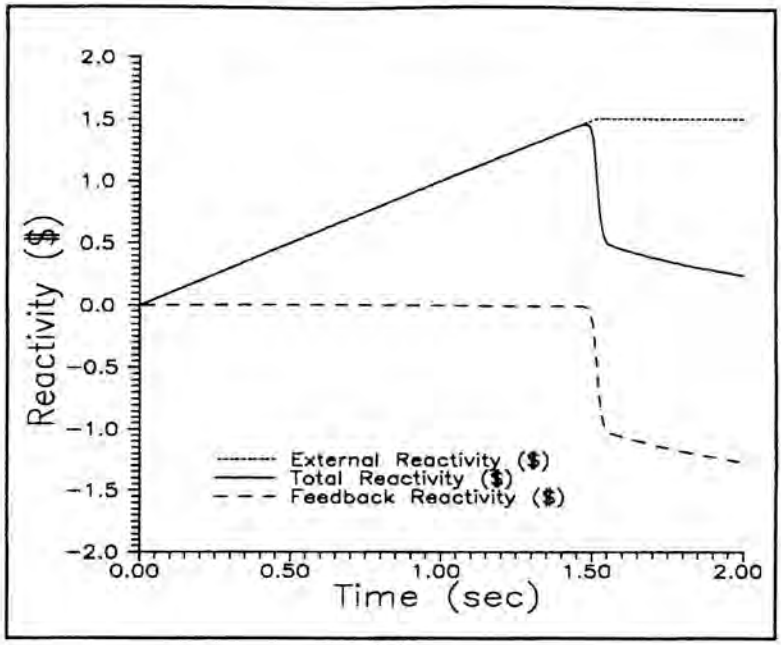

(a)

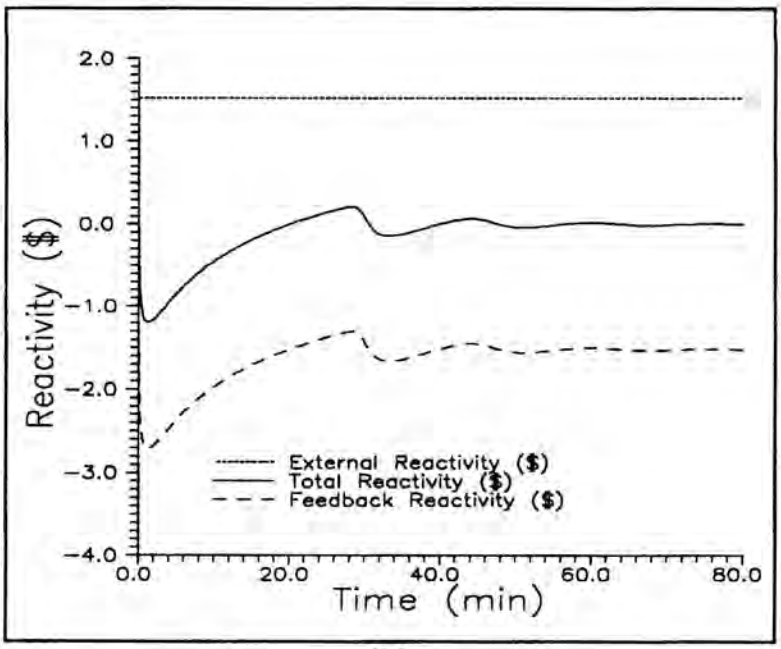

(b)

Figure 3.13 : Reactivity of a UO_3, 1-m x 1-m Slab, with a \$1.0/sec Reactivity Addition Rate on a (a) short time scale, and (b) long time scale.

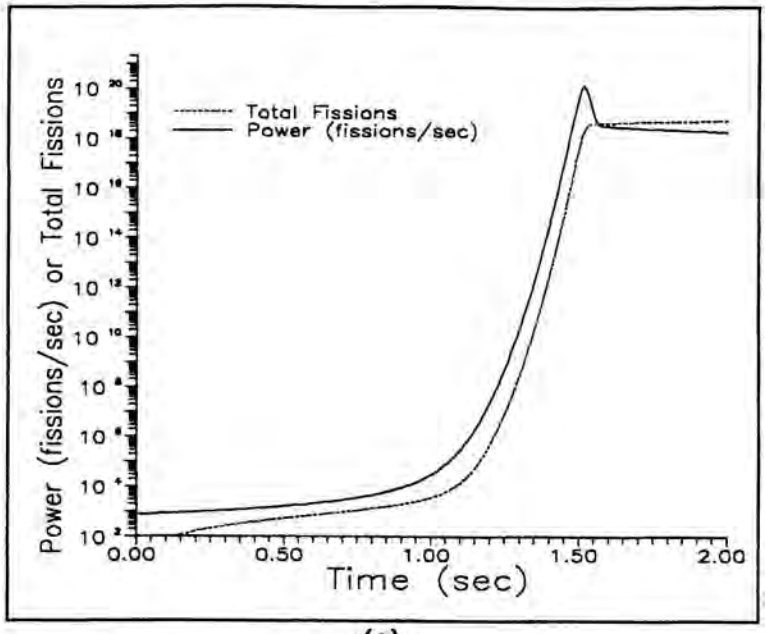

(a)

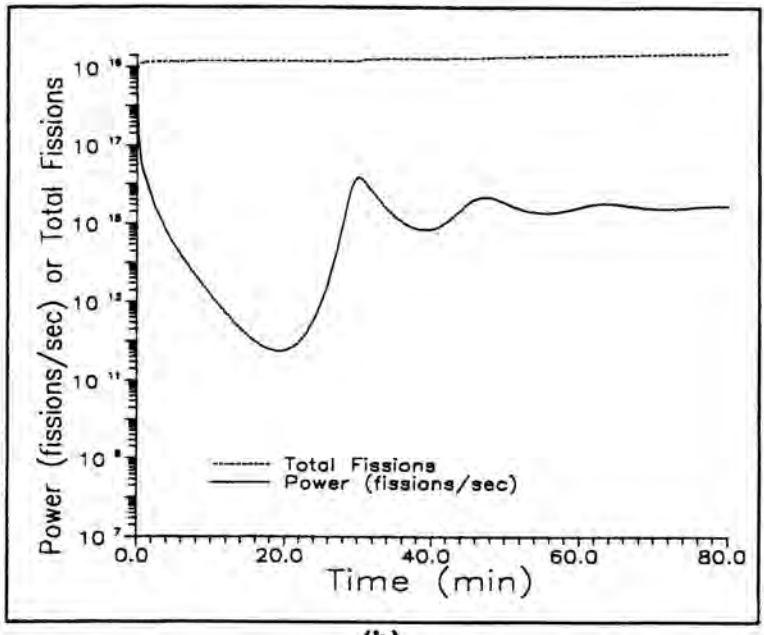

(b)

Figure 3.14 : Power and Total Fissions of a UO_3, 1-m x 1-m Slab, with a \$1.0/sec Reactivity Addition Rate on a (a) short time scale, and (b) long time scale.

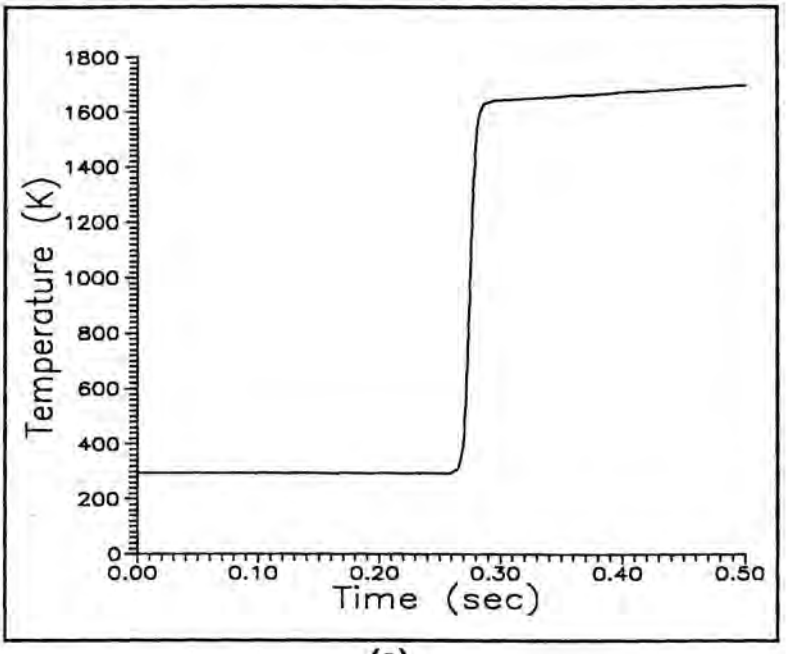

(a)

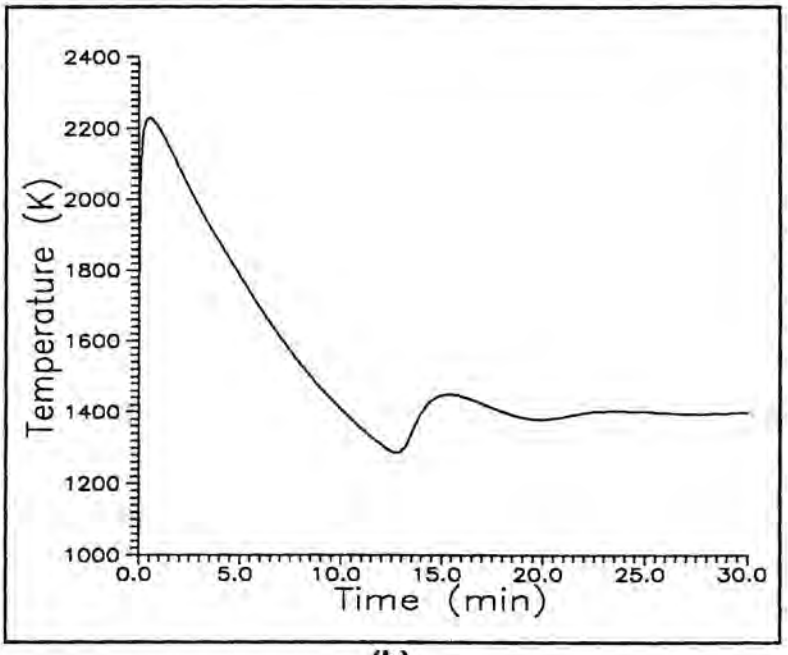

(b)

Figure 3.15 : Temperature of a UO_3, 1-m x 1-m Slab, with a \$10/sec Reactivity Addition Rate on a (a) short time scale, and (b) long time scale.

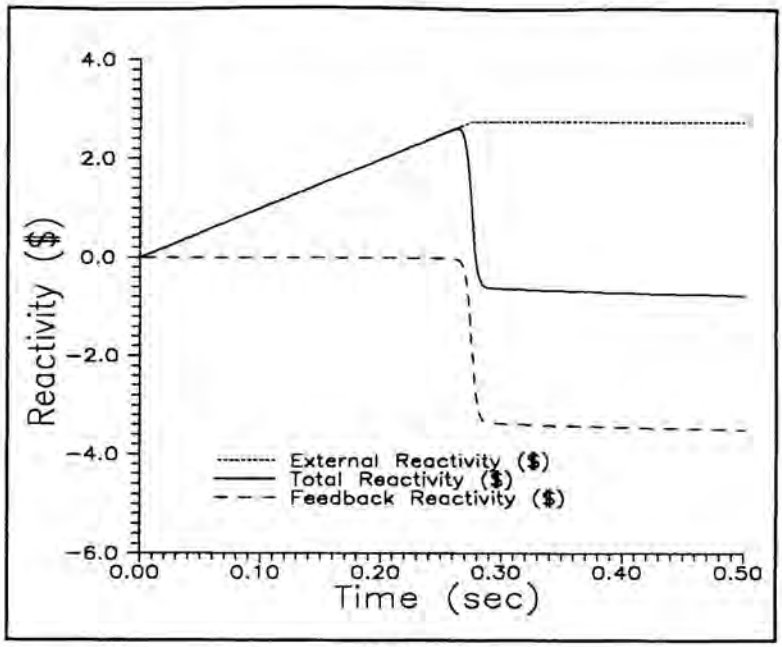

(a)

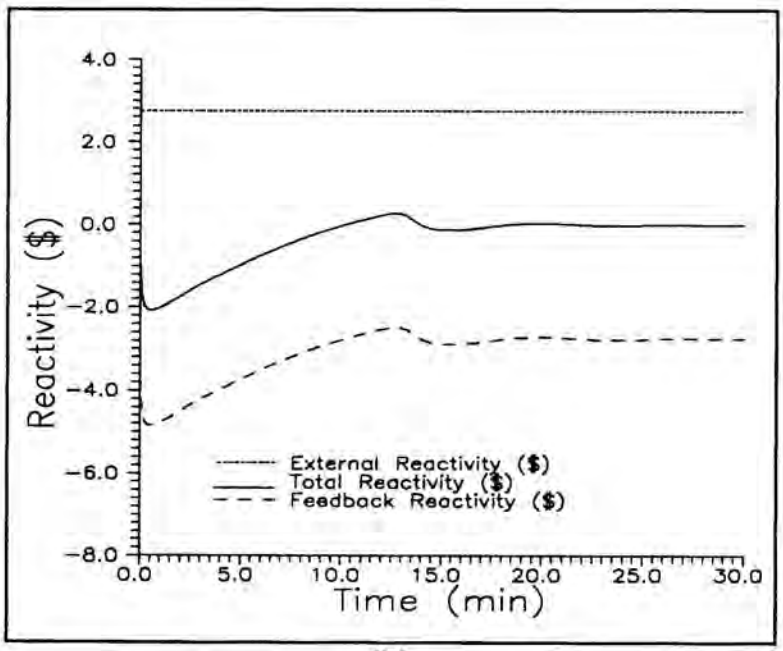

(b)

Figure 3.16 : Reactivity of a UO_3, 1-m x 1-m Slab, with a \$10/sec Reactivity Addition Rate on a (a) short time scale, and (b) long time scale.

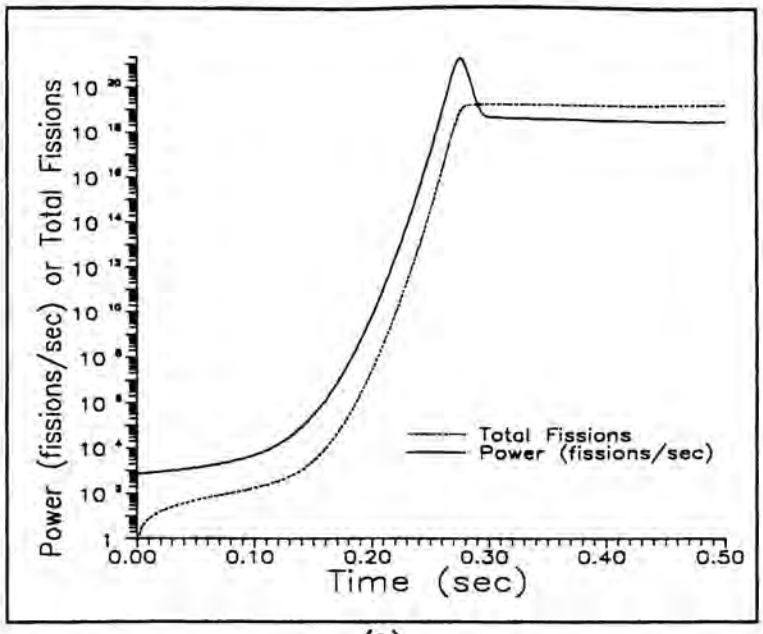

(a)

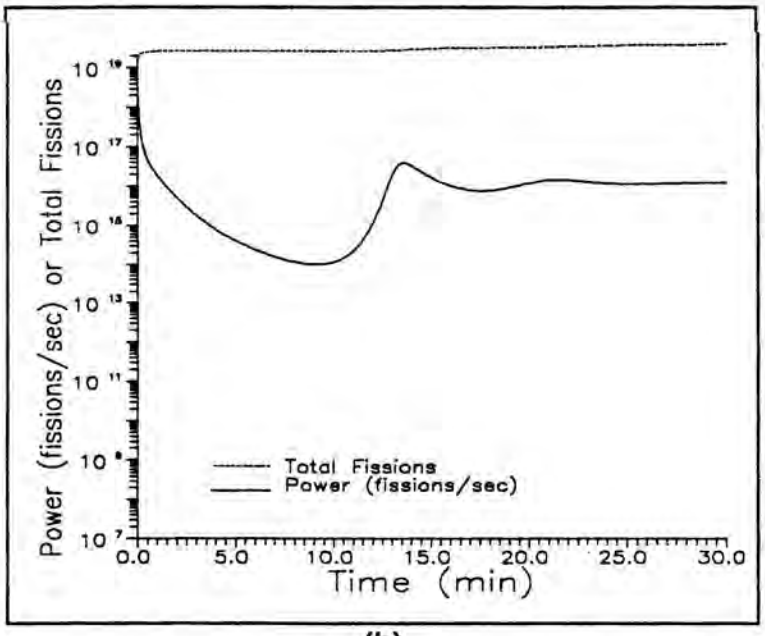

(b)

Figure 3.17 : Power and Total Fissions of a UO_3, 1-m x 1-m Slab, with a \$10/sec Reactivity Addition Rate on a (a) short time scale, and (b) long time scale.

3.6. Effect of a Change in Slab Dimension

The results of temperature, reactivity, power, and total fissions, for the UO_3, two-meter by two-meter powder slab with a \$1/sec reactivity addition rate are shown in Figures 3.18 - 3.20. Also shown in these figures, for comparison purposes, are the results for the UO_3, one-meter by one-meter, powder slab with a \$1/sec reactivity addition rate.

The temperature responses have the only significant differences due to changes in powder slab geometries. This is expected since the two-meter by two- meter slab system contains more mass and can therefore store more energy. Thus the peak temperature in the two-meter by two-meter slab is higher than occurs in the one-meter by one-meter slab.

The total fission results are slightly higher in the two meter by two meter case because the power peaks at a later time than the one meter by one meter case. This is also due to the temperature peaking at a later time thereby allowing more total fissions to occur.

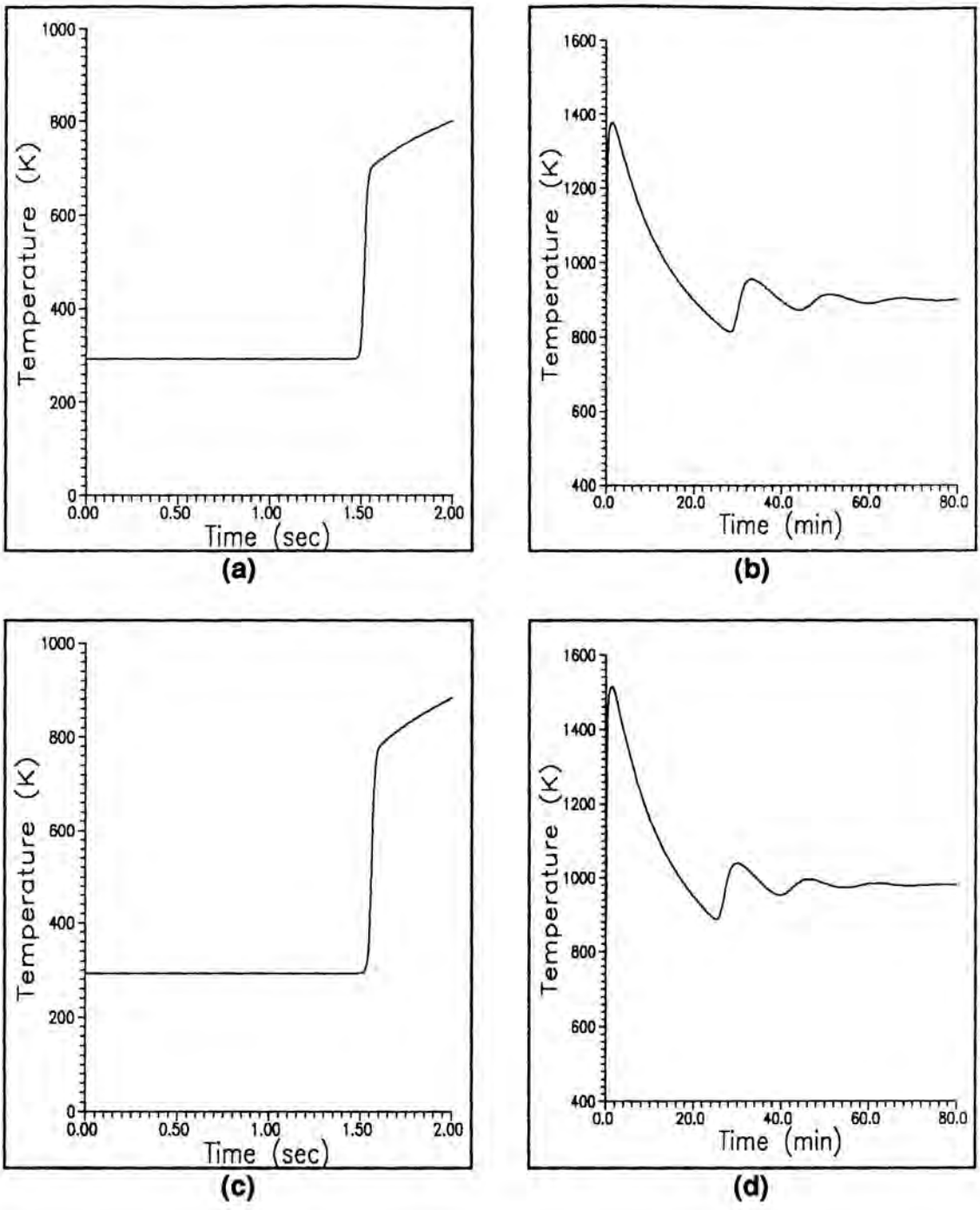

Figure 3.18 : Comparison of Temperature for a UO_3 Powder Slab, with a $1.0/sec Reactivity Addition Rate in a (a) & (b) 1-m x 1-m slab geometry, and (c) & (d) 2-m x 2-m slab geometry.

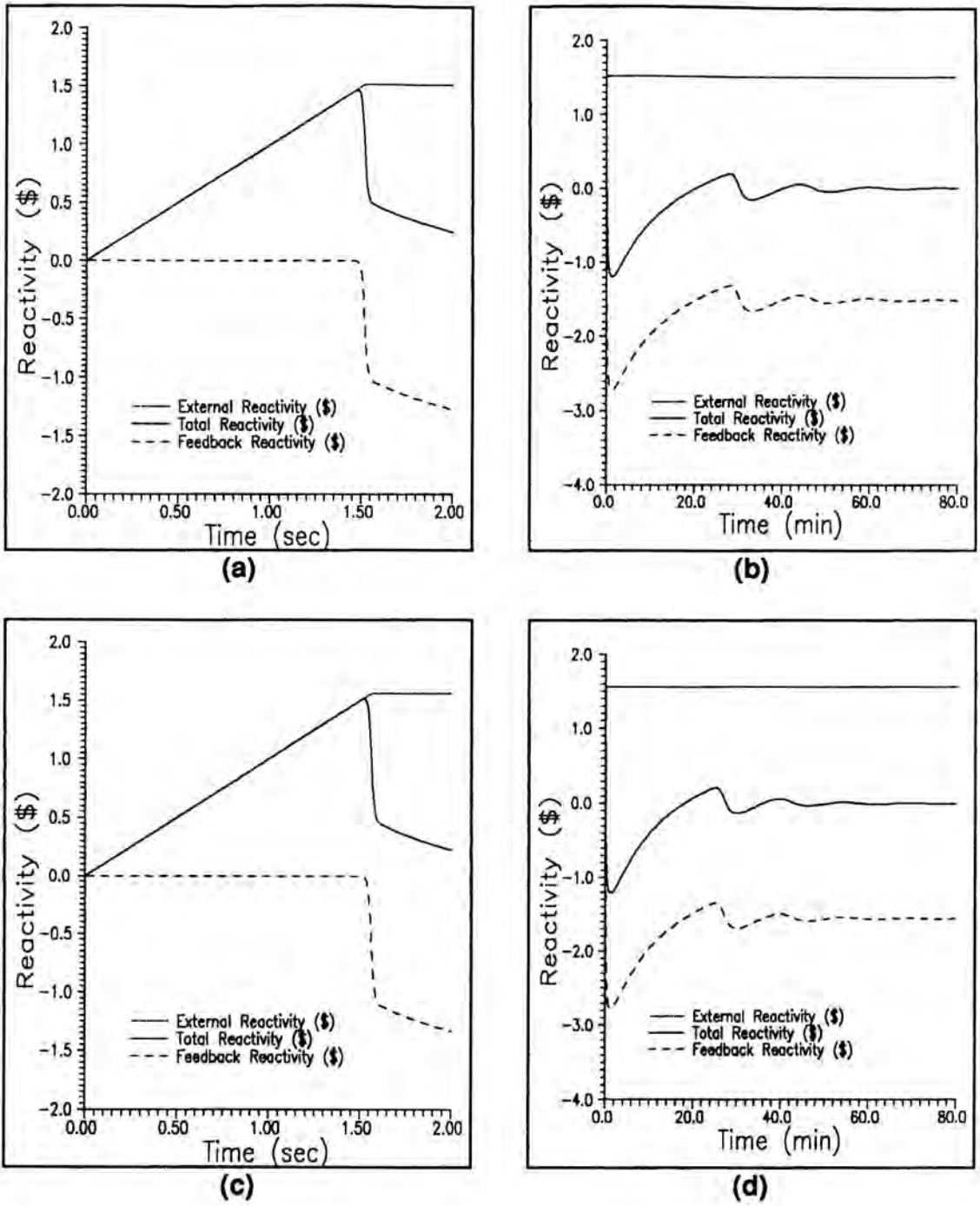

Figure 3.19 : Comparison of Reactivity for a UO_3 Powder Slab, with a \$1.0/sec Reactivity Addition Rate in a (a) & (b) 1-m x 1-m slab geometry, and (c) & (d) 2m x 2m slab geometry.

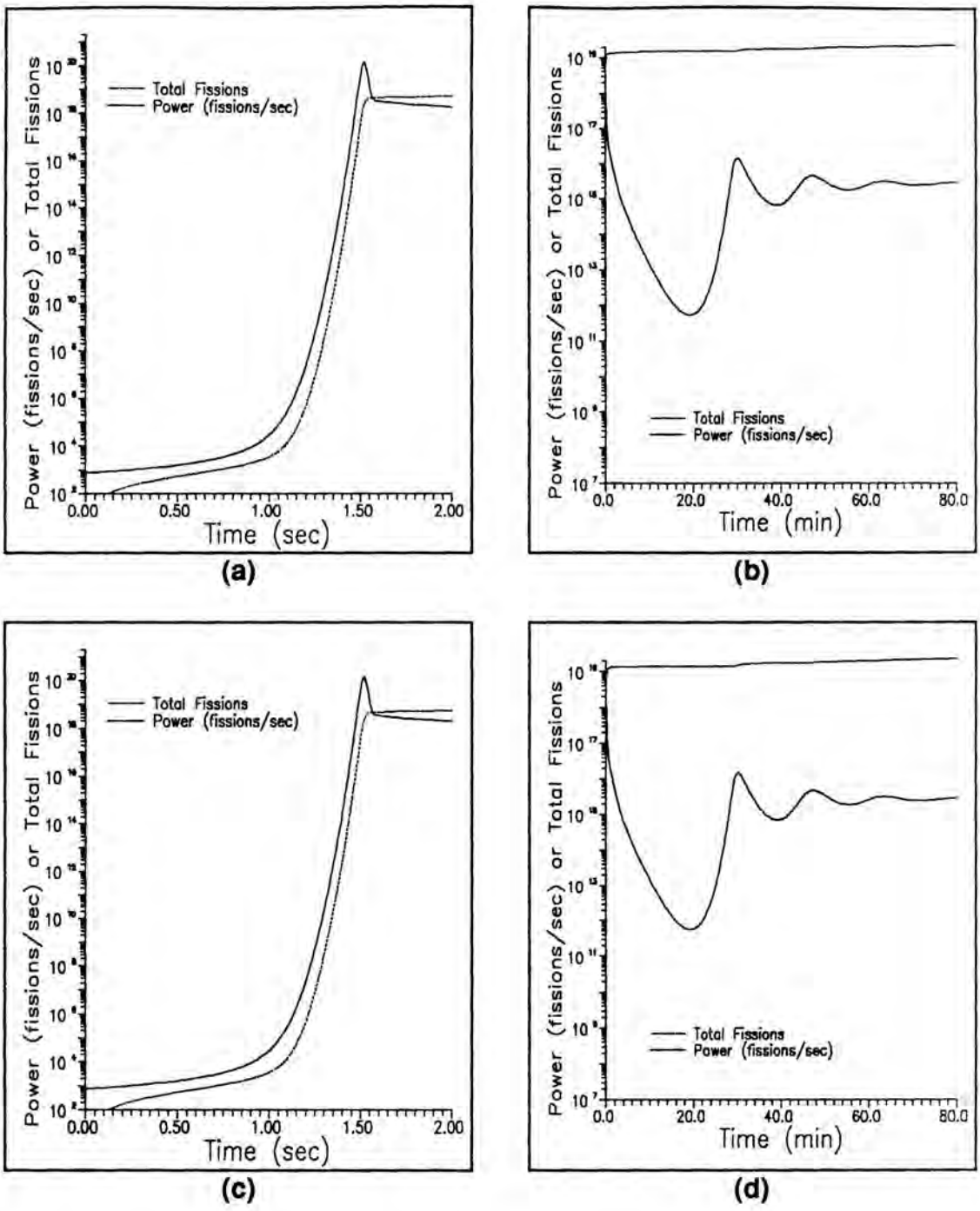

Figure 3.20 : Comparison of Power and Total Fissions for a UO_3, Powder Slab, with a \$1.0/sec Reactivity Addition Rate in a (a) & (b) 1-m x 1-m slab geometry , and (c) & (d) 2-m x 2-m geometry.

3.7. Effect of a Change in Powder Type

The results of temperature, reactivity, power, and total fissions for a one-meter by one-meter UF_4 powder slab with a \$1/sec reactivity addition rate are shown in figures 3.21 - 3.23. Also shown in these figures, for comparison purposes, are the results for the UO_3, one meter by one meter, powder slab with a \$1/sec reactivity addition rate.

The response curves show very little difference between the UO_3 and UF_4 cases. The temperature peaks higher in the UF_4 case because it takes slightly longer for the power to peak. This is due to a slightly lower initial power and slightly larger feedback coefficient in the UF_4 case. The difference in oscillations between the two cases is due to a larger feedback coefficient in the UF_4 case (see section 3.9).

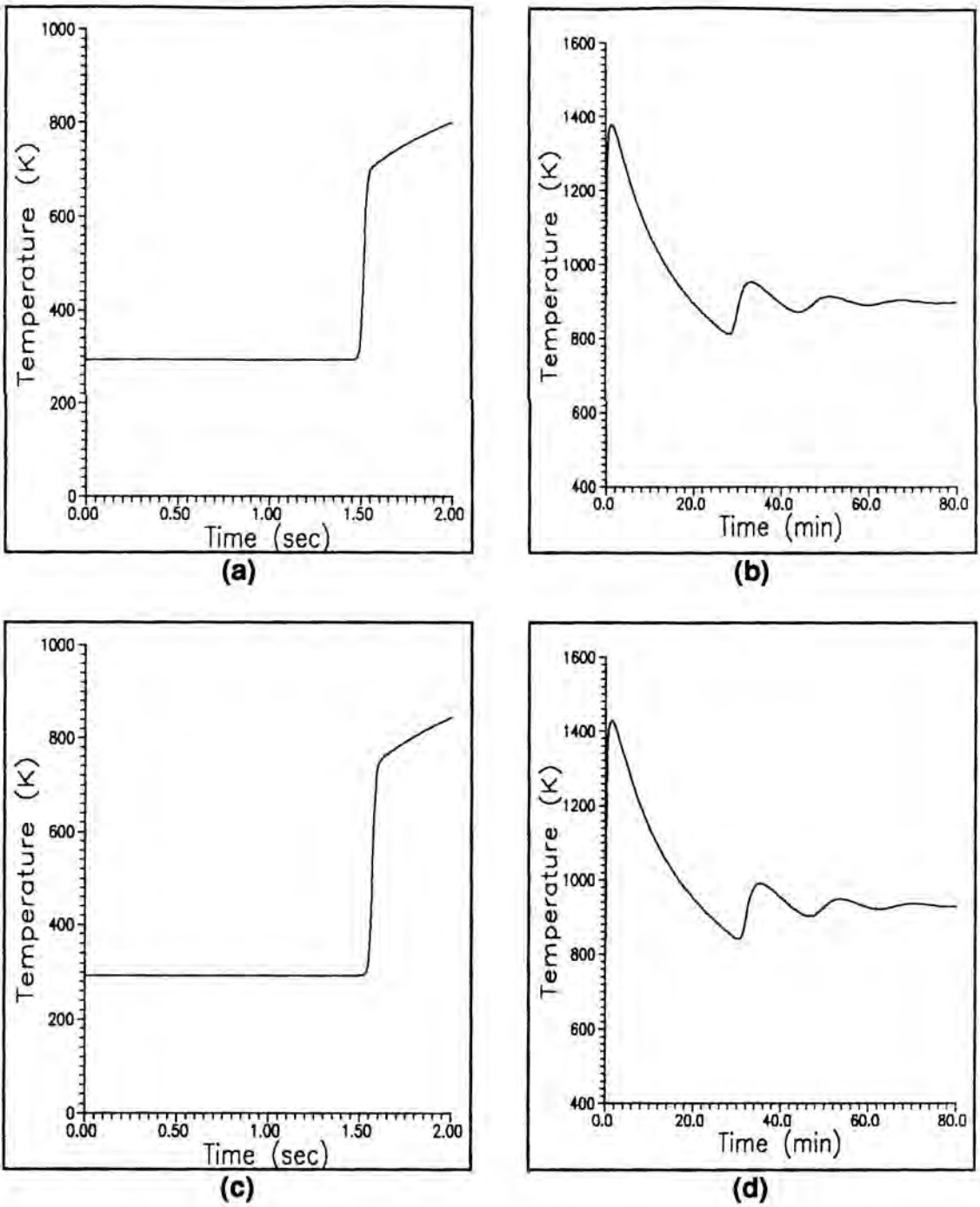

Figure 3.21 : Comparison of Temperature for a 1-m x 1-m Slab, with a $1.0/sec Reactivity Addition Rate, Containing (a) & (b) UO_3 powder, and (c) & (d) UF_4 powder.

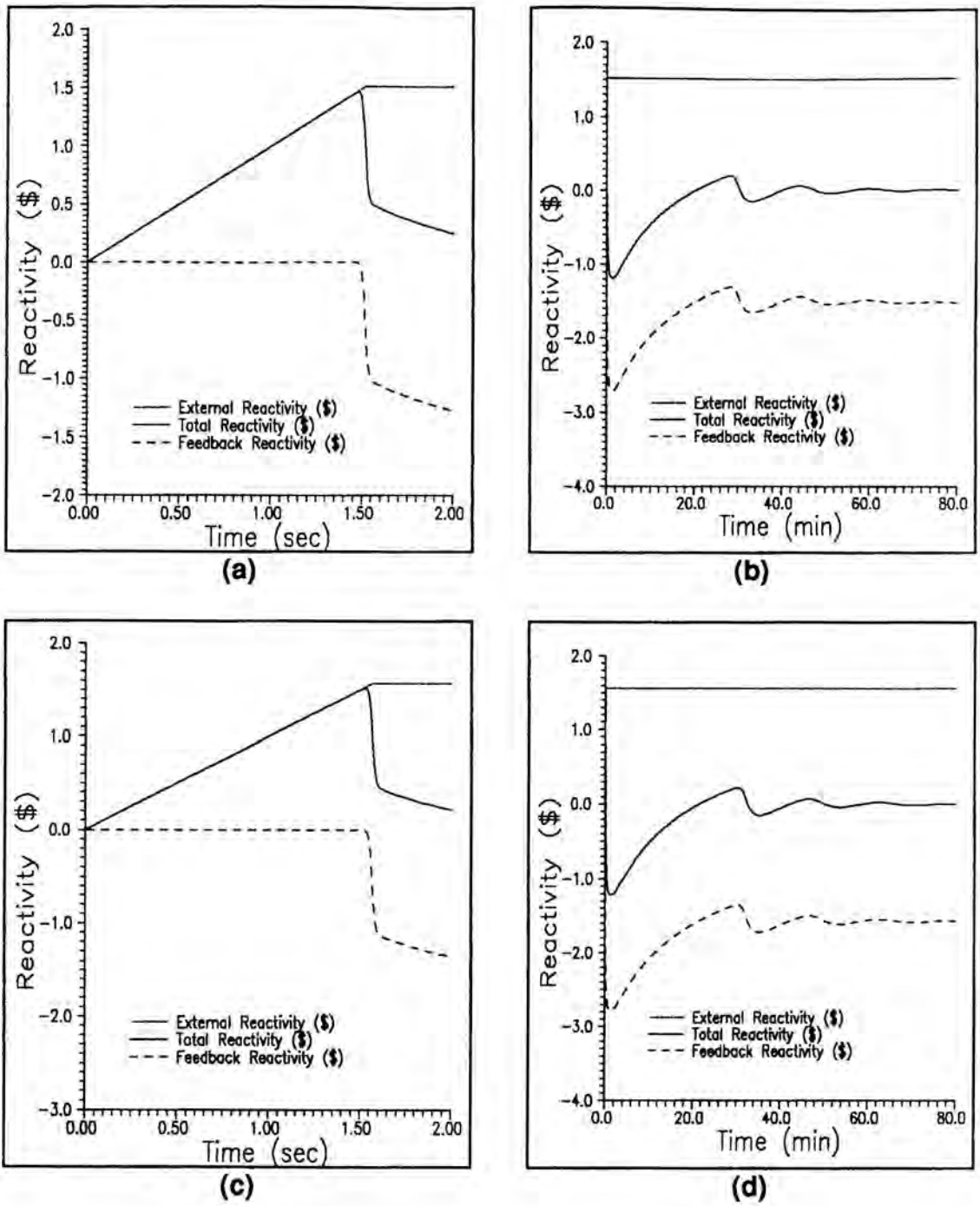

Figure 3.22 : Comparison of Reactivity for a 1-m x 1-m Slab, with a $1.0/sec Reactivity Addition Rate, Containing (a) & (b) UO_3 powder, and (c) & (d) UF_4 powder.

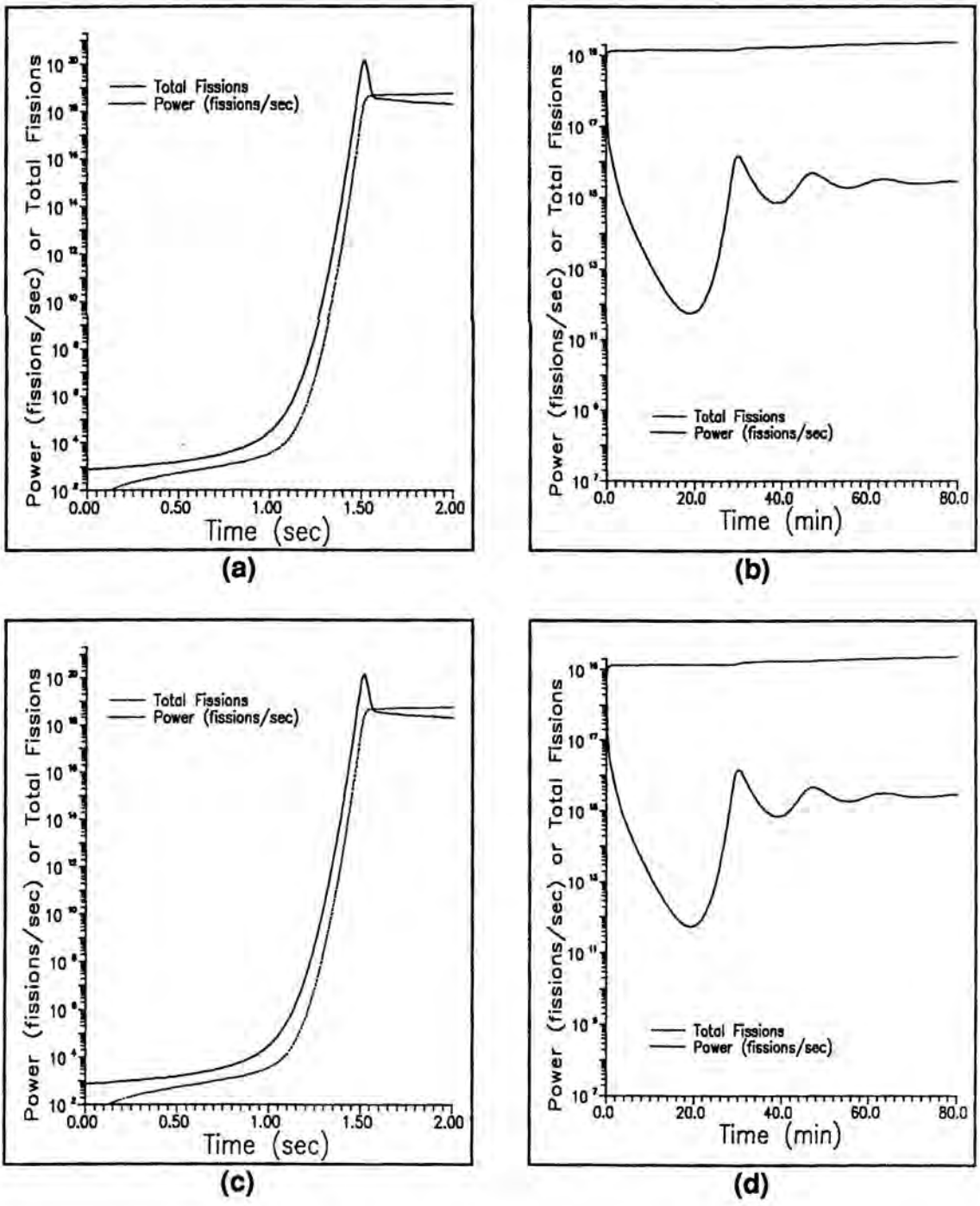

Figure 3.23 : Comparison of Power and Total Fissions for a 1-m x 1-m Slab with a \$1.0/sec Reactivity Addition Rate Containing (a) & (b) UO_3 powder, and (c) & (d) UF_4 powder.

3.8. Effect of a Constant Total External Reactivity Addition

The results of reactivity, power, and total fissions, for the UO_3, one-meter by one-meter, powder slab with a \$.1/sec, \$1.0/sec, and \$10/sec reactivity addition rates halted at a total external reactivity of \$2.5 are shown in Figures 3.24 - 3.29. These results are in contrast to previous results shown earlier in which the external reactivity addition was halted at the peak power.

The results of this analysis show that the power oscillations become very similar for a constant total external reactivity addition. The peak powers are still progressively higher with a higher reactivity addition rate. However, the total fissions as shown on the long time scale are very similar. This is because the power stays at a higher level after the power peak in each case due to the larger total external reactivity addition than for the cases where the total external reactivity ramp was halted at the power peak. The power does not decrease as fast for the higher total external reactivity addition and therefore, over a longer period of time, the total fissions for all cases approach the same value. The same power level is attained at equilibrium for all cases since the feedback coefficient in not changed.

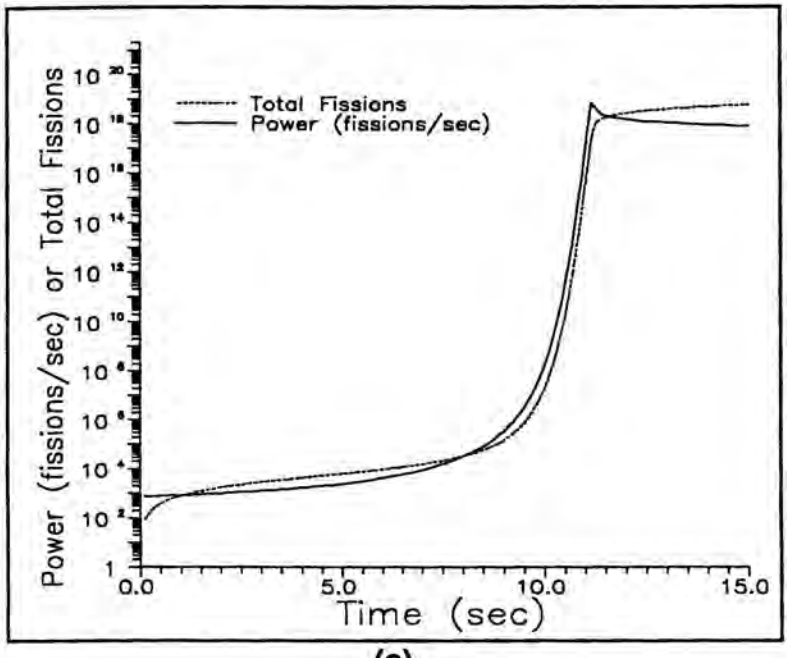

(a)

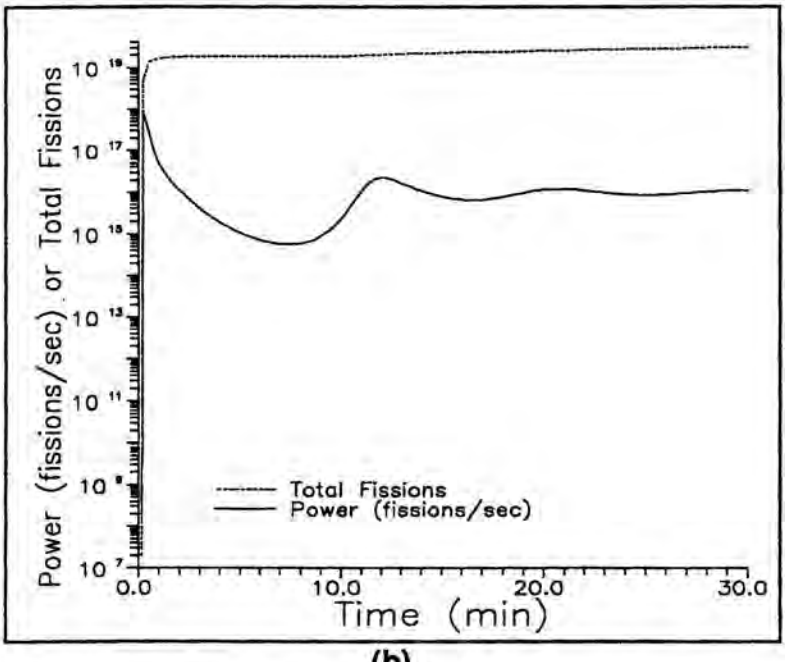

(b)

Figure 3.24 : Power and Total Fissions of a UO_3, 1-m x 1-m Slab, with a \$.10/sec Reactivity Addition Rate Stopped at \$2.5 of External Reactivity on a (a) short time scale, and (b) long time scale.

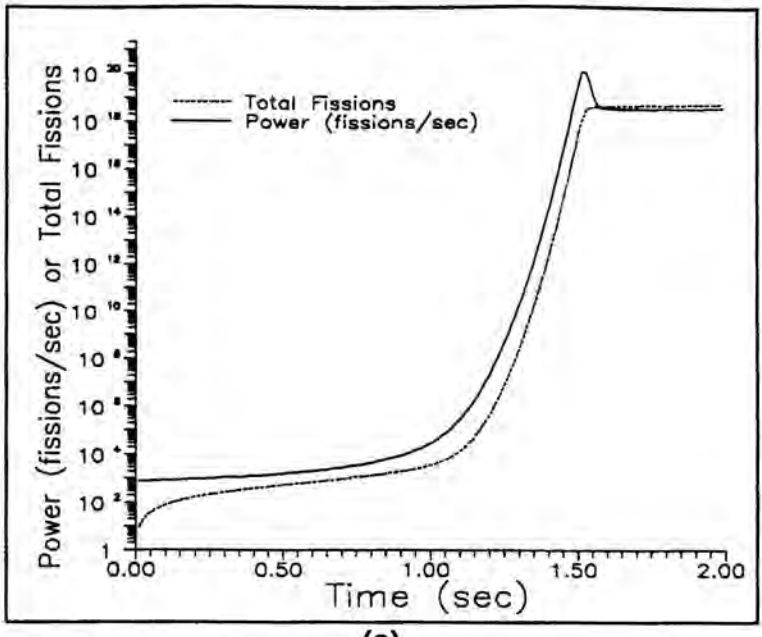

(a)

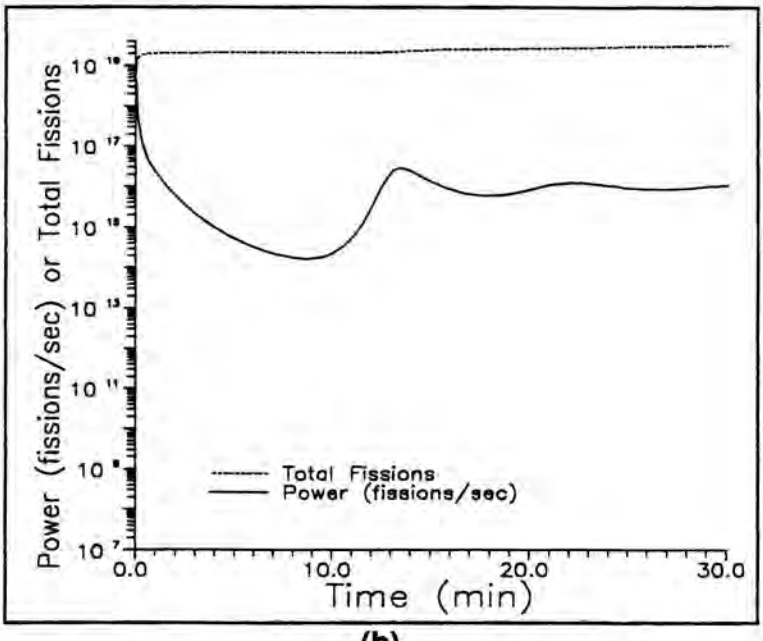

(b)

Figure 3.25 : Power and Total Fissions of a UO_3, 1-m x 1-m Slab, with a \$1.0/sec Reactivity Addition Rate Stopped at \$2.5 of External Reactivity on a (a) short time scale, and (b) long time scale.

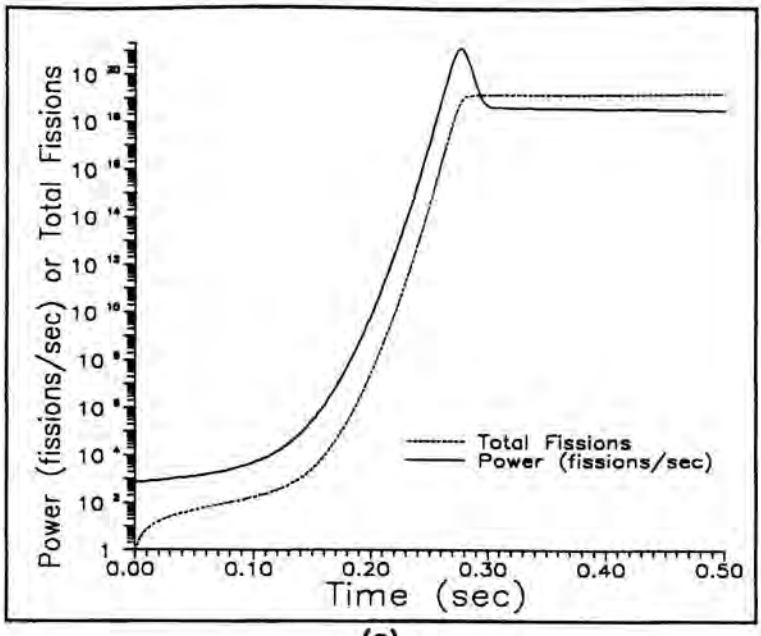

(a)

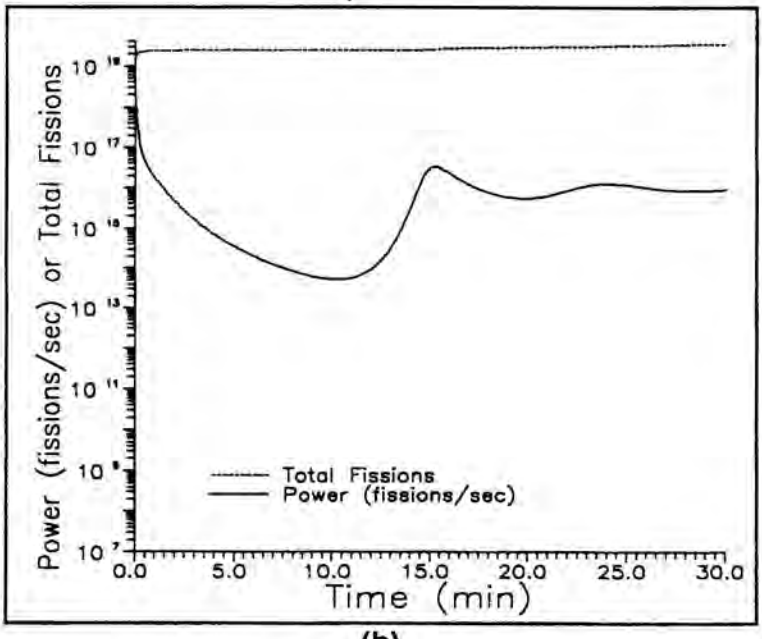

(b)

Figure 3.26 : Power and Total Fissions of a UO_3, 1-m x 1-m Slab, with a \$10/sec Reactivity Addition Rate Stopped at \$2.5 of External Reactivity on a (a) short time scale, and (b) long time scale.

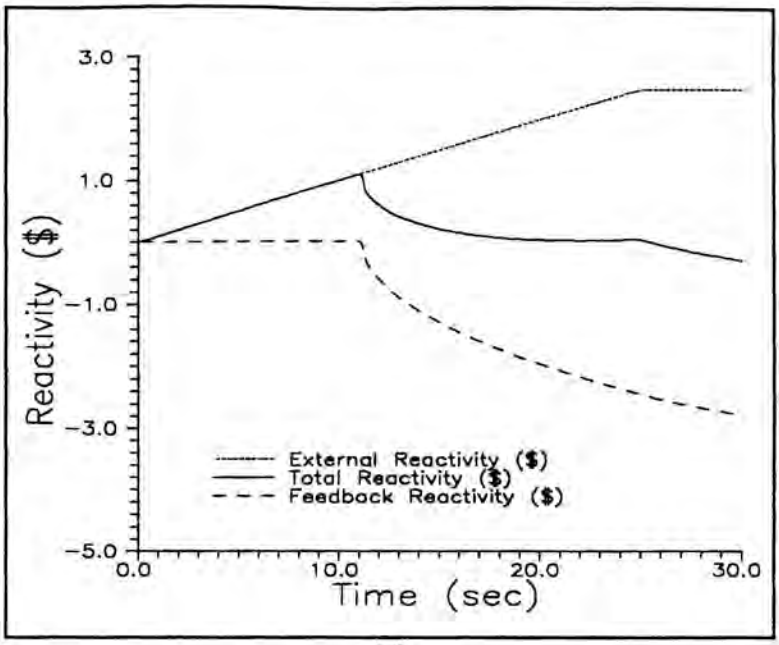

(a)

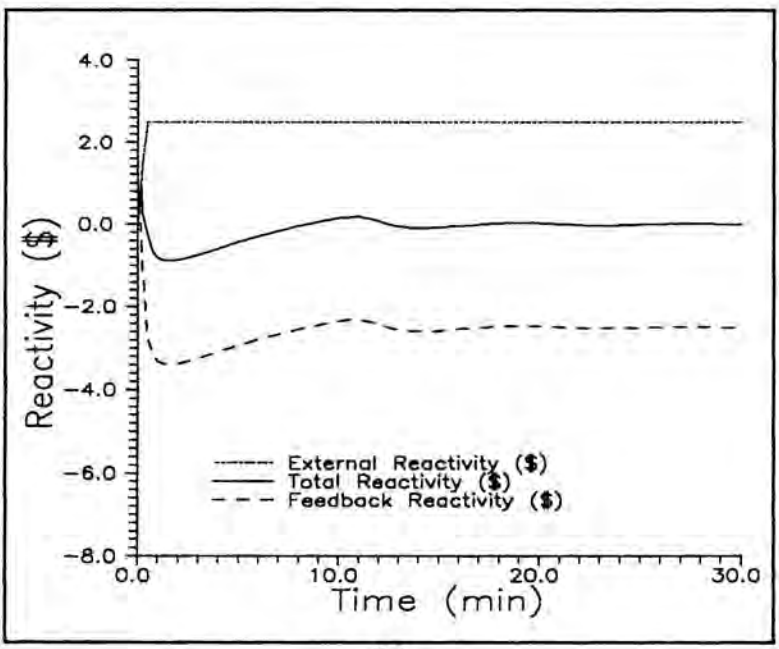

(b)

Figure 3.27 : Reactivity of a UO_3, 1-m x 1-m Slab, with a \$.10/sec Reactivity Addition Rate Stopped at \$2.5 of External Reactivity on a (a) short time scale, and (b) long time scale.

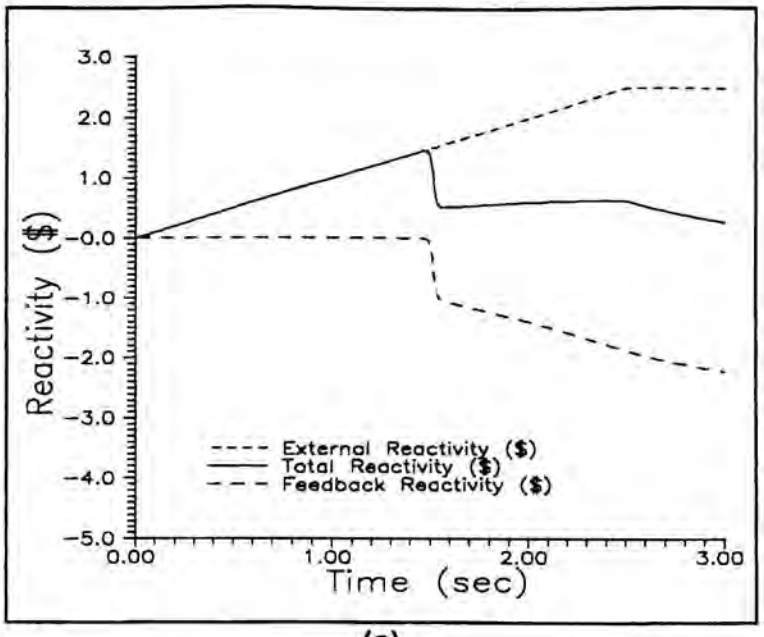

(a)

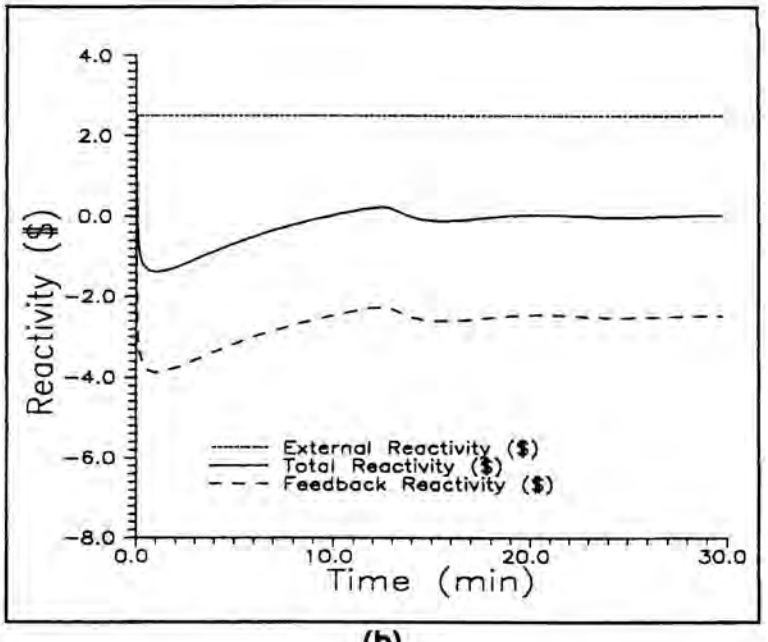

(b)

Figure 3.28 : Reactivity of a UO_3, 1-m x 1-m Slab, with a \$1.0/sec Reactivity Addition Rate Stopped at \$2.5 of External Reactivity on a (a) short time scale, and (b) long time scale.

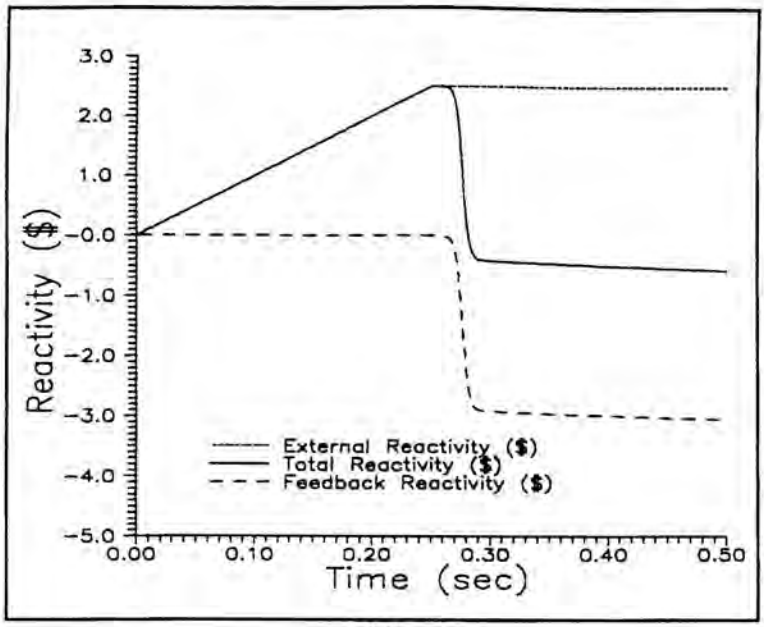

(a)

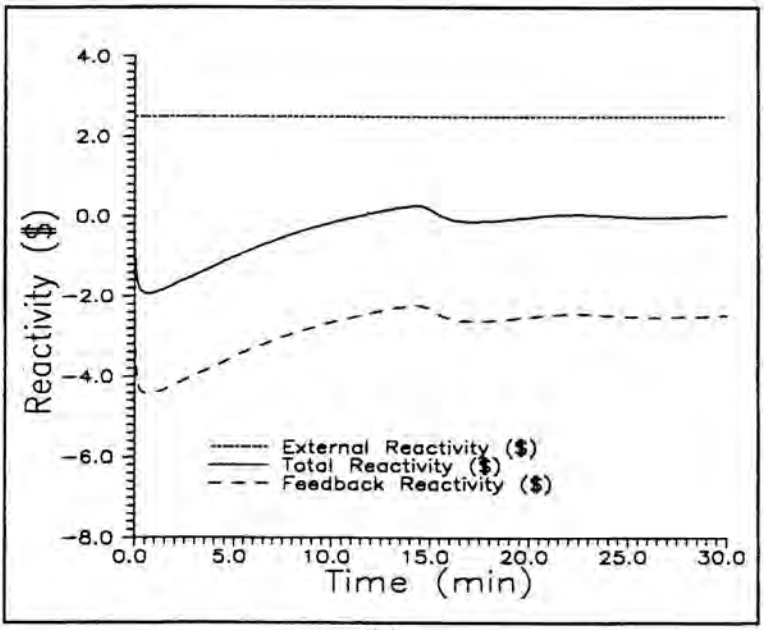

(b)

Figure 3.29 : Reactivity of a UO_3, 1-m x 1-m Slab, with a \$10/sec Reactivity Addition Rate Stopped at \$2.5 of External Reactivity on a (a) short time scale, and (b) long time scale.

3.9. Effect of an Uncertainty in the Feedback Coefficient

The results of reactivity, power, and total fissions, for the UO_3, one-meter by one-meter, powder slab with a $1/sec reactivity addition rate, with a reactivity feedback coefficient that is 10% too large and 10% too small are shown in figures

3.30 - 3.31. The results show that a difference in the feedback coefficient will cause a difference in the power oscillations of the system, but not the peak power. The power oscillates with a greater amplitude for the higher reactivity feedback coefficient and takes a longer time to settle out to equilibrium. The peak power occurs at essentially the same time in each case. The total fissions are also very similar in each case.

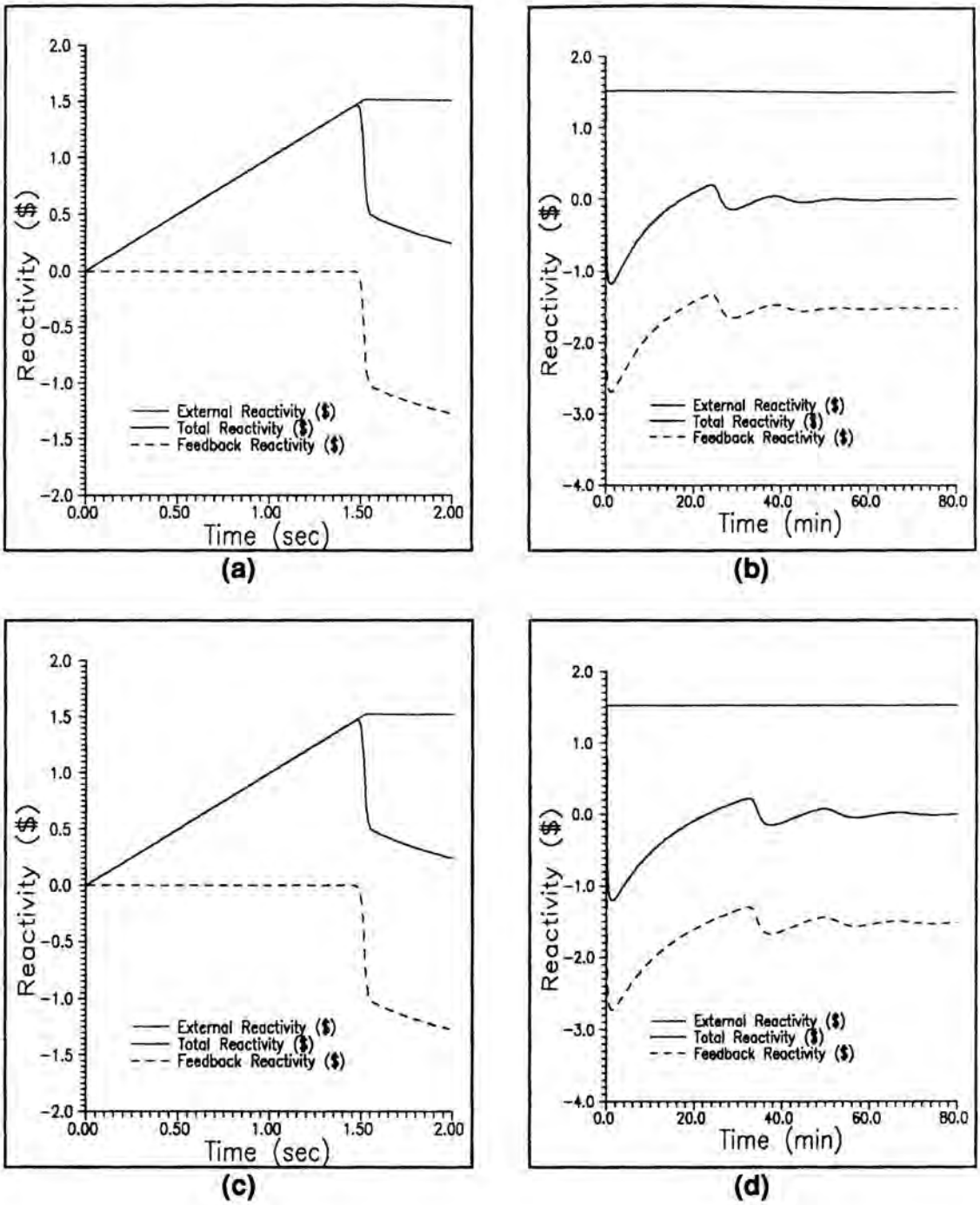

Figure 3.30 : Comparison of Reactivity for a UO_3, 1-m x 1-m Slab, with a \$1.0/sec Reactivity Addition Rate and a Reactivity Feedback Coefficient that is in (a) & (b) 10% too small, and in (c) & (d) 10% too large.

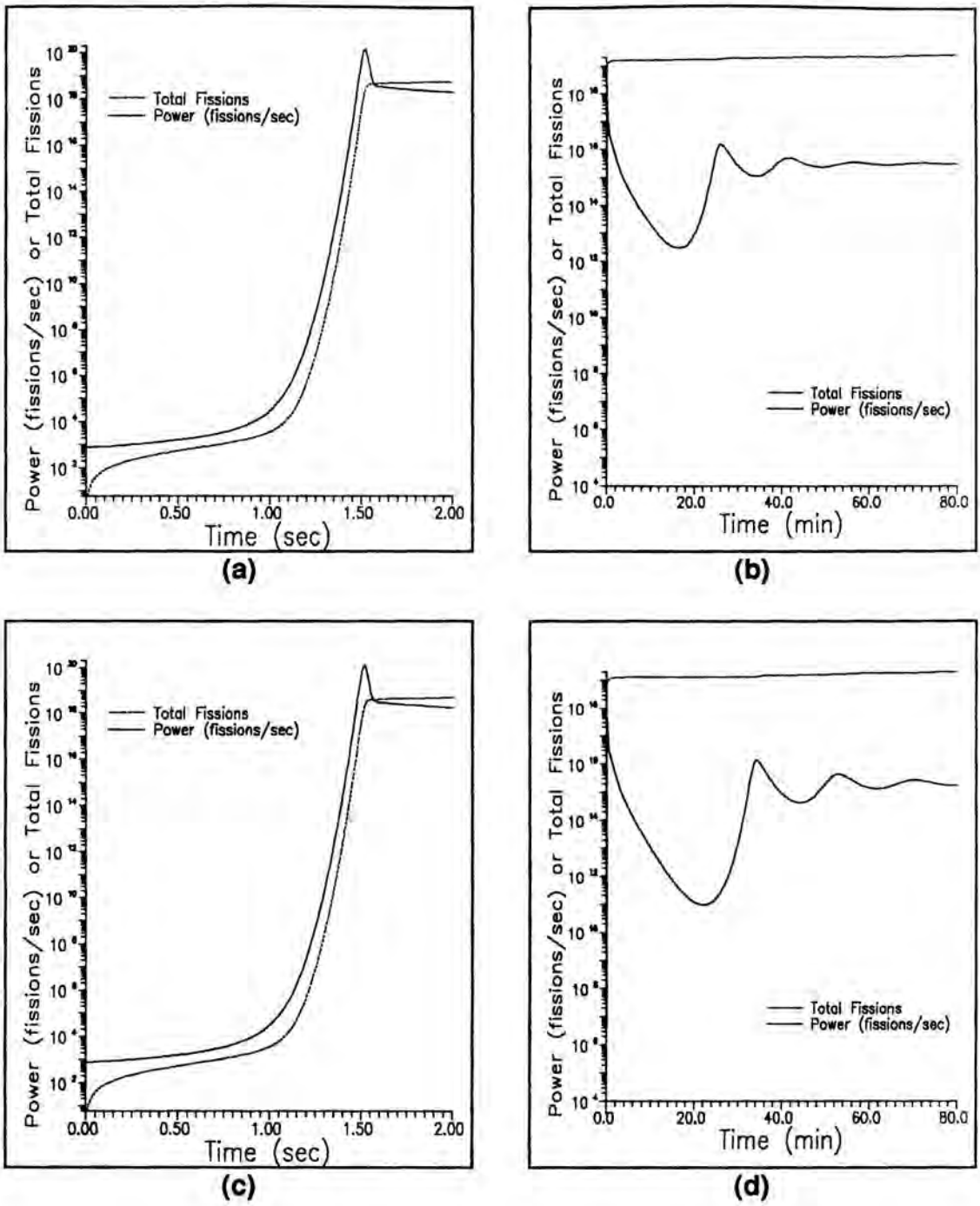

Figure 3.31 : Comparison of Power and Total Fissions for a UO_3, 1-m x 1-m Slab, with a \$1.0/sec Reactivity Addition Rate and a Reactivity Feedback Coefficient that is in (a) & (b) 10% too small, and in (c) & (d) 10% too large.

3.10. Powder Dispersal Effects

Analyses discussed thus far for dry HEU powder criticality accidents assume that no inherent shutdown mechanisms are present in the model. The system power peaks in a short time and then oscillates over a longer time until the system achieves an equilibrium temperature and power. A potential shutdown mechanism is the rapid expansion of the air occupying the interstitial volume in the powder.[29] The following section discusses this effect and presents a simple model for computing this effect.

3.10.1. Powder Dispersal Model

Dispersion of the dry HEU powder may be an important shutdown mechanism in the system. Air is assumed to be trapped inside the void space. As the system temperature changes, the powder density changes. The void space within the powder changes but the amount of air occupying the void space is assumed to remain constant. Using the ideal gas equation, PV=nRT, the pressure of the air inside the void space can be estimated. As the trapped air expands, it exerts a greater pressure on the powder, possibly dispersing it.

The first important parameter in the proposed dispersal model is the volume of void space that contains the air. If the density at time t, D(t), is divided by the theoretical density, the volume fraction of the powder particles is obtained. One minus the volume fraction of powder is the volume fraction of air space. The product of the total system volume, V_{sys}, and the volume fraction of air space is equal to the volume of the air space, V_{air}, in the powder slab as given by

$$V_{void}(t) = \left(1 - \frac{D(t)}{D_{theo}}\right)(V_{sys}) , \qquad (3.12)$$

where D_{theo} [UO_3] = 7.2 gm/cc, and
D_{theo} [UF_4] = 6.7 gm/cc.

This air space volume is used, along with the system temperature, $T_{sys}(t)$, to calculate the current pressure of the air trapped in the void space when the initial air pressure, $P_{air}(t)$, and air temperature, $T_{sys}(t)$, are known. The pressure, $P_{air}(t+\Delta t)$ at a new $T_{sys}(t+\Delta t)$ and a new $V_{air}(t+\Delta t)$ is known from the ideal gas law as

$$P_{air}(t+\Delta t) = \frac{P_{air}(t)\ V_{air}(t)\ T_{sys}(t+\Delta t)}{V_{air}(t+\Delta t)\ T_{sys}(t)} , \qquad (3.13)$$

where P(t) = 1 atm, and
$T_{sys}(t)$ = 293K.

This new pressure exerted by the air, $P_{air}(t+\Delta t)$, determines the pressure difference between the air voids and the outside air which is at atmospheric

pressure. This pressure difference gives rise to forces which may be sufficient to disperse the powder.

A very simple model for computing the effect of these forces on the powder is to assume that all of the powder particles are supported from below by all of the air trapped in the void spaces as shown in Figure 3.32. This artificial separation of the particles from the air permits a vertical force balance to be performed on the layer of powder particles as

$$\sum y\text{-}forces = [P_{air}(t) - P_{atm}]\ S - mg = m\ a(t)\ , \qquad (3.14)$$

where S = surface area air pressure is acting upon, (m^2)
m = mass of powder particles, (kg)
g = acceleration due to gravity, 9.8 (m/s^2)
a = resulting acceleration of m, (m/s^2)
t = time, (s).

Using equation 3.14, the acceleration of the powder particle layer may be calculated. If the pressure force of the rapidly expanding air is sufficient to cause this artificial layer of particles to accelerate quickly, then the force of the air in the real system (i.e., a uniform mixture of powder particles and air) is probably sufficient to disperse the powder pile - although no definite conclusions can be drawn from such a simple model. A more complex model for powder dispersal is presented in Appendix A.

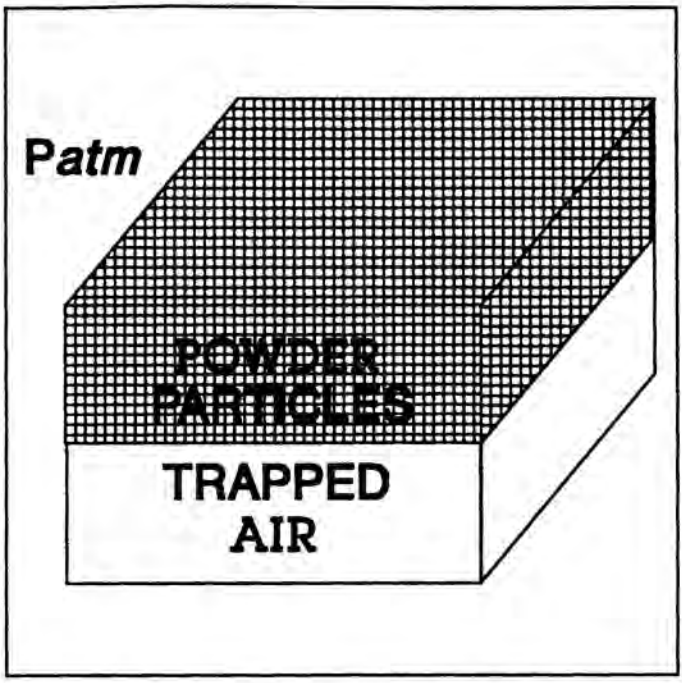

Figure 3.32 : Schematic of Simple Powder Dispersal Model

3.10.2. Results of the Powder Dispersal Model

The results of pressure and corresponding acceleration calculations using the powder dispersal model described above are shown in figure 3.33 for a UO_3, one-meter by one-meter slab. The acceleration calculated using this method is very high indicating that the powder will probably disperse; however, this model is probably too simplistic. The model does not consider the air that may escape the system without moving any powder particles. Also, the assumption of a contained void space is not necessarily accurate. In short, no definite conclusions regarding powder dispersal can be drawn from this very simple

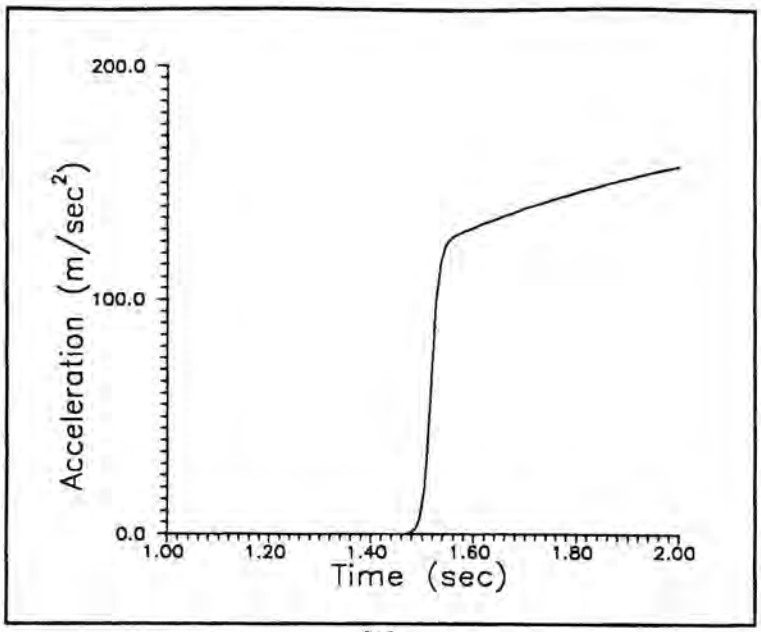

(a)

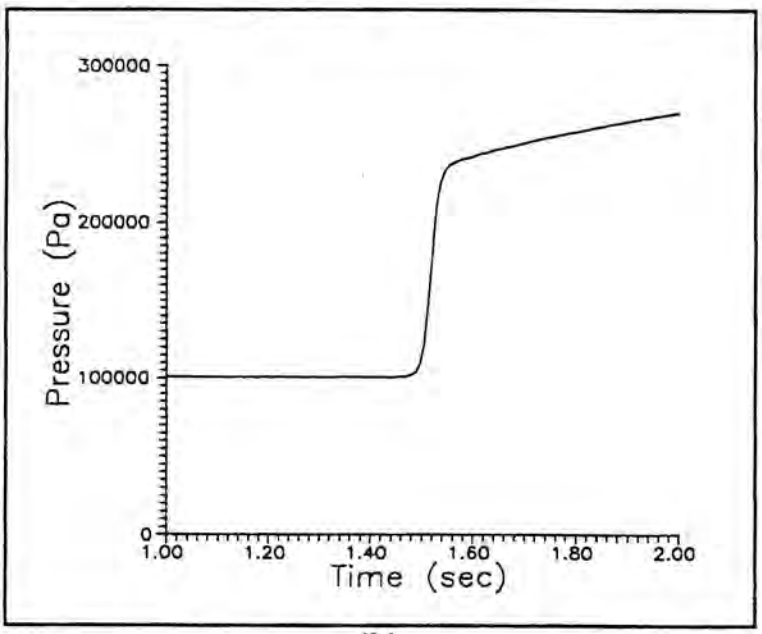

(b)

Figure 3.33 : Results of the Powder Dispersal Model for a UO_3, 1-m x 1-m Slab, with a \$1.0/sec Reactivity Addition Rate showing (a) acceleration, and (b) pressure.

model. A better model for dispersal is needed to accurately understand the motion of the powder particles (see Appendix A).

Chapter 4

VALIDATION EFFORTS

4.1. Comparison of SKINATH to Experiments and Other Codes

A modified version of the SKINATH code, named SKINATH-DP, is used for all of the calculations presented in Chapter 3. The original SKINATH code included a thermal-hydraulic model for a cylindrical reactor cooled externally by natural convection. Since no experimental or calculated data are available for the dry HEU powder system, other types of experimental data and computer code calculations were considered to compare with the SKINATH-DP results. Two facilities have cylindrical reactors, namely, DOSAR and SHEBA, and excursion data from these facilities has been modelled by the SKINATH-DP code. Reference 10 contains the necessary information to execute the SKINATH-DP code for both DOSAR and SHEBA. Comparison of results from the SKINATH-DP code are made with experimental data and with SLOPUS[10] code results for the SHEBA facility. The DOSAR facility calculations only provide a comparison between SKINATH-DP and SLOPUS results.

Other data available for validation efforts are from the CRAC experiments.[4] The CRAC experiments are not suited for the thermal-hydraulic model in the SKINATH-DP code. However, data are available to use Fuch's energy model for reactivity feedback. Results from SKINATH-DP using Fuch's energy model are

compared against the CRAC experimental data and results from the computer code CRITEX.

4.1.1. SHEBA Calculation

The SHEBA facility is a cylindrical reactor containing 5% enriched uranium solution located at Los Alamos National Laboratory. The reactor is 0.364 meters high and 0.56 meter in diameter. The heat capacity of the reactor is 4177. kJ/kg/K/l. The situation considered by SKINATH-DP is a step reactivity change of 7.0 cents and an initial power of 3.03×10^{-5} Watts. Table 4.1 presents the experimental results, results from the SLOPUS code, and results from SKINATH-DP where the thermal model for a powder has been replaced by the original cylindrical reactor model. The differences between these results are quite small, therefore SKINATH-DP as modified is judged to be an accurate tool for calculating criticality excursions for SHEBA-type systems.

Table 4.1 : Results for the SHEBA Facility

	Maximum Pulse Power (watts)	Time to First Pulse Peak (minutes)	Maximum Temperature Rise (°C)	First Pulse Yield (fissions)
Experiment	1450	48	4.5	2.8×10^{16}
SLOPUS	1470	47	4.6	3.0×10^{16}
SKINATH-DP	1345	49	2.5	2.6×10^{16}

4.1.2. DOSAR Calculation

The DOSAR facility is a cylindrical reactor containing 93% enriched uranium metal known as the Health Physics Research Reactor at the Oak Ridge National Laboratory. The reactor is 0.23 meters high and 0.20 meter in diameter. The heat capacity of the reactor is 1800 kj/kg/K/l. The situation executed by SKINATH-DP is a step change of 4.3 cents of reactivity and an initial power of 0.01 Watts. The temperature and power calculated by the modified SKINATH-DP code are compared to the SLOPUS results in figure 4.1. As may be observed, the modified SKINATH-DP code does well when compared to older codes such as the SLOPUS code.

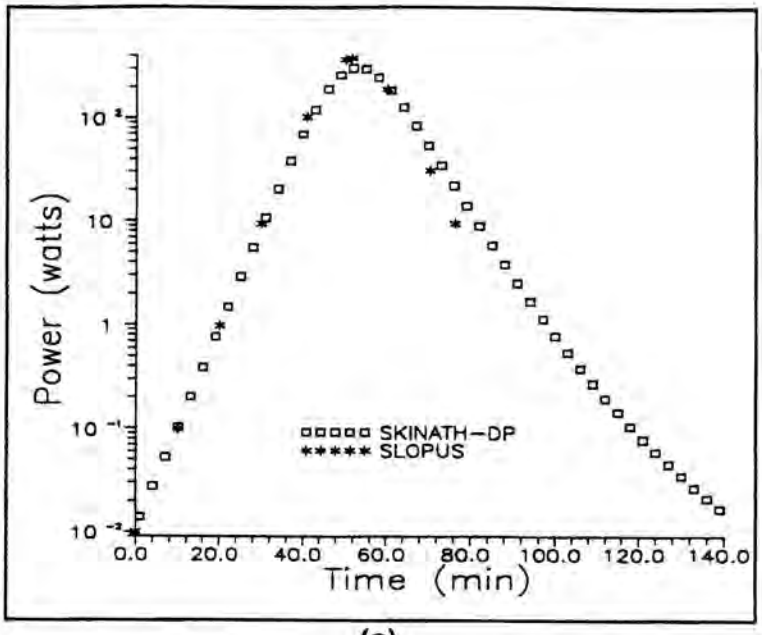

(a)

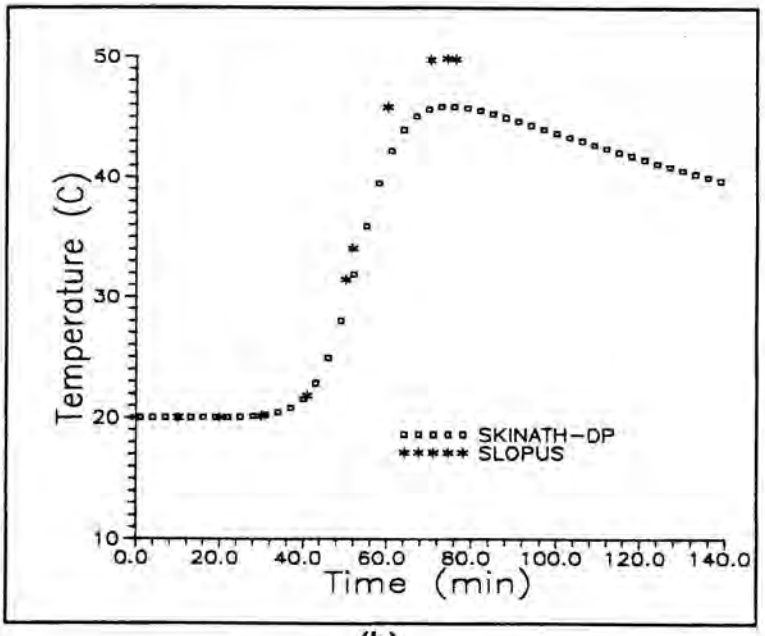

(b)

Figure 4.1 : Results of SKINATH-DP and SLOPUS for a Transient Calculation of the DOSAR Facility Showing (a) power, and (b) temperature.

4.1.3. CRAC Experiments Calculations

The CRAC fissile solution experiments can be modeled using a calculated quenching coefficient as described in the Fuch's energy model (see section 3.1). The Fuch's energy model uses a quenching coefficient, b, with units of Δk/k/fission. This quenching coefficient, b, is multiplied by the total fission yield to calculate the total feedback reactivity at time t. This reactivity is then subtracted from the external reactivity to calculate the total system reactivity at time t. Values for b are calculated using the data from the CRAC experiments.[2] These values are listed in table 4.2 for three CRAC experiments that were analyzed with the CRITEX code. Also listed in table 4.2 are the reactivity ramp rates for each experiment.

Table 4.2 : Input Parameters for CRAC Experiments Calculations[2]

CRAC NUMBER	Quenching Coefficient (k/k/fission)	Reactivity Addition Rate ($/sec)
10	4.86×10^{-20}	0.0772
12	2.06×10^{-20}	0.0156
19	6.27×10^{-20}	0.0870

The results of the experiments, the CRITEX code, and SKINATH-DP with Fuch's energy model are shown in Table 4.3. The CRITEX code does a better job of modeling the CRAC experiments because it contains an explicit thermal-

hydraulic feedback model for fissile solutions. However, SKINATH-DP with Fuch's energy model for thermal feedback is in reasonable agreement with both the CRITEX results and the experimental results.

Table 4.3 : Results of CRAC Experiments Calculations

CRAC #		Delay Time (sec)	Time of Peak (sec)	Peak Power (fissions/sec)	Energy in Pulse (fissions)
10	Experiment	n/a	6.6	2.00×10^{17}	4.30×10^{17}
	CRITEX	1.0	14.0	1.22×10^{17}	4.16×10^{17}
	SKINATH-DP	1.0	12.9	1.66×10^{17}	5.80×10^{17}
12	Experiment	n/a	65.0	1.00×10^{16}	3.70×10^{17}
	CRITEX	5.0	59.6	2.23×10^{16}	4.33×10^{17}
	SKINATH-DP	5.0	55.0	6.45×10^{16}	9.30×10^{17}
19	Experiment	n/a	16.2	6.70×10^{16}	3.50×10^{17}
	CRITEX	5.0	12.5	1.63×10^{17}	4.24×10^{17}
	SKINATH-DP	5.0	7.4	1.50×10^{17}	5.50×10^{17}

Chapter 5

CONCLUSIONS AND FUTURE WORK

5.1. Conclusions

The results presented in this thesis are for hypothetical criticality excursions involving dry highly-enriched uranium powders. This research serves as a first attempt at modeling neutronic and thermal effects of criticality excursions involving dry HEU powder. No inherent shutdown mechanisms are definitely established. The only shutdown mechanism considered is powder dispersal due to rapid air expansion. Therefore, according to the proposed model, the only definite shutdown mechanism for a dry(i.e., no water present) HEU powder excursion is fuel burnup. If the powder disperses, the system should shutdown much sooner. Other possible shutdown mechanisms should be explored to provide a better understanding of powder excursions.

The magnitude of the fission yield for all of the excursions considered in this work is about 10^{19} fissions. This yield is comparable to the results of other criticality accidents that have occurred to date.[1] However, the results are still an order of magnitude lower than those suggested by Woodcock.[5] Woodcock estimates 10^{20} fissions for a criticality excursion involving heterogeneous powder/liquid systems. The results presented in this thesis should be used with

caution since no experimental data for dry HEU powder systems is available for validation comparisons.

5.2. Future Work

Since this thesis is the first attempt at modeling a dry HEU powder criticality excursion, there are many areas for future improvement.

The code used to analyze the model developed for the HEU dry powder system is the SKINATH-DP code. The model used in SKINATH-DP is limited in its abilities because it does not consider spatial effects. The spatial effects of the power and temperature distributions could be important when powder dispersal or disassembly occurs (see Appendix A). Future analyses of dry HEU powder systems may need to include spatial effects in both the neutronic and thermal models.

If spatial effects are considered in the modeling of the system, other types of geometries may be explored. A hemisphere or cone of powder may describe the powder pile on the floor more accurately. These geometries may also make a powder dispersal model easier to implement. Particle motion may have important reactivity effects especially toward the shutdown of the system. The

powder dispersal model can be further improved to calculate the feedback reactivity caused by particle motion as done in the PAD code for metallic systems.[10]

Finally, the data available for UO_3 and UF_4 powders are limited. Important properties of the system, especially density, were modified from information for UO_2. It may not be possible to find more information about UO_3 and UF_4 since this data does not exist in the open literature. Also, the characteristics of the powder should be explored to determine the effect of very high temperatures and large temperature changes on the materials.

REFERENCES

REFERENCES

1. W.R.Stratton, "A Review of Criticality Accidents," DOE/NCT-04, Nuclear Criticality Technology, (March 1989).

2. W.T.Mee, D.A. Reed, R.G.Taylor, "Consequences of a Postulated, Moderated Criticality Accident at the Oak Ridge Y-12 Plant," Y/DD-384, Oak Ridge Y-12 Plant, (Sept.,1988).

3. G.E.Hansen, "Assembly of Fissionable Material in the Presence of a Weak Neutron Source," *Nucl. Sci. and Eng.*, **8**, 709 (Dec., 1960).

4. P.Lecorche, R.L.Seale, "A Review of the Experiments Performed to Determine the Radiological Consequences of a Criticality Accident," Y-CDC-12, Oak Ridge Y-12 Plant, (Nov.,1973).

5. E.R.Woodcock, "Potential Magnitude of Criticality Accidents," AHSB(RP)R-14, AHSB.

6. D.J.Mather, P.M.Shaw, "CRITEX - A Computer Program to Calculate Criticality Excursions in Fissile Liquid Systems," SRD R 380, UK Atomic Energy Authority. (July, 1984).

7. R.Kato et al., "The Code CREST to Simulate Criticality Accident Power Excursions in Fuel Solution," Mitsubishi Atomic Power Industries.

8. H.F.Lutz, "Nuclear Criticality Safety Assesment Calculations : Part I. Calculating Power Histories in Nuclear Excursions," M-164, Lawrence Livermore Nat. Lab., (1985).

9. H.L.Dodds, R.M.Westfall, "SKINATH - A Computer Program for Solving the Reactor Point Kinetics Equations with Simple Thermal Hydraulic Feedback," ORNL/CSD/TM-210, Oak Ridge National Laboratory, (Sept., 1984)

10. C.E.Newlon et al., "An Assesment of the Minimum Criticality Accident of Concern," H&R Technical Associates, H&R 82-2, Oak Ridge, TN (1982).

11. D.M.Peterson,W.R.Stratton,T.P.McLaughlin, "PAD : A One-Dimensional, Coupled Neutronic - Thermodynamic Computer Code," LA-6540-MS, Los Alamos Nat. Laboratory (December 1976).

12. F.Y.Barbry, "Review of Studies on Criticality Accidents Undertaken at CEA/Valduc," *Trans. Am. Nucl. Soc.*, **63**, 225 (June 1991)

13. J.P.Rozain, P.Fouillaud, D.J.Mather, A.M.Bickley, "Criticality Excursions in Wetted UO_2 Powder," *Trans. Am. Nucl. Soc.*, **63**, 228 (June 1991)

14. Personal Communication, Davis Reed, July 1990.

15. Personal Communication, Davis Reed, July 1991.

16. A.C.Hindmarsh, "LSODE and LSODI - Two New Initial Value Ordinary Differential Equation Solvers," ACM-Signum Newsletter, Vol.15, No 4 (1980).

17. G.R.Keepin, Physics of Nuclear Kinetics, Addison -Weley Publishing, Reading, Mass. (1965)

18. J.E.Calahan, K.O.Ott, "Delayed Neutron Data for Fast Reactor Analysis," *Nucl. Sci. and Eng.*, **50**, 208 (1973).

19. A.F.Henry, Nuclear-Reactor Analysis, MIT Press, (1975).

20. Staff of Technical Applications, Computing and Telecommunications Division at Oak Ridge National Laboratory, "SCALE: A Modular Code System for Performing Standardized Computer Analysis for Licensing Evaluation," NUREG/CR-0200, Vol.2, sect. f11, U.S. Nuclear Regulatory Commission (revised and reissued January 1990).

21. Staff of Technical Applications, Computing and Telecommunications Division at Oak Ridge National Laboratory, "SCALE: A Modular Code System for Performing Standardized Computer Analysis for Licensing Evaluation," NUREG/CR-0200, Vol.1, sect. c4, U.S. Nuclear Regulatory Commission (revised and reissued January 1990).

22. M.H.Rand, Thermochemical Properties of Uranium Compounds, Wiley & Sons, New York, (1963).

23. Churchill, Operational Mathematics in Engineering, McGraw Hill, (1960).

24. F.Incropera, D.De Witt, Fundamentals of Heat and Mass Transfer, John Wiley & Sons, (1985).

25. D.Halliday,R.Resnick, Fundamentals of Physics, John Wiley & Sons, (1974).

26. J.Belle, Uranium Dioxide : Properties and Nuclear Applications, Naval Reactors, Div. of Reactor Development, USAEC, (1961).

27. Nuclear Systems Materials Handbook, Vol. 1, Design Data, Part IV - Nuclear Fuels, Hanford Engineering Laboratory, Richland, WA.

28. Staff of Technical Applications, Computing and Telecommunications Division at Oak Ridge National Laboratory, "SCALE: A Modular Code System for Performing Standardized Computer Analysis for Licensing Evaluation," NUREG/CR-0200, Vol.2, sect. f7, U.S. Nuclear Regulatory Commission (revised and reissued January 1990).

29. Personal Communication, Tom Radcliffe, July 1991.

30. Personal Communication, Davis Reed, March 1991.

31. G.E.Hansen, C.C.Byers, J.J.Koelling, "Fission and Explosive Energy Releases of PuO_2 and PuO_2-UO_2 Assemblies," *Trans. Am. Nucl. Soc.*, (Nov. 1976)

APPENDIXES

Appendix A

A MORE COMPLEX POWDER DISPERSAL MODEL[29]

A more complex dispersal model of the dry HEU powder system would involve knowledge of the spatial power distribution in the slab. This is not currently calculated with the program used in this work but a spatial power profile can be assumed to understand the more complex powder dispersal model.

A more complex powder dispersal model would involve dividing the slab into several different regions in the vertical direction (i.e., the Y direction). The powder slab is represented as a set of smaller powder slabs stacked on top of one another, separated by slabs of air pockets (see Figure A.1). The power generation in each slab is known from the spatial power distribution and the temperature of the air pockets is computed from an energy balance on each air pocket. The pressure of each air pocket can then be calculated with the ideal gas equation, PV=nRT or by equation 3.10. With a pressure profile calculated, the acceleration of the particle slabs can be calculated along with their subsequent motion.

The motion of the powder slabs is due to the pressure difference between the air pocket trapped below a set of powder slabs and the air

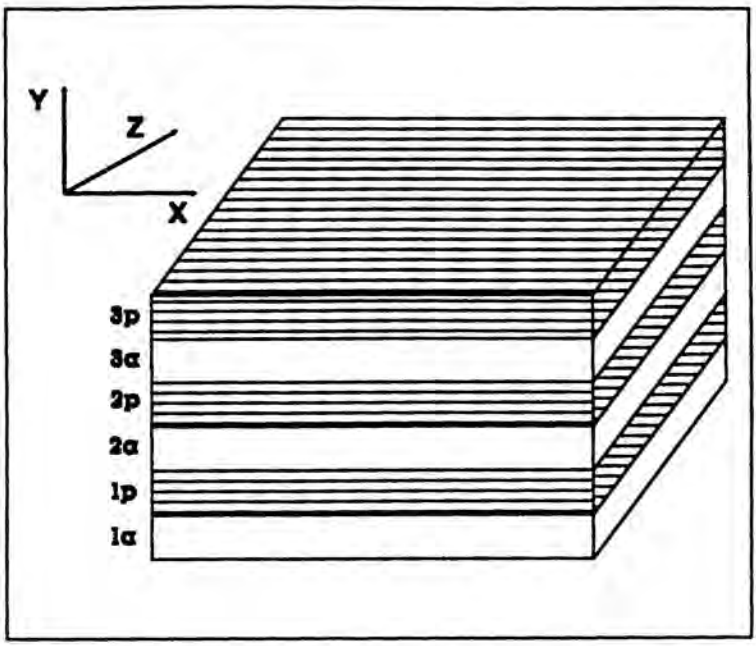

Figure A.1 : Slab Configuration for the more Complex Powder Dispersal Model

pressure outside the entire system. The air pocket, which is at a higher pressure than the outside of the system, is assumed to accelerate all powder slabs above it. Now the mass that was shown in equation 3.11 to calculate the acceleration is equal to the total mass of particle slabs sitting above it. Examining figure A.1 shows that the air slab located in position 1a would accelerate all of the particle slabs above it; 1p, 2p, and 3p. This would be true for air pocket 2a; 2p and 3p, and air pocket 3a; 3p.

The accelerations are integrated once to calculate the particle slab velocities of the slabs above the air pocket and integrated twice to calculate the particle slab positions. The flow of air particles from one air pocket to the air

pocket above it will occur because of leakage through the above powder slab. To account for this, Bernoulli's equation is used to calculate the velocity of air particles travelling through the powder using a friction loss factor, k.

$$v_{air} = \left(\frac{2\, g\, \Delta p}{k \rho} \right)^{\frac{1}{2}} \qquad \text{(A.1)}$$

This friction loss factor for this system is not known and would probably have to be determined experimentally.

Integrating the resulting air velocity between air pockets gives the amount of air mass that is transferred from one pocket of air to another. This air mass is used in the ideal gas equation, PV=NRT, to calculate the pressure at the next time step and next temperature value.

This calculational scheme is used throughout the system to calculate pressure forces, accelerations, velocities, etc. for each slab of air or powder in the system. The calculation will end when the gas expansion caused by energy generation and gas leakage through the particle layers reaches an equilibrium with the gravity force. The final result will be rectangles of powder expanded in the +Y direction (see Figure A.2)

The model presented does not account for motion in the X or Z dimensions. If the calculation of motion in these directions is desired,

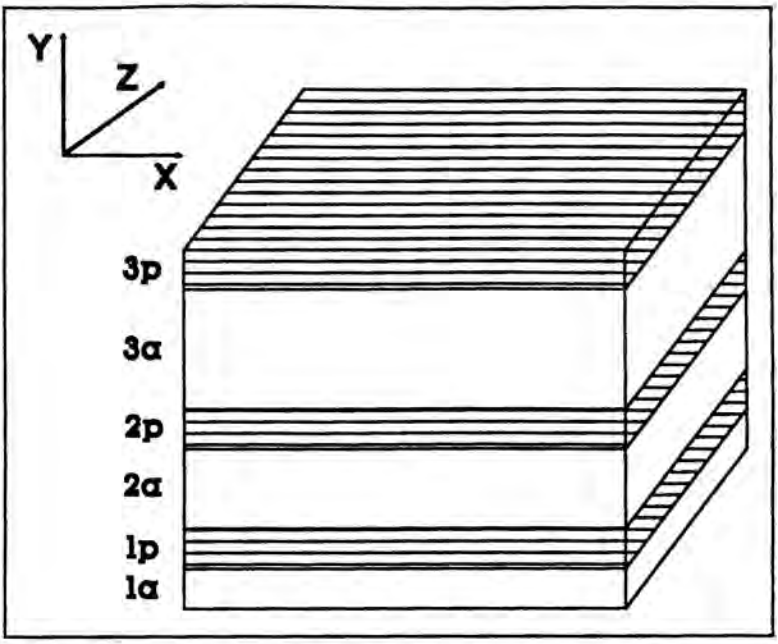

Figure A.2 : Final Result of Air and Powder Slab Configuration

parallelpipeds of powder pockets and air pockets would be used instead of slabs.

This model predicts the movement of the powder inside the total system. If the movement is rapid enough, powder dispersal may take place. It is not known, however, how much powder motion would be needed to completely disperse the powder. The negative reactivity caused by air expansion is also important because of the change in density. This would only be known by performing a spatial k_{eff} calculation at each new powder position; that is, reactivity feedback due to material relocation.

Appendix B

EFFECT OF MOISTURE ON DRY HEU POWDER SYSTEM

Effect on k_{eff}

At a late stage in this project, it was discovered that the dry HEU powder, UO_3, may contain as much as 1.5w/o moisture in the form of H_2O attached to UO_3.[30] This results in an H/U of about 0.5. Analyzing a one meter by one meter slab at 3.5 gm/cc with an H/U ratio of 0.5 yields a k_{eff} that is 10% higher than without moisture present. Also previous work has shown that water is the basic disassembly material even in the case of extremely small amounts.[31]

This change in k_{eff} of the system is not likely to create much change in the results presented in this thesis. The temperature feedback coefficient calculated with the combined effects of density and volume change does not change much when the coefficient is recalculated with the moisture present. Figure B.1 shows the results of a temperature feedback coefficient calculation with a 0.5 H/U ratio present.

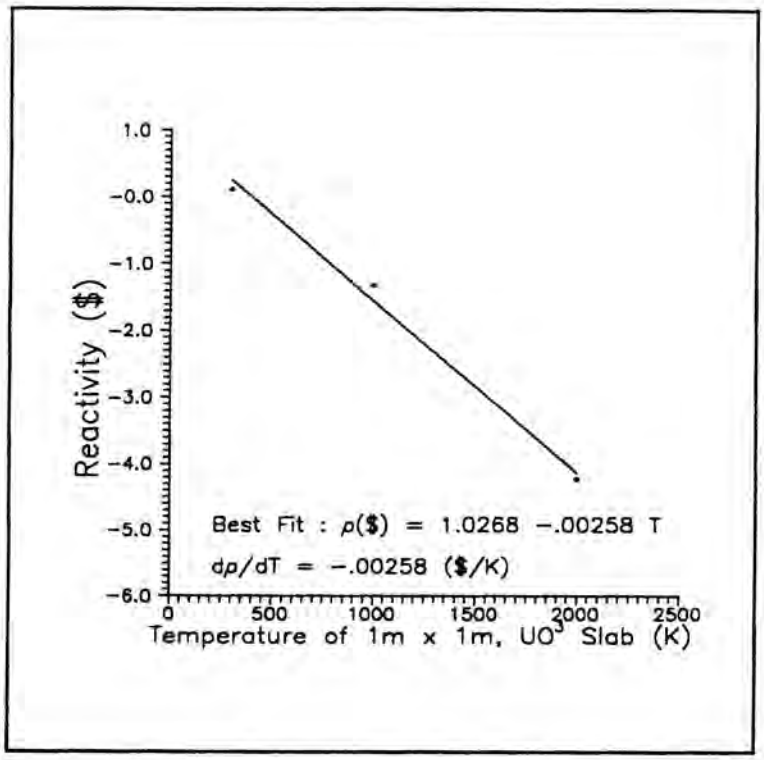

Figure B.1 : Reactivity Feedback Coefficient for a UO_3, 1-m x 1-m Slab With 1.5w/o Water Present.

Changes in the Thermal Model

The most important concern with the presence of water is the change in the thermal equations. Since water is present, the energy produced in the powder particles will not only be transferred into the air voids but will also be absorbed into the water that is present. Water can absorb greater amounts of heat than air resulting in the production of water vapor. The production of water vapor will serve to further increase the pressure exerted by the void spaces, possibly dispersing the powder even sooner. A brief discussion of the thermodynamics of the system with water present is presented next.

The presence of moisture in the system creates a problem is the calculation of one bulk temperature for the entire system. The heat transferred to the air pockets in the powder pile is neglected in the energy balance model. However, the presence of water in the system cannot be neglected because of its high heat capacity. Therefore, the heating of the water present in the system can only be analyzed by separate energy balance equations for the water and powder.

The energy balance equation for the powder would be similar as shown before except for the presence of another loss term in the energy rate equation. The heat lost from the powder to the water would be described by a heat

transfer coefficient from powder to water, h_p, times the surface area of powder that is transferring heat to the water, A_p, times the difference in powder and water temperatures.

$$\frac{dT_p}{dt} = \frac{1}{m_p C_p}[\epsilon FP - Q_{loss} - h_p A_p(T_p - T_w)]. \qquad \text{(B.1)}$$

The heat transfer coefficient from powder to water would have to be estimated from a correlation of convective heat transfer from small particle spheres to liquid water. The area of the powder that transfers heat to the water must be estimated from the amount of water present and the volume of the void space that it occupies. This means that a certain percentage of the powder particles are in contact with water and transfer their heat directly to the water. This heat transfer increases the internal energy of the water. Equation B.2 shows the energy balance equation for the water

$$\Delta U_{water} = h_p A_p(T_p - T_{water}) , \qquad \text{(B.2)}$$

where ΔU = change in interval energy of the water.

The energy transferred to the water will be first increase the temperature of the water up to the saturation point. Therefore,
$\Delta U = m_{water}\, C_{p,water}(T_{water} - T_{water,0})$. The initial pressure of the water can be assumed as the pressure of the air voids. Once the liquid water has reached

saturation temperature, the subsequent energy transferred will produce water vapor.

The production of water vapor is determined from the heat of vaporization, h_{fg}. The introduction of energy into the liquid water will convert some of the liquid to vapor. The amount of mass converted is simply equal to the amount of energy deposited divided by h_{fg}

$$m_v = \frac{\Delta E}{h_{fg}}. \qquad \text{(B.3)}$$

This vapor production will cause an increase of the pressure in the void space due to an increase in the gas density occupying the void space. This causes a decrease in the specific volume of the water vapor occupying the void space. Using steam tables and the new smaller value of the specific volume for saturated vapor, the new increase in values for saturation pressure, P_{sat}, and temperature, T_{sat} are found. The heat of vaporization will also change. The temperature of the water is now equal to the new T_{sat} and the next amount of energy is used to vaporize the next amount of liquid water using the new heat of vaporization. This process of increasing the saturation pressure and temperature will continue until all available liquid water is converted into vapor.

The vapor that is now contained in the void spaces will continue to absorb energy which changes its internal energy. This is the same equation presented for the change in internal energy of the liquid water with the correct specific heat; namely, equation B.2.

The vaporization of the water inside the system creates problems for the dry HEU powder system. The incorporation of the change of state of water from liquid to vapor is not easy to handle because of the need for steam table lookups. However, the production of water vapor in the void space and the corresponding pressure increase can be used in the powder dispersal model to predict higher pressures in the void space perhaps dispersing the powder even sooner than predicted with no water present.

APPENDIX C

SKINATH-DP CODE LISTING

The following pages show a sample input file, screen output, and the code listing of the SKINATH-DP code used in this research. The actual calculated values are written to files labeled according to the input file name. A complete output file is not shown to save space. The SKINATH-DP code was executed on the VAX workstations in the Nuclear Engineering Department of the University of Tennessee.

```
1
754.9,2.4e-5
0.,1.,0.
-.00247,169.0
1.,.3010,293.,293.
.008,.008,2.0
1.5,0.
10
```

Figure C.1 : Sample Input File for SKINATH-DP

```
ENTER INPUT FILENAME :
ex1

POWDER SPECIFICATION : UO3

SLAB SIZE SPECIFICATION : 1 METER X 1 METER

INITIAL POWER : 0.346E+07  GENERATION TIME : 0.240E-04

REACTIVITY INSERTION :
REAC =  0.00E+00  +  .100E+01 T  + 0.00E+00

DOPPLER COEFFICIENT :  -.247E-02

VOLUME CHANGE COEFFICIENT : 0.169E+03

THE INITIAL SLAB VOLUME :  0.301E+00

0.8000E-02  0.8000E-02  .2000E+01

0.1500E+01  0.0000E+00

 1
```

Figure C.2 : First Page Output Screen for SKINATH-DP
Which is an Echo of the Input File.

Time (sec)	Time (min)	Total Fission	Power(fission/s)	Temperature
0.800000E-02	0.133333E-03	0.605011E+01	0.758462E+03	0.293000E+03
0.800000E-02	0.133333E-03	0.605011E+01	0.758462E+03	0.293000E+03
0.160000E-01	0.266667E-03	0.121407E+02	0.764303E+03	0.293000E+03
0.240000E-01	0.400000E-03	0.182799E+02	0.770518E+03	0.293000E+03
0.320000E-01	0.533333E-03	0.244694E+02	0.776887E+03	0.293000E+03
0.400000E-01	0.666667E-03	0.307104E+02	0.783387E+03	0.293000E+03
0.480000E-01	0.800000E-03	0.370039E+02	0.790018E+03	0.293000E+03
0.560000E-01	0.933333E-03	0.433510E+02	0.796782E+03	0.293000E+03
0.640000E-01	0.106667E-02	0.497528E+02	0.803684E+03	0.293000E+03
0.720000E-01	0.120000E-02	0.562104E+02	0.810727E+03	0.293000E+03
0.800000E-01	0.133333E-02	0.627248E+02	0.817916E+03	0.293000E+03
0.880000E-01	0.146667E-02	0.692974E+02	0.825253E+03	0.293000E+03
0.960000E-01	0.160000E-02	0.759293E+02	0.832743E+03	0.293000E+03
0.104000E+00	0.173333E-02	0.826217E+02	0.840391E+03	0.293000E+03
0.112000E+00	0.186667E-02	0.893760E+02	0.848201E+03	0.293000E+03
0.120000E+00	0.200000E-02	0.961934E+02	0.856177E+03	0.293000E+03
0.128000E+00	0.213333E-02	0.103075E+03	0.864325E+03	0.293000E+03
0.136000E+00	0.226667E-02	0.110023E+03	0.872650E+03	0.293000E+03
0.144000E+00	0.240000E-02	0.117038E+03	0.881157E+03	0.293000E+03
0.152000E+00	0.253333E-02	0.124122E+03	0.889851E+03	0.293000E+03
0.160000E+00	0.266667E-02	0.131276E+03	0.898737E+03	0.293000E+03
0.168000E+00	0.280000E-02	0.138502E+03	0.907823E+03	0.293000E+03
0.176000E+00	0.293333E-02	0.145802E+03	0.917114E+03	0.293000E+03
0.184000E+00	0.306667E-02	0.153177E+03	0.926616E+03	0.293000E+03
0.192000E+00	0.320000E-02	0.160628E+03	0.936337E+03	0.293000E+03
0.200000E+00	0.333333E-02	0.168159E+03	0.946283E+03	0.293000E+03
0.208000E+00	0.346667E-02	0.175770E+03	0.956461E+03	0.293000E+03
0.216000E+00	0.360000E-02	0.183463E+03	0.966879E+03	0.293000E+03
0.224000E+00	0.373333E-02	0.191240E+03	0.977546E+03	0.293000E+03
0.232000E+00	0.386667E-02	0.199104E+03	0.988468E+03	0.293000E+03
0.240000E+00	0.400000E-02	0.207057E+03	0.999655E+03	0.293000E+03
0.248000E+00	0.413333E-02	0.215099E+03	0.101112E+04	0.293000E+03

Figure C.3 : Second Page Output Screen for SKINATH-DP Which Shows Excursion Results.

Figure C.4 : Listing of SKINATH-DP

```
C*********************************************************************
C                                                                     *
C     THIS VERSION OF SKINATH SOLVES SIMPLE POINT KINETICS            *
C     WITH THERMODYNAMIC MODEL FOR HEU DRY POWDER                     *
C     SYSTEM                                                          *
C                                                                     *
C                                                                     *
C THE Y-VECTOR CONTAINS THE TOTAL NUMBER OF FISSIONS, THE             *
C FISSION RATE, SIX PRECURSOR CONCENTRATIONS, AND                     *
C THE TEMPERATURE.                                                    *
C                                                                     *
C NOTE THAT THE FISSION RATE IS PROPORTIONAL TO THE                   *
C SYSTEM POWER.                                                       *
C                                                                     *
C                                                                     *
C*********************************************************************
C
      IMPLICIT REAL*8(A-H,O-Z)
      CHARACTER*12 INFILE,OUTFL1,OUTFL2,OUTFL3
      COMMON /DATAIN/ AMDA(6),B(6),RHOEX(3),TC,T0,GEN,BT,RHOCOF,
     *RHODEN,DEN0,DENT,RHOVL,VOL0,VOLT,QLOSS,SIDEX,REACEX,
     *IPOWDER,EXST
      DIMENSION RWORK(200),IWORK(200),Y(9)
      EXTERNAL F
      PRINT*,' ENTER INPUT FILENAME :'
      READ(*,'(A12)') INFILE
      OUTFL1='O1'//INFILE
      OUTFL2='O2'//INFILE
      OUTFL3='O3'//INFILE
C
      DO I=1,12
       IF (INFILE(I:I).EQ.' ') THEN
        IMAX=I-1
        GO TO 10
       ENDIF
      END DO
       IMAX=12
C
10    OPEN(11,file=INFILE(1:IMAX),STATUS='unknown')
      DO I=1,12
       IF (OUTFL1(I:I).EQ.' ') THEN
        IMAX1=I-1
        GO TO 11
```

```
      ENDIF
     END DO
      IMAX1=12
11    OPEN(21,file=OUTFL1(1:IMAX1),status='unknown')
C
     DO I=1,12
      IF (OUTFL2(I:I).EQ.' ') THEN
       IMAX2=I-1
       GO TO 12
      ENDIF
     END DO
      IMAX2=12
C
12    OPEN(22,file=OUTFL2(1:IMAX2),STATUS='unknown')
     DO I=1,12
      IF (OUTFL3(I:I).EQ.' ') THEN
       IMAX3=I-1
       GO TO 13
      ENDIF
     END DO
      IMAX3=12
C
13    OPEN(23,file=OUTFL3(1:IMAX3),STATUS='unknown')
C
     READ(11,*) IPOWDER
     READ(11,*) P0,GEN
     READ(11,*) RHOEX(1),RHOEX(2),RHOEX(3)
     READ(11,*) RHOCOF,RHOVL
     READ(11,*) SIDEX,VOL0,T0,TC
     READ(11,*) DT1,DT2,TSTOP
     READ(11,*) EXST,SWITCH
     READ(11,*) IFLAG
c
C
C   NEUTRONIC INPUT
C
     M = 6
     AMDA(1)=.0129D+0
     AMDA(2)=.0311D+0
     AMDA(3)=.134D+0
     AMDA(4)=.331D+0
     AMDA(5)=1.26D+0
     AMDA(6)=3.21D+0
     B(1)=.00023D+0
```

```
      B(2)=.00142D+0
      B(3)=.00136D+0
      B(4)=.00244D+0
      B(5)=.00070D+0
      B(6)=.00027D+0
C
      Y(9)=T0
      Y(2)=P0
      Y(1)=0.0D+0
      REACTOT = 0.0D+00
      BT = 0.0000D+00
      DO 1 I=1,M
      BT=BT+B(I)
 1    Y(I+2)=B(I)*Y(2)/AMDA(I)/GEN
C     THE EXTERNAL REACTIVITY PERTURBATION IS NEXT.
      BTD = BT
C
      RHOEX(1)=RHOEX(1) * BTD
      RHOEX(2)=RHOEX(2) * BTD
      RHOEX(3)=RHOEX(3) * BTD
      RHOCOF =  RHOCOF * .0065
      RHOVL =  RHOVL * .0065
c
      DEN0=3500.
C
C     GENERAL INPUT
C
C
      NEQ = 9
      ITOL = 1
      RTOL = 1.D-08
      ATOL = 1.D-08
      ITASK = 1
      ISTATE = 1
      IOPT = 1
      LRW = 200
      LIW = 200
      MF = 22
      ICOUNT = 1
      IWORK(6)=10000
      T = 0.D+0
      DT=DT1
      TOUT = DT
C
```

```
C
      IF(IPOWDER.EQ.1) THEN
        WRITE(6,*) ' POWDER SPECIFICATION : UO3'
        WRITE(6,*) ' '
      ELSEIF(IPOWDER.EQ.2) THEN
        WRITE(6,*) ' POWDER SPECIFICATION : UF4'
        WRITE(6,*) ' '
      ELSE
        WRITE(6,*) ' ERROR :: INVALID POWDER SPECIFICATION'
        WRITE(6,*) ' '
        GO TO 81
      ENDIF
      IF(SIDEX.EQ.1.) THEN
        WRITE(6,*) ' SLAB SIZE SELECTION : 1 METER X 1 METER'
        WRITE(6,*) ' '
      ELSEIF(SIDEX.EQ.2) THEN
        WRITE(6,*) ' SLAB SIZE SELECTION : 2 METER X 2 METER'
        WRITE(6,*) ' '
      ELSE
        WRITE(6,*) ' ERROR :: INVALID SIZE SPECIFICATION'
        WRITE(6,*) ' '
        GO TO 81
      ENDIF
C
      WRITE(6,44)P0,GEN
        WRITE(6,*) ' '
      WRITE(6,*) ' REACTIVITY INSERTION : '
      WRITE(6,45) RHOEX(1)/BTD,RHOEX(2)/BTD,RHOEX(3)/BTD
        WRITE(6,*) ' '
      WRITE(6,46) RHOCOF / .0065
        WRITE(6,*) ' '
      WRITE(6,48) RHOVL / .0065
        WRITE(6,*) ' '
      WRITE(6,49) VOL0
        WRITE(6,*) ' '
      WRITE(6,43) DT1,DT2,TSTOP
        WRITE(6,*) ' '
      WRITE(6,43) EXST,SWITCH
        WRITE(6,*) ' '
      WRITE(6,*) IFLAG
C
C
4     CALL LSODE(F,NEQ,Y,T,TOUT,ITOL,RTOL,ATOL,ITASK,ISTATE,IOPT,
```

```
     XRWORK,LRW,IWORK,LIW,JEX,MF)
c
c     CALCULATE THE PRESSURE OF AIR IN THE SYSTEM
c
C     THDEN IS THE THEORETICAL DENSITY OF THE POWDER
      THDEN = 7200
C
      VOLAIR = (1 - DENT/THDEN) * VOLT
      PRESAIR = (((1 - DEN0/THDEN) * VOL0) / VOLAIR) * (Y(9) / TC)
      PRESAIR = PRESAIR * 1.01D5
      ACCEL   = (PRESAIR - 1.01D5) * SIDEXT**2/ MASST
C
C
      TIMEM = T/60.D+0
C
      IF(ISTOP.NE.1) THEN
       IF(T.GT.SWITCH) GO TO 88
      ENDIF
C
      IF(T.GT.EXST) GO TO 2
        REACEX = RHOEX(1)+RHOEX(2)*T+RHOEX(3)*T*T

2     REACFB= RHOCOF * (Y(9)-TC)
      REACTOT= REACFB + REACEX
      REACFBD =REACFB /BTD
      REACEXD=REACEX/BTD
      REACTOTD=REACTOT/BTD
C
      WRITE(21,43) T,TIMEM, Y(1),Y(2),Y(9)
      WRITE(22,43) T,TIMEM,REACTOTD,REACEXD,REACFBD
      WRITE(23,43) T,TIMEM,PRESAIR,ACCEL
      IF(IFLAG.EQ.1) THEN
        WRITE(6,51) T,REACTOTD,REACEXD,REACFBD,Y(1),Y(2),y(9)
      ENDIF
C
43    FORMAT('  ',13E14.6)
44    FORMAT(' INITIAL POWER :  ',E11.3,' GENERATION TIME :  ',E11.3)
45    FORMAT(' REAC = ',E11.3,' + ',E11.3,' T  + ',E11.3,' T**2')
46    FORMAT(' DOPPLER COEFFICIENT : ',E11.3)
47    FORMAT(' DENSITY COEFFICIENT : ',E11.3)
48    FORMAT(' HEIGHT CHANGE COEFFICIENT  : ',E11.3)
49    FORMAT(' THE INITIAL SLAB VOLUME : ',E11.3)
51    FORMAT('  ',13E11.3)
      IF(ISTATE.LT.0) GO TO 80
```

```
      IF(T.GE.TSTOP) GO TO 81
      ICOUNT = ICOUNT + 1
      TOUT =DFLOAT(ICOUNT)*DT
      IDUM = MOD(ICOUNT,27)
      IF(IDUM.NE.0) GO TO 4
      GO TO 4
 88    ICOUNT= 0
      DT=DT2
      TOUT=DT
      ISTOP=1
      GO TO 4
 80    WRITE(6,90) ISTATE
 90    FORMAT(1H0,' ERROR HALT....ISTATE =',I3)
  81   CONTINUE
C
C
C
C
C     SEE SUBROUTINE F FOR AN EXPLANATION OF TK,Y1TK,AND Y2TK

      STOP
      END
      SUBROUTINE F(NEQ,T,Y,YDOT)
C   THIS ROUTINE IS REQUIRED BY LSODE.  SEE LSODE
C   DOCUMENTATION.
      IMPLICIT REAL*8 (A-H,O-Z)
      COMMON /DATAIN/ AMDA(6),B(6),RHOEX(3),TC,T0,GEN,BT,RHOCOF,

     *RHODEN,DEN0,DENT,RHOVL,VOL0,VOLT,QLOSS,SIDEX,REACEX,
     *IPOWDER,EXST
      DIMENSION Y(NEQ),YDOT(NEQ)
C
C  THERMAL-HYDRAULIC INPUT
C
C
C 'EPSIL' IS THE AMOUNT OF ENERGY IN JOULES RELEASED PER
C  FISSION
      EPSIL =3.204E-11
C 'CP' IS THE SPECIFIC HEAT OF THE POWDER
      IF(IPOWDER.EQ.1) THEN
C  UO3 POWDER
      CP = 14.78 * (22.1 + 2.64D-3*Y(9) - 2.65D+5/Y(9)**2)
      ELSEIF(IPOWDER.EQ.2) THEN
C  UF4 POWDER
```

```
      CP = 13.45 * (25.7 + 7.00D-3*Y(9) - 0.06D+5/Y(9)**2)
      ENDIF
C 'DENT' IS THE DENSITY OF THE POWDER IN KG/M3
      DENT=DEN0 * (1 + 2.04E-5*(T0-273) + 8.7E-9*(T0-273)**2)/
     <(1+2.04E-5*(Y(9)-273)+8.7E-9*(Y(9)-273)**2)
C
C     CALCULATE THE VOLUME CHANGE

C
       VOLT = VOL0 * (DEN0/DENT)
       HCHNG=(DEN0/DENT - 1) / 3
       SIDEXT=(1+HCHNG) * SIDEX
       HEIGHT = VOLT/SIDEXT**2
C
C  THIS NEXT SECTION CALCULATES THE PARAMTERS NEEDED
C  FOR THE ENERGY LOSS FROM THE SYSTEM
C
C 'TF' IS THE FILM TEMPERATURE
      TF = (Y(9) + TC)/2
C 'GRAV' IS THE ACCELERATION DUE TO GRAVITY

      GRAV=9.8
C 'ALPHA' IS THE THERMAL DIFFUSIVITY OF THE COOLANT

      ALPHA = 1.D-6 * (-32.39 + .2055*TF - 5.98D-5*TF**2
     <+ 5.57D-8*TF**3)
C 'TNU' IS THE KINEMATIC VISCOSITY OF THE COOLANT

      TNU = 1.D-6 * (-2.451 + .044018*TF + 7.787D-5*TF**2)
C 'THERMALK' IS THE THERMAL CONDUCTIVITY OF THE COOLANT

      THERMALK = 1.D-3 * (13.68 + .004456*TF + .000128*TF**2
     <- 9.939D-8*TF**3 + 2.452D-11*TF**4)
C 'CLENGTOP' IS THE CHARACTERISTIC LENGTH OF THE TOP OF THE
C  SLAB
      CLENGTOP = SIDEXT/4
C 'CLENGSID' IS THE CHARACTERISTIC LENGTH OF THE SIDE OF THE
C  SLAB
      CLENGSID = HEIGHT
C CALCULATE THE RAYLEIGH NUMBER FOR THE TOP
      RALTOP = GRAV*(Y(9)-TC)*CLENGTOP**3/(ALPHA*TNU*TF)
C CALCULATE THE RAYLEIGH NUMBER FOR THE SIDE
      RALSID = GRAV*(Y(9)-TC)*CLENGSID**3/(ALPHA*TNU*TF)
C CHECK FOR WHICH CORRELATION TO USE FOR THE TOP
```

```
      IF (RALTOP.GT.1D7) THEN
        HBARTOP = .15*RALTOP**.33*(THERMALK/CLENGTOP)
      ELSEIF (RALTOP.LT.0.) THEN
         HBARTOP=0.
      ELSE
        HBARTOP = .54*RALTOP**.25*(THERMALK/CLENGTOP)
      ENDIF
C
C CHECK FOR WHICH CORRELATION TO USE FOR THE SIDE
C
      IF (RALSID.GT.1D9) THEN
        HBARSID = .10 * RALSID**.33*(THERMALK/CLENGSID)
      ELSEIF (RALSID.LT.0.) THEN
         HBARSID=0.
      ELSE
        HBARSID = .59 * RALSID**.25*(THERMALK/CLENGSID)
      ENDIF
C EMIS IS THE EMMISIVITY OF THE POWDER
      TEMPC=Y(9)-273
      IF(TEMPC.LT.1020) THEN
        EMIS = .850
      ELSEIF(TEMPC.LT.1600) THEN
        EMIS = .680058 + .000575996 * TEMPC - 4.593E-7*TEMPC**2
      ELSE
        EMIS = .40
      ENDIF
C BOLT IS BOLTZMANN'S CONSTANT
      BOLT = 5.67D-8
C CONCK IS THE THERMAL CONDUCTIVITY OF THE CONCRETE
      CONCK = 1.4
C CONCL IS THE LENGTH OF THE SLAB OF CONCRETE
      CONCL = .20
C QLOSS IS THE TOTAL ENERGY LOSS IN THE SYSTEM
      QLOSS = (HBARTOP * SIDEXT**2 * (Y(9)-TC))
     <+ ((HBARSID * HEIGHT * SIDEXT * (Y(9)-TC)) * 4)
     <+ ((CONCK/CONCL) * SIDEXT**2 * (Y(9)-TC))
     <+ (EMIS * BOLT * (SIDEXT**2 + 4 *SIDEXT*HEIGHT)
     <* (Y(9)**4 - TC**4))
C
      IF(T.GT.EXST) GO TO 2
        REACEX = RHOEX(1)+RHOEX(2)*T+RHOEX(3)*T*T
2     REACFB= RHOCOF * (Y(9)-TC)
C
C CALCULATE THE CURRENT MASS OF THE SYSTEM
```

```
C
      MASST= DEN0*(VOL0 + REACEX / RHOVL)
C
      REACTOT = REACEX + REACFB
      YDOT(1) =        Y(2)
C         HI THERE AGAIN
      SUM = 0.D+0
      DO 1 I = 3,8
      YDOT(I) = B(I-2)*Y(2)/GEN-AMDA(I-2)*Y(I)
1     SUM = SUM + AMDA(I-2)*Y(I)
      YDOT(2) = (REACTOT - BT)*Y(2)/GEN + SUM
      YDOT(9)= (EPSIL*Y(2)- QLOSS)/(CP*MASST)
      RETURN
      END
```

VITA

William D. Newmyer was born in Hershey, Pennsylvania on October 29, 1967. At the age of two, he moved to Palmyra, Pennsylvania where he attended elementary school. He was graduated from Palmyra Area High School in June, 1985. The following August, he entered The Pennsylvania State University where he received a Bachelor of Science degree in Nuclear Engineering in December, 1989.

In the January of 1990, he accepted a fellowship at The University of Tennessee, Knoxville and began study toward a Master of Science degree in Nuclear Engineering. This degree was awarded in December, 1991.

William lives in Pittsburgh, Pennsylvania with his wife, Martie, where he works for Westinghouse Electric Corporation as a Core Design Engineer in the Commercial Nuclear Fuels Division.